Peripheral Mechanisms for Fine Tactile Perception: behavioural and modelling approach

Davide Deflorio

A thesis submitted to the University of Birmingham

For the degree of Doctor of Philosophy

September 2022

School of Psychology

College of Life and Environmental Science

University of Birmingham

UNIVERSITY OF
BIRMINGHAM

University of Birmingham Research Archive

e-theses repository

This unpublished thesis/dissertation is copyright of the author and/or third parties. The intellectual property rights of the author or third parties in respect of this work are as defined by The Copyright Designs and Patents Act 1988 or as modified by any successor legislation.

Any use made of information contained in this thesis/dissertation must be in accordance with that legislation and must be properly acknowledged. Further distribution or reproduction in any format is prohibited without the permission of the copyright holder.

Abstract

The tactile system is highly complex. The properties of its central and peripheral components determine the way external stimuli are transformed into perception. At the very first stage, first-order tactile neurons respond to skin mechanical deformation and their activation convey a representation of the sensed object (i.e., encoding). However, there are several open questions regarding which factors can significantly influence the peripheral neural response and hence, perception. The goal of the work presented in this thesis is to provide new evidence about the link between skin properties, object's characteristics, first-order tactile neurons response and discriminative judgments.

Chapter One provides an overview of the tactile system with a focus on the peripheral components (e.g., skin, first-order tactile neurons), as well as a summary of the relevant behavioural findings on tactile perception in Young and Elderly. Chapter Two outlines the methods used in this work including psychophysics, a device to present tactile stimuli in a controlled fashion, skin measurement techniques, and manufacturing of fine-textured stimuli. Chapter Three provides an in-depth review of computational models that simulate the response of first-order neurons and how they can be applied for psychophysical research. Chapter Four is the first empirical chapter that evaluates the effects of skin and mechanoreceptive afferent properties on spatial tactile sensitivity in young and elderly participants assessed with the 2-point discrimination task. Chapter 5 is the second empirical chapter that investigates the effects of the interaction between finger and surface properties on the detection sensitivity for a single microdot in young participants with active exploration. Chapter Six summarises the findings of the research undertaken in my doctoral studies and discusses their implications for understanding the sensory mechanisms underlying tactile perception. Overall, the findings presented in this thesis suggest that the progressive loss of mechanoafferent units contribute to the decline in tactile spatial acuity as predicted by a

population model of the afferent response, and provide new evidence on the complex effects of frictional changes and the role of skin biomechanics on the detection of a microdot.

Acknowledgements

I would like to thank all the people that have helped me throughout my doctoral research. My supervisors Max Di Luca, Alan Wing, and Marta Arroyo provided many stimulating ideas and were supportive in their attempts to mitigate the impact of the Covid-19 pandemic. Other people have contributed with their insightful comments on the manuscripts and suggestions for analysis, the manufacturing of the stimuli, the set-up of the experimental equipment, and emotional support. These are Chris Miall, Winnie Chua, Diar Karim, Pavel Penchev, Benoit Delhaye, Claudio Zito, Al Loomes, Roberta Roberts, David Acunzo, Damiano Grignolio, Min Susan Li. This thesis was supported by a collaborative studentship between the University of Birmingham and Procter and Gamble.

Table of Contents

List of Publications

Deflorio, D., Di Luca, M., & Wing, A. M. (2022). Skin and mechanoreceptor contribution to tactile input for perception: a review of simulation models. *Frontiers in Human Neuroscience*, *16*.

[This publication was used for sections 1.2.1, 1.2.2, 1.3.1, 1.3.2 and form the basis for Chapter 3]

Deflorio, D., Di Luca, M., & Wing, A. M. (under review). Finger properties and afferent density in the deterioration of tactile spatial acuity with aging. *Journal of Physiology*

Conferences

Deflorio, D., Di Luca, M., & Wing, A. M. (January 2021). Two-point discrimination task in young and elderly: a psychophysical and computational study. *Experimental Psychology Society.* Organised by University of Kent (online conference).

Deflorio, D., Di Luca, M., & Wing, A. M. (September 2021). Computational models of tactile neurons of the finger pad: a review. *Symposium on Applied Perception.* Hosted by Inria centre at Rennes University (online conference).

Contribution

The design, programming, experimental set-up, pilot testing, data collection, data analysis and manuscript writing in all studies of this dissertation were carried out by myself with the advice of my supervisors Max Di Luca and Alan Wing, Marta Arroyo and the technical help of collaborators.

List of Figures

Chapter 4. Finger properties and afferent density in the deterioration of tactile spatial acuity with aging.

Chapter 5: Surface geometry and moistened finger affect friction and detection threshold for a single microdot.

List of Tables

Chapter 1

Tactile System and Tactile Perception: A review of the literature

1.1 Overview

The sense of touch allows us to interact with the external world successfully and independently. It enables us to perceive the relative position and state of our muscles, joints, and tendons (kinesthetics/proprioception), to discriminate material properties and to identify objects (cutaneous/tactile), and eventually to act and interact with the external world (haptics), including affective and social exchange. The proprioceptive and cutaneous systems can be thought of as functionally distinct, although they are strictly intertwined (i.e., haptics) and many similarities are present in terms of underlying mechanisms (e.g., sensor response to static vs dynamic mechanical deformation).

The tactile system is hierarchically organized (Figure 1.1). In brief, the origin of tactile sensation is at the periphery with the acquisition of the information through the mechanical deformation of the skin and the subsequent response of the mechanoreceptors. The signal is relayed upstream to the spinal cord, and then to the brainstem and the cortex.
In this work, the leminiscal cutaneous tactile system with mechnoreceptor input is treated in isolation from pain and proprioceptive inputs to facilitate the description of its elements and the interpretation of the findings in relation to human tactile perception and discriminative judgments.

The focus of this thesis is on the peripheral mechanisms underlying tactile perception. The goal is to gain a better understanding of how, and to what extent, finger properties, including skin and (simulated) mechanoafferent units, and object characteristics can influence the sensitivity to discriminate or detect near-threshold stimuli. To address these questions, I

have employed psychophysics in combination with measurements of finger properties, recording of contact dynamics, and simulations of the response of first-order tactile neurons.

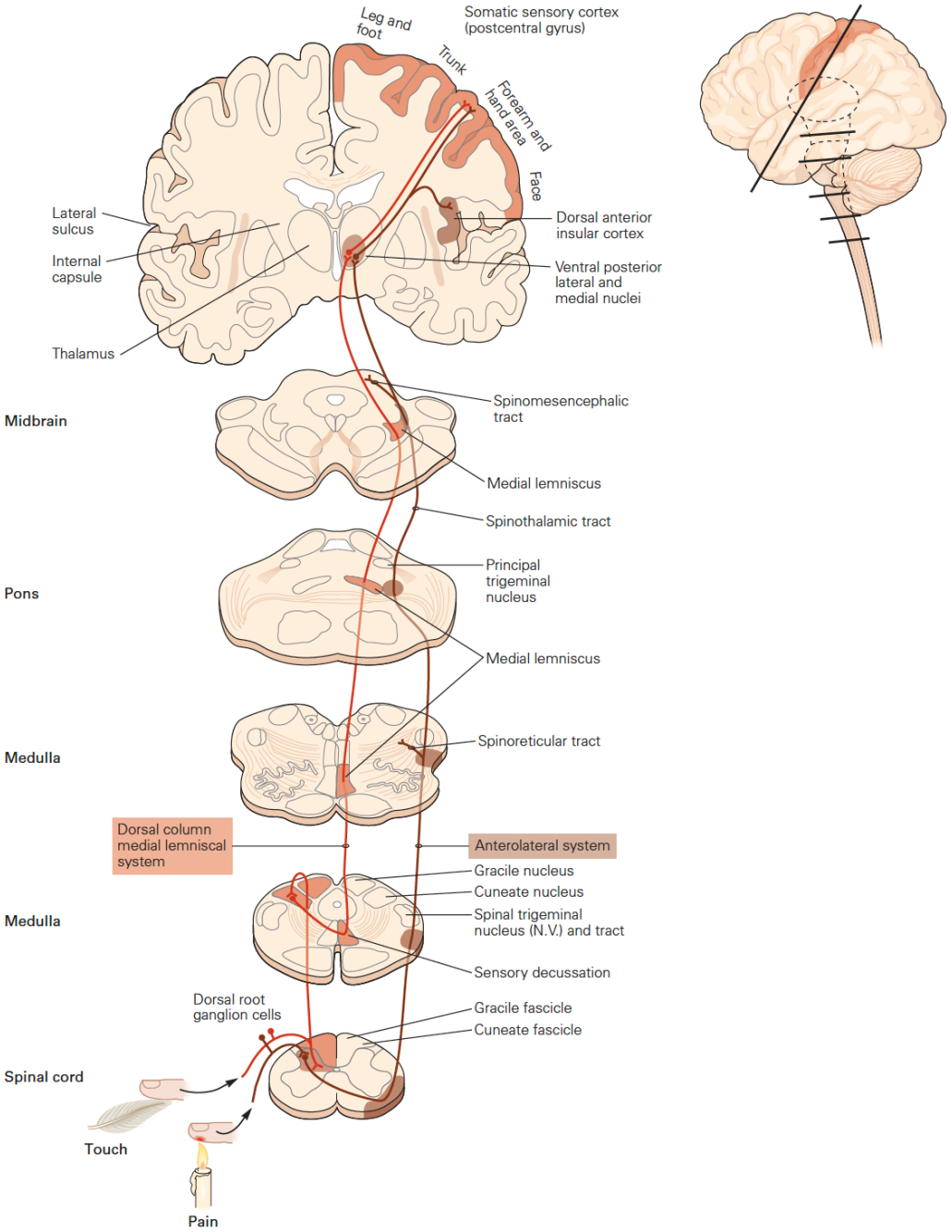

Figure 1.1. Schematic representation of the tactile system pathway from the finger to the cortex. Image from Kandel et al, Principles of Neural Science (2021).

In the next paragraphs, I outline the basic components of the tactile system in more detail with a focus on the peripheral components. This will help the reader with the remaining sections of this chapter which include an overview of the known peripheral transduction mechanisms that enable tactile perception. In addition, I will summarise behavioural findings from the literature on tactile perception, including healthy Young and Elderly people, which served as the basis on which to build the two experiments presented here. In the last section, I introduce the goal of the research undertaken in my doctoral studies and provide an overview of the following chapters.

1.2 Cutaneous Tactile System

1.2.1 Composition and properties of glabrous skin

Skin is a highly complex material, and it varies significantly across the body with consequences for our perceptual abilities. An important distinction is between the hairy skin on the forearm and the glabrous skin of the finger pads. The latter is markedly more involved in tactile discriminative judgments thanks to its composition and the presence of a large number of receptors sensitive to small skin deformations that support tactile perception even down to the order of microns (LaMotte and Srinivisan 1991)

In classifying objects on a range of different properties, such as texture, hardness or shape, we employ specific exploratory movements with the digits that are optimal for extracting cues relevant to those properties (Lederman and Klatzky, 1987). The contact (e.g., sliding vs pressing) between the glabrous skin and the properties of the touched object (e.g., fine or coarse texture and compliance, Figure 1.2) and the physical details of the interaction (e.g., normal and tangential force and displacement) determine how the skin deforms and the mechanoreceptors are activated, and in turn how the stimulus features are coded by the activity of sensory neurons (Bensmaia and Hollins, 2003; Muniak et al., 2007; Weber et al., 2013; Greenspon et al., 2020).

However, the relationship between specific stimuli and the resulting spatiotemporal deformation of the skin is not straightforward but, in fact, is quite nonlinear. This is because the skin is a highly complex medium composed of multiple layers having different load- and time-dependent properties (Daly, 1982; Wang and Hayward, 2007). These comprise epidermis, dermis, and subcutaneous tissue (hypodermis), which is not part of the dermis but is important in providing attachment of the skin to the bones and muscle.

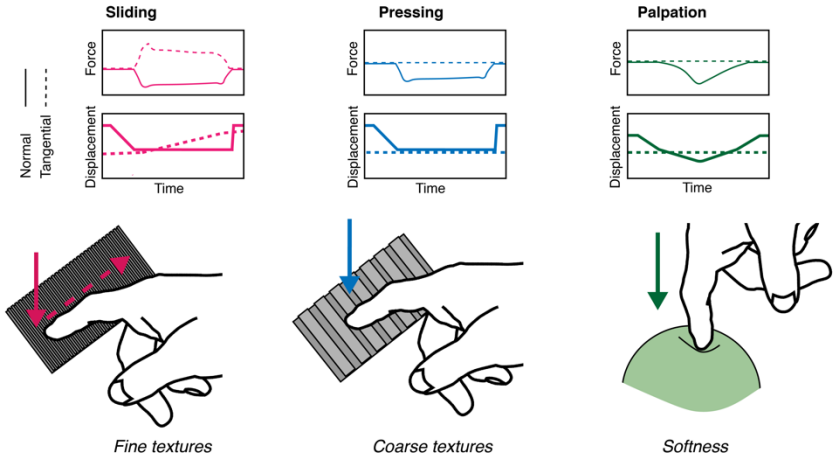

Figure 1.2. Schematic view of exploratory movements. Surface texture (e.g., periodicity of a spatial grating, or roughness of sandpaper) may be felt by static pressing or sliding contact of the index finger with the normal and tangential force components as shown. Sliding is critical in discriminating very fine texture as it generates skin vibrations which reflect the sensed surface.

The epidermis is the outer skin layer and is further subdivided into multiple layers, of which the stratum corneum is the outermost one contacting the external world. The thickness of the stratum corneum is highly variable across individuals ranging between 0.1 to 0.7 mm at the finger pad (Fruhstorfer et al., 2000). This property is relevant as it might indirectly contribute to skin friction by affecting the distensibility of the skin when sliding (Liu et al., 2015). The composition and higher thickness of the dermis (1 to 4 mm) make it functionally more important than the stratum corneum. The dermis hosts most of the mechanoreceptors and nerve endings involved in conveying information about touch and temperature (Figure 1.3). It

contains sweat glands and sebaceous glands which contribute to the hydration of the skin which affect its frictional properties, the contact dynamics, and in turn the way we interact with objects (Adams et al., 2013; Andrè et al., 2011).

The dermis can be histologically divided into two regions: the papillary region and the reticular region. The papillary region consists of loose connective tissue with fingerprint-like projections called papillae which extend to the epidermis and form the papillary ridges of the fingerprint. These irregularities contribute to how the skin responds to mechanical stimuli, mainly by affecting the contact area, and so the friction between the finger and the object (Arvidsson et al., 2017; Duvefelt et al., 2016), as well as the distribution of stress fields (Gerling and Thomas, 2005).

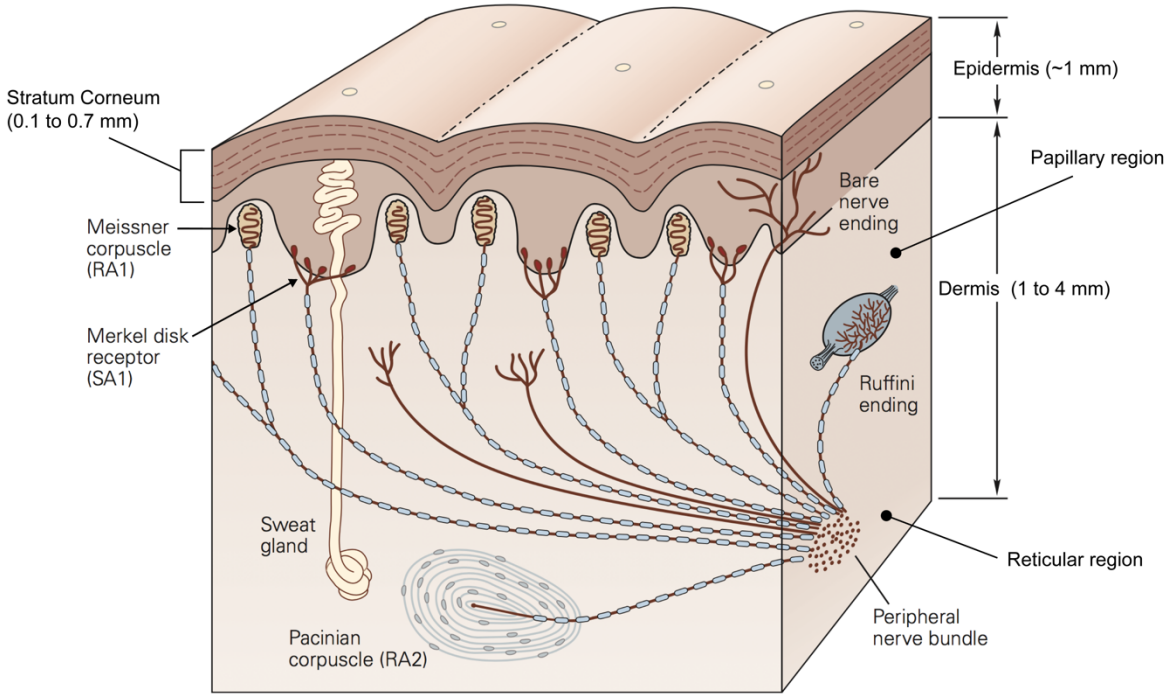

Figure 1.3. Schematic representation of a cross section of the glabrous skin showing different layers, mechanoreceptors and other components. Republished with permission of McGraw Hill LLC, from Principles of Neural Science, Kandel E et al, 5/E, 2013 permission conveyed through Copyright Clearance Center, Inc.

On the other hand, the reticular region constitutes the bulk of the dermis and acts as the support structure. As such, it constrains the deformation that the dermis can undergo. The connective tissue of which the reticular region is made, is very dense and incorporates both collagen fibres, which have high tensile strength and form the main supporting structure, and elastomeric fibres, which are elastic and thus enable the skin to return to its original shape following deformation. Together the two sets of fibres possess directionally specific mechanical properties as well as viscoelastic qualities (Daly, 1982). In fact, the skin behaves differently when subject to stresses and strains along or across the finger. Such anisotropy is reflected by the higher tension of the skin across the Langer's lines (Langer, 1861). Langer discovered these lines when he observed that a circular incision on a corpse changed into an oval shape. These tension lines may be due to the orientation of the collagen fibres which are parallel to them (Gibson et al., 1969).

Viscoelastic materials exhibit relations between stress (applied force) and strain (displacement) that lead to time-dependent nonlinear behaviours. These behaviours include stress relaxation, hysteresis, and creep which can last several seconds. Stress relaxation is measured by stretching and holding the skin and measuring the force required to hold the skin at a given distance. At low strains, the skin responds as an elastic body so that the force required is the same over a long time-interval. At high strains, it behaves as a viscoelastic body requiring a force decreasing logarithmically with time (Daly, 1982; Pan et al., 1997). In addition, the stress-strain relationship is further characterised by a nonlinear response. Under low uni-axial loading the skin is relatively soft but it gets stiffer for high loads for both normal (Maurel et al., 1998) and tangential displacement (Nakazawa et al., 2000). Hysteresis is defined as the strain energy loss between loading and unloading phases due to internal friction, that is the skin deformation decreases during unloading more slowly than it increases during loading. The energy loss is high, repeatable, and invariant for long loading-unloading cycles (e.g., 20 to 80 seconds), but it diminishes for faster cycles (e.g., 5 or 10 seconds) (Wang and Hayward, 2007). Mechanical creep is the continuous extension of the

skin under a constant force. It has been shown that skin creep can be divided in three parts: an initial purely elastic deformation, a viscoelastic phase, and a constant creep phase (Agache et al., 2000). This phenomenon begins with the realignment of the collagen fibres that are rearranged in parallel to one another when stretched (inherent extensibility). During stretching, water in the collagen network is displaced, and elastic fibres are micro-fragmented resulting in mechanical creep and a more viscous skin (Wilhemi et al., 1998).

Skin properties can be highly variable across different individuals. For example, changes in skin elasticity correlate with age, gender (Yang et al. 2018), occupation, and history of exposure to environmental factors such as the sun (Langton et al. 2017). In particular, with ageing, the elastomeric proteins become sparser and their orientation changes resulting in less elastic skin (Yang et al., 2018). In a modelling study it has been shown that the lower elastic modulus observed in the elderly affects the distribution of stresses and strains during static indentation and lateral sliding. As a result, skin vibrations that are generated by sliding the finger across a surface are higher in amplitude and frequency range which may influence the response of the mechanoreceptors (Amaied et al., 2015).

Skin properties are also affected by factors in the testing environment. Although skin hydration is regulated by the glands located in the dermis, it is highly susceptible to environmental conditions such as temperature and humidity, the application of water, or other formulations. For example, Sandford and colleagues (2012) measured the skin stiffness of the arm when exposed to different levels of relative humidity at constant temperature. They found that skin hydration increases with relative humidity and that skin stiffness has a positive relation with the hydration level. This is relevant because skin hydration is also positively correlated with friction (Andrè et al. 2011) which affects vibration in sliding and contributes to how the tactile receptors are activated.

1.2.2 First-order tactile neurons

Tactile perception is mediated by mechanoreceptors located in the dermis that are sensitive to skin mechanical deformation. They are connected to Group II Aβ afferent fibres which transmit the information to synapses in the dorsal spinal cord, and on through the thalamus and then to somatosensory cortex for central processing. The receptor organs, the connected fibres, and the cell body (located in the dorsal root of the spinal cord) are referred to as first-order tactile neurons or mechanoafferent units.

There are four types of mechanoreceptors that differ from one another in terms of their morphology, distribution, and response properties (Figure 1.4). These properties include: i) adaptation or the rate at which the neural response subsides to a constant static stimulus (slow and rapidly adapting receptors); ii) the receptive field characteristics, or the area of the skin to which each mechanoreceptor can respond to. Type 1 fibre (i.e., SA1 and RA1) refers to small receptive fields while type 2 fibre (i.e., SA2 and RA2 or PC) refers to large receptive fields. This property depends in part on the depth of the mechanoreceptors with superficial receptors (i.e., SA1 and RA1) having small receptive fields and deeper receptors (i.e., SA2 and RA2 or PC) large receptive fields; iii) frequency sensitivity profile to vibratory stimuli (e.g. sinusoid) which may be defined in terms of absolute threshold (the minimum amplitude that elicits a spike for a specific frequency) and tuning threshold (the minimum amplitude that elicits at least one spike per cycle); iv) the spike timing, or the precise and repeatable occurrence of individual spikes.

Adaptation rate and receptive field properties are commonly used to categorise the type of receptor. Meissner corpuscles are referred to as rapidly adapting type 1 receptors (RA1). Located close to the skin surface at the base of the epidermis (0.5 to 1 mm below skin surface), they respond preferentially to changes in applied load in a frequency range from 1 to 300 Hz (most sensitive between 5 and 50 Hz) (Kandel et al., 2021; Bolanowski et al., 1988). Their response subsides quickly to static deformation of the skin. The superficial

location of Meissner corpuscles results in a relatively small (type 1) receptive field. Pacinian corpuscles are rapidly adapting type 2 receptors (RA2 or PC). This type of receptor can be found at a deeper layer of the skin, in the dermis (2-3 mm), and they respond to changes in applied pressure for a wide range of frequencies from 5 to 800 Hz (most sensitive between 30 and 500 Hz) (Kandel et al., 2021; Bolanowski et al., 1988). The depth of Pacinian corpuscles contributes to their large receptive field (type 2) characteristic. Similar to Meissner's, the response of Pacinians to sustained indentation fades out rapidly.

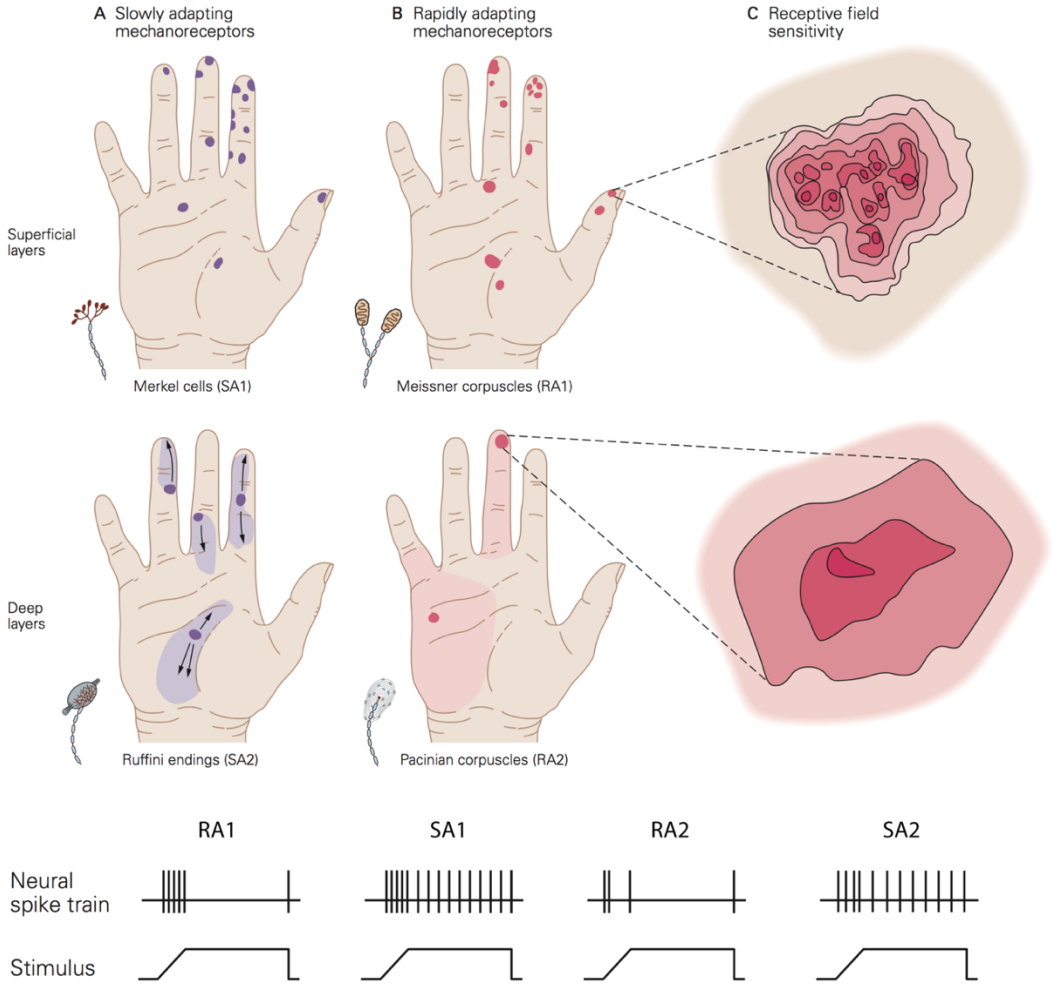

Figure 1.4. Top image shows a schematic view of the distribution, size, and sensitivity map of the receptive field of the four afferent types. Bottom image shows the typical adaptation of the four afferent types in response to a ramp-and-hold indentation. Republished with permission of McGraw Hill LLC, from Principles of Neural Science, Kandel E et al, 5/E, 2013 permission conveyed through Copyright Clearance Center, Inc.

Merkel cells constitute slowly adapting type 1 units (SA1) located close to the skin surface (small receptive field) at the tip of the epidermal sweat ridges (0.5 to 1 mm below the skin surface). They respond to the dynamic onset and the subsequent sustained static pressure with slow adaptation to frequencies up to 100 Hz (most sensitive between 0.3 and 5 Hz) (Kandel et al., 2021; Bolanowski et al., 1988). Finally, Ruffini endings are mainly located around the nail bed and to a lesser extent in the deeper layer of the dermis (2-3 mm). Ruffini endings respond to stretching during both the dynamic and static phase of skin indentations. They were classically thought to be connected to SA2 fibres, but more recent evidence suggests that only a very few SA2 fibres are likely to innervate Ruffini endings (Parè at el., 2003).

It has been estimated that human adult skin has around 200.000 to 270.000 neural fibres linked to mechanoreceptors (Corniani and Saal, 2020), but their density varies across the body with a higher concentration in the hand, feet, and face. The glabrous skin of the young adult hand alone has 17.000, which are more prevalent on the finger pad (Johansson and Vallbo, 1979). The number of Meissner and Merkel's cells decrease with ageing, with the age group 60-90 years old having 4 to 6 times fewer receptors than younger adults between 20 and 49 years of age (Garcia-Piqueras et al., 2019). The morphology of mechanoreceptors also changes with ageing. For example, Meissner's corpuscles become smaller and denervated. Importantly, these receptor changes may contribute to the deterioration of tactile spatial sensitivity observed with ageing.

The size of receptive fields is correlated with the density of receptors and the sensitivity of a specific body part. Thus, the higher density of receptors at the finger pad and the smaller receptive fields lead to higher sensitivity than, for example, the palm of the hand where receptors are more sparsely distributed (Figure 1.4). In the finger pad there are about 100 SA1 units and 150 RA1 units per cm^2 corresponding to an average centre to centre spacing of their receptive fields of 1 mm and 0.82 mm, respectively. Importantly, the receptive field is

a functional concept which depends on the stimulus parameters, as first noted by Johansson (1978). In fact, it has been shown that the receptive field area of SA1 and RA1 fibres increase linearly as the indentation depth increases with estimated minimum area of 5 mm^2 for both and median areas of 11 mm^2 for SA1 and 12.6 mm^2 for RA1 (Vega-Bermudez and Johnson, 1999). Although the afferent spacing and receptive field size is related to and might limit the tactile spatial sensitivity of a specific body area, these are not the only factors involved. In particular, RA1 and SA1 fibres innervate multiple receptor organs and, at the same time, each receptor is linked to multiple fibres. An RA1 fibre innervates 10 to 30 Meissner corpuscles on average and each Meissner corpuscle is innervated by 2 to 5 RA1 fibres. This innervation branching allows the combination of information from several adjacent regions of the skin and contributes to localised hotspots with higher sensitivity in type 1 units. Having multiple “hotspots” may benefit the perception of fine spatial features such as the detection of small changes in edge orientation, important for fine manual dexterity (Pruszynski et al., 2018). All these properties enable RA1 and SA1 receptors and associated fibres to transmit detailed spatial representations of an object’s geometry when in contact with the skin.

In contrast to RA1 and SA1 receptors, Pacinian corpuscles (RA2) are more sparsely distributed (Johansson and Valbo 1979), and only a single afferent fibre is connected to each Pacinian receptor. Their receptive fields are relatively large (5 to 10 times that of SA1) (Johansson and Valbo, 1980) which makes these fibres unsuitable for resolving fine spatial details. Nonetheless, the high sensitivity of RA2 to sub-micron vibrations of the skin, over a wide range of high frequencies, plays a major role in the detection of very fine features during dynamic exploration. For example, LaMotte and Srinivasan (1991) found that RA2 fibres responded consistently during a sliding movement over a texture composed of bars with a height of only 0.05 μm. They showed that these values are in agreement with human detection thresholds suggesting that RA2 units might play a major role for detecting this sort of micro feature. SA2 fibres, instead, tend to be distributed near the fingernails, which makes

them less sensitive than RA1 and SA1 to the transient components of sensations, and it has been shown that they might contribute to the perception of applied force on the finger pad (Brothers and Hollins, 2014). However, the role of Ruffini receptors is still not fully determined, as most neurophysiological studies on touch have been conducted on monkeys' glabrous skin which is devoid of SA2 fibres.

1.2.3 Spinal cord

First order-tactile neurons are composed of a single axon, called primary afferent fibre, with two branches. One projects to the periphery and innervates the receptor organs and the other terminates either in the grey matter of the dorsal portion of the spinal cord or projects to the brainstem (Kandel et al., 2021). The local branches are involved in reflex circuits while the distal branches convey tactile information to the brain for perception. The distal branches of the first-order tactile neurons cluster together to form different spinal nerves which transmit the information from a specific area of the skin which is named dermatome. The afferent pathway that conveys tactile signals from the hand ascends in the ipsilateral dorsal column to the cuneate nucleus in the brainstem. Here, they form the first synapses of the somatosensory pathway connecting to second-order neurons. The second-order fibres decussate to form the medial lemniscus and terminate in the contralateral portion of the thalamus.

1.2.4 Thalamus and Somatosensory areas

The thalamus is located in the centre of the brain (diencephalon) and acts as link between peripheral sensory neurons and the somatosensory areas. Rather than being a simple relay station, the thalamus can prevent or enhance the signals coming from the periphery, thanks to the inhibitory neurons populating the outer shell of the thalamus, named reticular nucleus (Kandel et al., 2021).

The thalamus is a well-organised structure composed of 50 nuclei which receives and transmits information from a specific sensory modality to the neocortex. Cutaneous and proprioceptive information is relayed through the ventral posterior nucleus and the ventral posterior superior nucleus, respectively, and transmitted to the primary somatosensory cortex, S1 (Kaas, 2008). S1 is also extensively connected to higher level cortical areas where the somatotopic information is processed further. These include the secondary somatosensory areas (S2), the posterior parietal cortex, and the primary motor cortex.

S1 is located in the postcentral gyrus of the parietal lobe and comprises 4 distinct areas: Brodmann's area 3a, 3b, 1, 2. Each of these areas have its own somatotopic map. According to the inputs they receive, these maps are tuned to a specific touch sub-modality and are involved in different aspects of touch. Area 3a receives proprioceptive information from muscles and joints. Area 3b receives signals coming from SA1 and RA1 fibres, while area 1 receives inputs from SA2 and RA2 fibres. Area 2, instead, is activated by both cutaneous and proprioceptive inputs. These maps are characterised by the so-called cortical magnification. That is, the amount of cortex dedicated to a specific body part is related to the importance of that body part to the sense of touch. In particular, body areas with higher innervation density of mechanoreceptors (e.g., hand, tongue, toe) are represented in larger portion than those with fewer receptors (e.g., trunk).

An important aspect of the cortical neurons devoted to touch is their receptive field characteristics which differ considerably from the receptive fields of first-order neurons. Primary afferents innervating mechanoreceptors on the fingertip have receptive fields covering a very small area. Instead, the receptive field of a cortical neuron in area 3b can cover one or two fingertips (Gardner, 1988). This is because each of these cortical neurons receives inputs from 300 to 400 primary afferents allowing the integration of information from adjoining receptors. The RF size becomes even larger as the signal progresses through higher-level cortical areas The RFs of area 1 and area 2 can cover several fingertips or

larger portions of different fingers (Gardner, 1988). The cortical RFs of area 3b are characterised by an excitatory region adjacent to or overlapping with an inhibitory region (DiCarlo et al., 1998; Sripati et al., 2006a). These patterns of excitation and inhibition are thought to be created by feed-forward and feedback connections at the level of the dorsal column nuclei, the thalamus and the cortex (Andersen et al., 1964; Alloway and Burton, 1991).

The structure of the receptive fields has important functional implications. For example, surrounding inhibitory regions may prevent the spread of activity to nearby neurons resulting in an enhanced neural image of the tactile details or enabling direction (Warren et al., 1986) and orientation sensitivity (Bensmaia et al., 2008). These properties enable the representation of tactile stimuli in an increasingly abstract manner as the information moves from lower to higher level cortical areas. Thus, the neural response becomes more and more tuned to a particular class of stimuli or a particular feature (e.g., orientation, direction of motion) rather than the position of the stimulus in their receptive field.

The response of first-order neurons is very sensitive to stimulus parameters such as amplitude and speed while neurons in area 3b and 1 are relatively insensitive to these changes. For example, Bensmaia et al. (2008) showed that many neurons in area 3b and 1 respond to the preferred orientation (i.e., orientation tuning) regardless of whether the stimulus is scanned or indented into the skin and their response does not depend on the amplitude nor the speed of the contact. Area 2 receives information from multiple fingers which provide the information to detect to overall shape and size of an object held in the hand. Neurons in this area also receive proprioceptive feedback, such as the hand posture and the necessary force to hold the object. Thanks to the integration of different types of information, area 2 subserves the identification or discrimination of objects.

Somatosensory area S2 is located posterior to S1 in the parietal operculum and, like S1, it contains four distinct somatotopic maps (Kandel et al., 2021), although these maps are less detailed than those in S1. For example, Ruben et al., (2001) showed that there are no separate representations of the second and fifth finger in S2, in contrast to what has been observed in S1 (Shoha, and Grinvald, 2001). Importantly, this area not only receives its inputs from S1 but is also activated by visual inputs (Robinson and Burton, 1980; Hihara et al., 2015) and modulatory feedback from higher-level cortical areas (Romo et al., 2002). S2 is critical to perceiving the spatial properties of objects such as roughness and shape (Murray and Mishkin, 1984) as well as temporal features of vibratory stimuli (Ryun et al., 2017; Harrington and Downs, 2001). However, its response does not reflect exactly the stimulus properties as is the case for first-order tactile neurons and to a lesser extent S1 neurons, but it results from an interaction of somatosensory inputs and cognitive processes such as the attentional state (Hsiao et al., 1993) or memory for previous tactile stimuli (Romo et al., 2002)

To conclude, central somatosensory areas have the important function of processing the information from the mechanoreceptors to transform the highly specific information encoded by thousands of receptor organs to a more abstract representation. This representation enables surface and object discrimination, and eventually the interaction with tactile objects by combining proprioceptive and cutaneous inputs from neighbouring skin areas to support manipulative movements involving supplementary motor area (SMA) and primary motor cortex (M1). In the next section, I provide an overview of the transduction of mechanical inputs into meaningful neural response and highlight the contribution of each mechanoreceptor type to the encoding of tactile stimuli.

1.3 Transduction and Encoding of Mechanical Inputs

People are able to detect and discriminate many different classes of stimuli. Such sensitivity is due to the ability to code spatiotemporal patterns of the stimulation by leveraging the

properties of individual receptors, combining skin pressure information close to the indentation site (static component) with the variations of pressure (i.e., vibrations/waves) that propagate away from the contact points (dynamic component) throughout the hand up to the wrist (Shao et al. 2016). Interestingly, the stimulation originating from long-distance propagation of waves to remote receptors can be used in isolation for sensory discrimination in some instances (Libouton et al., 2012).

The experimental findings for static and sliding touch suggest that tactile perception relies on at least two different neural mechanisms (Duplex Theory, Katz, 1925). Coarser features are thought to be encoded by the spatial activation of the afferent population which closely matches the spatial layout of the stimulus indented into the skin. Fine feature perception, by contrast, is thought to rely on the temporal patterning of individual afferents generated by stroking movement or vibrating stimuli. In fact, the encoding of tactile information may involve a spatial or a temporal code depending on the circumstances. The former refers to firing rate variations between afferents. The latter, in contrast, employs firing rates variations of individual afferents over time and their precise spike timing.

1.3.1 Spatial code

In a seminal study, Phillips and colleagues (1988) showed that during static contact, the spatial layout of the indentation is reflected in the spatial activation of SA1, and to a lesser extent, RA1 fibres. They repeatedly indented each letter of the alphabet into the finger of rhesus monkeys while shifting the position of the letter on each iteration. Then, they plotted the generated action potentials of the 89 recorded afferents (34 SA1, 36 RA1, and 19 RA2) to build a Spatial Event Plot (SEP). These plots showed that SA1 responses carry fine spatial details of the image, while RA1 plot are less sharp, and RA2 plots even more blurred (Figure 1.5). In fact, SA1 and RA1 have small receptive fields and are present at high density which make them suited to resolve fine spatial details. However, it is not clear

whether the innervation density limits tactile acuity or whether there are factors that allow perception of features with a resolution beyond the spacing of afferents.

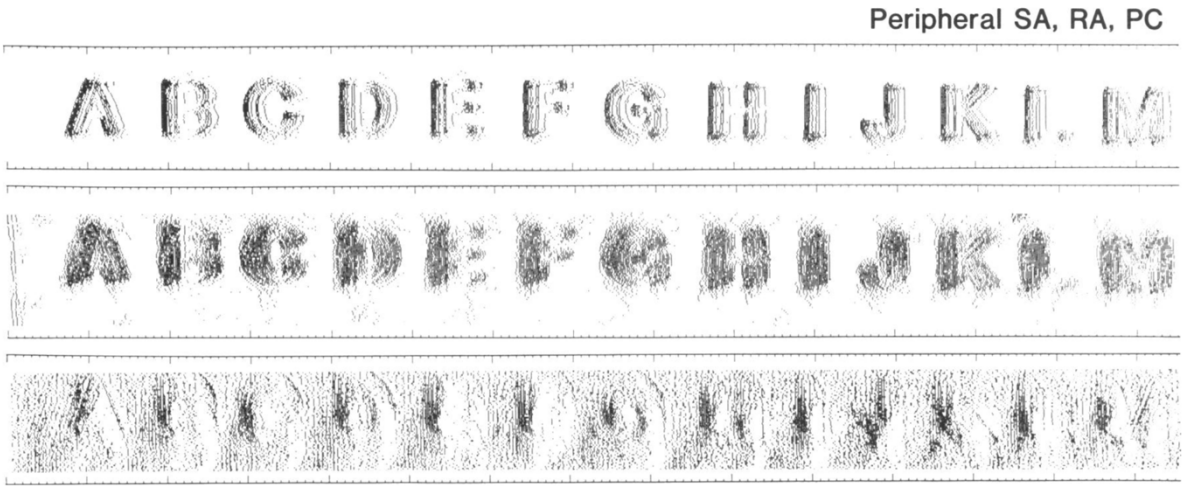

Figure 1.5. Somatosensory Evoked Potentials (SEP) in rhesus monkeys for several indented letters. Rows from top to bottom show SEPs from one SA1, one RA1, and one RA2, respectively. Image reproduced with the author's permission (Phillips, Johnson and Hsiao, 1988).

Afferent spacing was initially considered as a limit to the resolution of fine details by static touch, but several studies showed that hyperacuity (Westheimer, 1975) is present in the tactile as well as in other sensory modalities. For example, it has been shown that edge orientation thresholds are around 20° in a 2-IFC discrimination task (Bensmaia et al., 2008). The authors suggested that tactile discrimination of bars is poor when compared to the visual counterpart, but they are similar in the extent to which the resolution limit is set by the respective innervation density of both modalities. However, in a recent study using a tactile pointer-alignment task, Pruszynski et al. (2018) showed that participants can detect much smaller changes in the orientation of edges (i.e., 3° for edges spanning the entire fingertip – 10 mm). These findings are in contrast with the traditional view that tactile spatial resolution is limited by the afferent density and the centre-to-centre spacing of the receptive fields (Friedman et al., 2002; Dodson et al., 1998). Pruszynski et al. (2018) used a modelling approach to show that implementing complex receptive fields with multiple hotspots of high sensitivity can enable the tactile system to resolve fine details near the limit of receptive field

spacing. These results suggest that tactile orientation discrimination can be as good as vision. Recently, Jarocka et al. (2021) provided further evidence that the spatial sensitivity of SA1 and RA1 is defined by the complex structure of their receptive fields having high responsive subfields and not only their spacing. They estimated that the subfield acuity is approximately 0.4 mm, which would allow resolution of details finer than the innervation density.

1.3.2 Temporal code

A temporal code is observed for the perception of fine or micro features such as microdots and textures. In a series of studies, LaMotte and colleagues (LaMotte and Srinivasan, 1991; LaMotte and Whitehouse, 1986; Johansson and LaMotte, 1983) showed that people can detect very small dots, on an otherwise smooth surface, of only 1 micron height with a diameter of ~600 microns (3 microns with ~230 microns diameter and 6 microns height with a diameter of ~40 microns) and very fine textures (parallel bars 45 microns wide and spaced ~100 microns) of only 0.1 microns height, when compared against a smooth surface in a 2AFC task. They found that lateral sliding is essential for these fine features to be perceived, as no sensitivity to the same set of stimuli was found with static touch. Neurophysiological recordings suggest that rapidly adapting mechanoreceptors (RA1 and RA2) have a primary role in the perception of the microdots and fine textures as they are sensitive to low amplitude and high-frequency vibrations (LaMotte and Srinivasan, 1991). The sliding movement is necessary to elicit skin vibrations (Manfredi et al., 2014) that in turn trigger the vibratory response of both types of rapidly adapting fibres.

Importantly, the neural response accurately reflects the skin oscillations with sub-millisecond precision. Mackevicius et al. (2012) showed that sinusoidal vibrations elicit a phase-locked response in first-order neurons which depends mainly on the frequency of the vibrations rather than their amplitude. On the other hand, firing rates were highly affected by the stimulus amplitude resulting in similar population firing rates across different frequencies.

This suggests that precise spike timing is relevant to perception in this context and is likely a better candidate than firing rate to encode the frequency of vibrations and to detect or discriminate fine textures. These findings are in line with the early work of Morley and Goodwin (1987) who observed that the temporal firing patterns of first-order tactile neurons is phase-locked to the spatial frequency of the grating.

Spike timing has also been proposed to enable the encoding of spatial features such as curvature or the direction of applied force. In particular, Johansson and Birznieks, 2004 showed that the relative timings of the first spikes across afferents can be informative of whether the probe in contact with the fingertip is flat or rounded, and whether the movement happened in proximo-distal or lateral direction. The authors suggested that first spike latencies might underlie rapid object manipulation as it requires only a few spikes elicited from the initial contact with the skin. However, Delhaye et al. (2019) showed that a spatial code based on the variations of firing rates across the afferent population is also rapid enough to be considered as a potential coding strategy for spatial features and hence object manipulation.

It is worth mentioning that it is unlikely that the different mechanoreceptor types work in isolation. Instead, tactile perception arises from the contribution of all the different units and their interaction (see Saal and Bensmaia, 2014). For example, Weber et al. (2013) showed that the perceived roughness of a wide range of textures is driven by three types of tactile unit. On the one hand, coarser textures elicit an informative response from all afferent types but are best resolved from the spatiotemporal activation of SA1 fibres which is generated by the spatial layout of the texture in contact with the skin. On the other hand, finer features are mainly conveyed by the precise spike timing of RA and PC fibres (and to a less extent SA1 type). Briefly summarised, Weber et al (2013) showed that combining the response of RA1, RA2, and SA1 provides a more accurate prediction of the perceived texture than the response of a single unit type. Similarly, grip control can be achieved by a combination of the

perceived object curvature, direction of motion (i.e., slip), onset or offset of contact, and applied pressure which are mediated by the four different classes of afferent fibres (Jenmalm et al., 2003; Birznieks et al., 2001; Westling and Johansson, 1987).

1.4 Tactile perception

Our ability to detect and discriminate tactile features has been studied widely. Research on tactile perception focused on determining human capabilities has provided evidence regarding human sensitivity to a range of stimuli including coarse and fine textures, grating and edge orientation, 2-point discrimination, vibration detection and discrimination, and fine features such as a single dot placed on an otherwise smooth surface.

To facilitate the presentation of the behavioural findings that informed the research undertaken in my doctoral studies, it is useful to make a distinction between studies employing static (e.g., ramp-and-hold stimuli indented orthogonally into the skin) versus dynamic stimuli (e.g., sinusoidal vibrations, sliding movement over textures). The former is commonly used to assess spatial acuity while the latter is employed to target vibrotactile sensitivity. This distinction is related to the fact that tactile perception is thought to rely on at least two different mechanisms that enable the perception of the whole range of tactile stimuli that we encounter. This notion stems from the duplex theory elaborated by Katz (1925) in the beginning of the 20th century who first noted that the sense of touch relies on both spatial and temporal cues.

The following sections outline behavioural findings and considerations that informed the research presented in Chapters 4 and 5. The next section presents the reader with an overview of the 2-point discrimination task in relation to tactile spatial acuity and ageing touch. Then, I highlight the relevant information on vibrotactile sensitivity in the context of active touch and the importance of studying skin-object interaction.

1.4.1 Spatial Acuity and the 2-point discrimination task

Tactile spatial acuity refers to the ability to discern the spatial configuration of stimuli indented orthogonally into the skin. It is used to evaluate somatosensory system function, to assess the sensitivity across different body parts, or to study the effects of a variety of factors on discrimination abilities. One of the classical paradigms to assess spatial acuity is the 2-point discrimination task which originated from the pioneering work of Weber (1835) who first attempted to map tactile sensitivity across different body parts. Blindfolded participants are presented with two closely spaced stimuli (e.g., pins or needles) and they have to report whether they feel the two stimuli as distinct. The separation distance is varied so to determine the minimum distance needed to perceive the two pins accurately. More recently, variations in spatial acuity across different body regions, as summarised by Weinstein (1968), are shown in Figure 1.6. The author confirmed Weber's map reporting higher sensitivity at the level of the fingertips of about 2 mm, lower sensitivity on the palm of about 10 mm, and 40 mm on arm, thigh, and back.

The 2-point discrimination task has been adapted through the years to overcome the limitations embedded in the original design. Initially, only the two-point stimuli at various distances were presented with no comparisons with single point stimuli. In this case, participants are likely to adopt subjective criteria for responding "two" producing highly variable results (Weber, 1935). To avoid subjective bias, a common approach is to present the single point stimulus on every trial to allow direct comparison of the spatial configuration of the two stimuli. Johnson and Phillips (1981) used this method to investigate the spatial neural mechanisms underlying tactile perception. Their stimuli were 0.5 mm diameter flat-ended pins presented singly and in pairs on each trial. They found that subjects could discriminate the two-pins correctly even when presented at zero separation distance. They noticed that having the same diameter for the single point and the two-point stimuli resulted in different overall contact area, shape and dimension that could be used to perform the task. To overcome this issue, contact area can be evened up and shape differences

minimised by choosing pins with different diameters. The Aesthesiometer™ was designed for this purpose. This device features three pins, one with larger diameter and two with a diameter that together sum up to the diameter of the single pin.

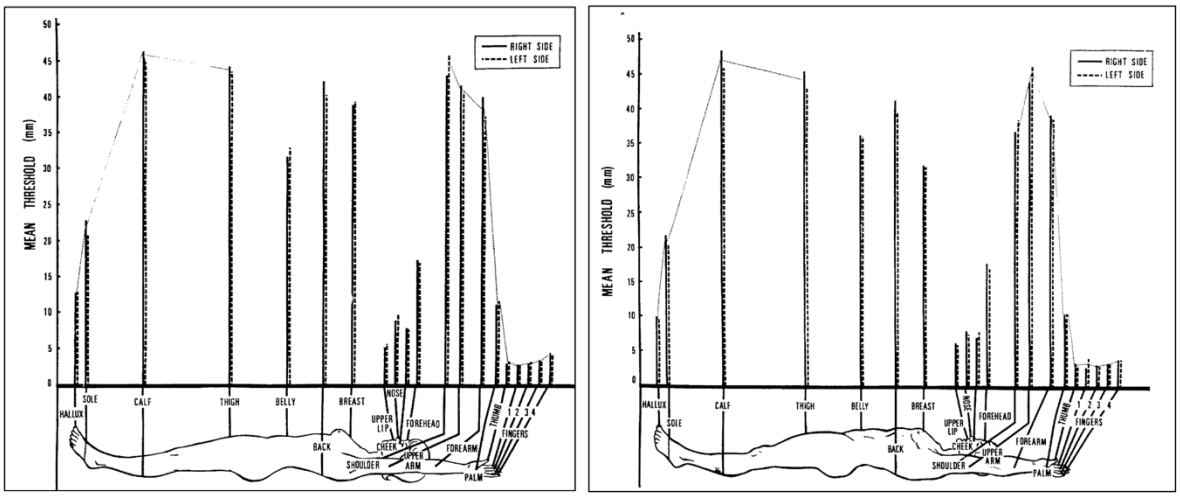

Figure 1.6. Weinstein's map of tactile spatial sensitivity for female subjects (left) and male (right). The schematic figure shows the mean 2-point threshold in millimetre as function of body region tested. The figure also shows the threshold for left and right body side (Weinstein 1968).

Another limitation is the variability of results across studies driven by the type of stimuli employed. The 2-point stimuli used include paper clips, compass with flat or sharp ends, Aesthesiometer™, Disk-Criminator™ (wheel device with fixed-distance stimuli), and brass needles. Furthermore, stimulus presentation can be achieved either actively by participants pressing their finger on the stimuli (Kalisch et al., 2009), or passively by either the experimenter (Dellon et al., 1987) or a computer-controlled device (Phillips and Johnson, 1981a) pressing the stimulus onto the skin. The latter is preferred as it ensures that a consistent pattern of indentation is achieved.

In general, it is important to provide an exact description of how a tactile test was performed to allow a better comparison between studies and allow reproducibility of results, but this is not always the case (see Table 1.1). In particular, the findings of Yokota et al. (2020) highlight the importance of controlling indentation speed and depth which can affect the

estimated thresholds. Notwithstanding these limitations, the 2-point discrimination paradigm can still be a useful method to evaluate discriminative touch and to help gauge the difference between different populations (e.g., young versus elderly, patients with sensory conduction compromised by carpal tunnel compression of the nerve versus control) as long as the indentation parameters are carefully controlled (Lundberg and Rosén, 2004).

Study	Stimuli	Stimulation	Method	Estimated Threshold
Weinstein (1968) N = 48 (24 female); mean age = 22 years	Aesthesiometer™	Hand-held stimuli	Method of limits	~ 2 mm (results not reported in detail)
Johnson and Phillips (1981) N = 14 (12 female); age range = 17-25 years	0.5 mm diameter flat-ended steel needles mounted on a rotating disk (same diameter for single and two points stimuli)	Computer-controlled stimuli indented on immobilised finger. 3 levels of force (10, 30, 80 g)	Method of constant stimuli (2-IFC)	0 mm (results not reported in detail) No effect of force
Crosby and Lee Dellon (1989) N = 20 (10 female); age range = 22-62 years; mean age = 39.8 years	1. Aesthesiometer™ 2. Paper clip 3. Disk-Criminator™	Stimuli indented manually by the experimenter	Method of limits	1. 2.6 ± 0.67 mm 2. 2.3 ± 0.57 mm 3. 2.3 ± 0.44 mm
Kalisch et al. (2009) N = 19, all right-handed (12 female); mean age = 24.5 ± 4.6 years; age range = 19-35 years	0.2 mm diameter flat-ended brass needles (same diameter for single and two points stimuli)	Participants moved their finger onto the stimuli. Indentation depth partially controlled by arresting the down movement with a stopper at fixed position	Method of constant stimuli (either single- or two-point stimulus presented on each trial). Respond 'one-point' if unsure	Right hand: 1.48 ± 0.05 mm Left hand: 1.46 ± 0.05 mm
Tong et al. (2013) N = 24 (10 female); median age = 21 years; age range = 18-26 years	Digital calliper with tips width 0.25 mm and thickness 0.5 mm. For single-point one tip was used. For two-points both tips touched the finger	Stimuli indented manually by the experimenter	Bayesian adaptive procedure (2-IFC)	75% threshold not reported 95% threshold = 1.2 mm

Won et al. (2017) N = 40 (20 female); mean age = 27.1 ± 3 years; age range = 21-37 years	Drawing compass with blunt tips	Stimuli indented manually by the experimenter	Method of limits (two-point stimulus presented on each trial)	Male: 2.1 ± 0.6 mm Female: 1.9 ± 0.6 mm
Yokota et al. (2020) N = 36 (16 female); mean age = 21.1 ± 0.8 years; 15 subjects attended Exp.1 and 21 attended Exp.2; 7 subjects involved in both experiments	Pins features not reported	Computer-controlled stimuli Exp. 1: 4 indentation speeds a) 1 mm/s b) 5 mm/s c) 10 mm/s d) 20 mm/s with indentation depth fixed at 0.5 mm Exp. 2: 3 indentation depths a) 0.5 mm b) 1 mm c) 2 mm with indentation speed fixed at 10 mm/s	Method of constant stimuli (either single- or two-point stimulus presented on each trial). Respond 'one-point' if unsure	Exp. 1: a) 3.67 ± 0.71 b) 3.07 ± 0.72 c) 3.09 ± 0.76 d) 3.28 ± 0.76 Exp. 2: a) 3.14 ± 0.51 b) 3.00 ± 0.04 c) 3.03 ± 0.9

Table 1.1. Summary table of relevant studies measuring the two-point discrimination thresholds obtained for the distal phalange of the index finger. The table highlights the variability of results depending on the stimuli used, indentation protocol and psychophysical method used.

Besides the two-point discrimination test, there are other tasks that are commonly used to evaluate tactile spatial resolution with static touch. These include grating discrimination which can be used to test the ability to discern between a smooth surface and a grooved surface (Craig, 1999), gap detection and letter recognition (Phillips and Johnson, 1981a), braille-like patterns which can be presented in pair and participants are asked to report whether the two stimuli have the same layout or not (Kauffman et al., 2002), and edge orientation (Pruszynski et al., 2018).

1.4.2 Spatial acuity and Ageing touch

The spatial acuity tests listed in the previous section have been used not only to characterise the tactile sensitivity of healthy young adults, but also to assess the evolution of the sense of touch throughout the lifespan. The extensive literature on ageing touch reveals that our ability to discriminate the spatial properties of tactile stimuli is negatively affected by ageing across a variety of tasks. In relation to the two-point paradigm, several authors reported poorer performance in older participants (Stevens, 1992; Woodward, 1993; Kalisch et al., 2009; Bowden and McNutty, 2013). For example, Stevens (1992) used an adaptive staircase to measure the 2-point threshold for the index finger in three age groups: 18-33, 41-63, and 66-91 years. Results showed a progressive worsening with age (Figure 1.7). Namely, the mean threshold for the young group was 1.95 ± 0.69 mm, for the middle age group was 2.68 ± 0.44 mm, and 5.03 ± 1.88 mm for the elderly group.

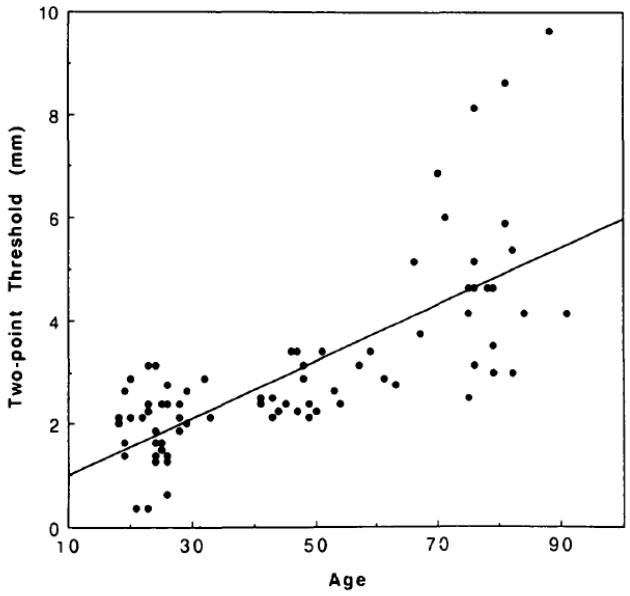

Figure 1.7. Two-point threshold in millimetre plotted as a function of age. Image from Stevens (1992)
Further evidence come from the work of Stevens and Cruz (1996) who employed three different tasks to measure sensitivity threshold for young (mean age 22.7 years) and elderly participants (mean age 77.5 years). They used the gap detection, line orientation and line length discrimination task and reported that the thresholds were about three times larger for the older group in all tests. Similar findings were shown for grating orientation discrimination by Goldreich and Kanics (2003). They observed a linear decrease of sensitivity across the lifespan for both sighted and blind participants.

Interestingly, the effect of age seems to be greater at the level of the toes and fingers compared to other body parts such as calf and tongue (Stevens and Choo, 1996). Several anatomical and morphological changes affect the glabrous skin of the finger with age including lower skin elasticity and hydration (Skedung et al., 2018), decreased Young's modulus (Yang et al., 2018), deterioration of the mechanoafferent units in terms of morphology, size, and number (Garcia-Piqueras et al., 2019), and demyelination process affecting the nerve fibres (Peters, 2002).

In general, ageing offers an opportunity to leverage the intrinsic decline of the tactile system to gather evidence regarding the peripheral mechanisms underlying tactile perception. An open question regards the relative contributions of skin and mechanoafferent properties to the decline of spatial acuity observed with ageing. In particular, it is not clear to what extent changes in skin elasticity, stiffness, hydration and mechanoafferent density are linked to the worsening of tactile discrimination ability.

1.4.3 Vibrotactile sensitivity

Vibrotactile sensitivity can be defined as the ability to detect and discriminate stimuli that elicit an oscillatory response in the skin. Similar to spatial acuity, vibrotactile sensitivity tests provide insights into the functioning of the peripheral tactile system. A common test is the detection of a vibrating probe in static contact with the skin which can vary in frequency and amplitude (Bolanowski et al., 1980).

Vibrational inputs activate the rapidly adapting receptors (RA1 and PC) which are very sensitive to small amplitude vibrations over a wide range of frequencies (up to 1000 Hz) and prove essential to detect and discriminate fine-textured stimuli such as gratings (Hollins et al., 2001), raised dots (LaMotte and Srinivasan, 1991), or abrasive paper (Miyaoka et al., 1999). Tactile temporal sensitivity allows us to perceive textural information far beyond what

is achievable by vision (Heller, 1989) or audition alone (Lederman, 1979). It also provides rich information regarding other surface properties such as stickiness/slipperiness which contribute to object identification and manipulation.

People are very sensitive to vibration cues which allow us to perceive object's features down to micron and nanometre scale. Johansson and LaMotte (1983) showed that people are able to detect a single dot placed on an otherwise smooth surface of 1 micron height with a diameter of ~600 microns, 3 microns height with ~230 microns diameter, and 6 microns height with a diameter of ~40 microns. Participants were able to perform the task only in the presence of a sliding movement, in contrast to when the task involved only pressing on the surface. In a follow-up study, LaMottte and Whitehouse (1986) observed that increasing the scanning speed affected the detection threshold as well as the magnitude estimation of the dot height. Increasing stroke velocity from 1.5 mm/s to 10 mm/s resulted in d' increase from 0.49 to 2.3 for a dot with ~600 microns diameter and 4 microns height while it did not affect d' for a dot with ~600 microns diameter and 15 microns height. The magnitude estimation increased 4-fold when increasing the speed from 1.5 mm/s to 10 mm/s for both dots, but no further change was observed when the scanning speed was 40 mm/s.

The characteristics of exploratory movements used in touching determine the way we perceived object features. For example, the effects of skin-object interaction on discrimination abilities have been shown for roughness discrimination tasks (Aktar et al., 2017; Skedung et al., 2018). However, it is still not clear how the detection of near-threshold stimuli, such as microdots of only few microns height, is affected by manipulations of friction and surface roughness which in turn would alter the forces acting on the skin and its biomechanical response.

1.5 Research Proposals and Overview of Chapters

Overall, this thesis focuses on determining the effects of intrinsic (i.e., ageing) and extrinsic (i.e., caused by environmental factors) peripheral changes that happen at the level of the finger on perceptual threshold in the context of static as well as dynamic touch. In particular, the goal is to provide new evidence to better understand the relationship between finger properties, skin mechanics and tactile perception. To this end, I combined psychophysics with measurements of finger properties, force recordings, and simulations of the response of first-order tactile neurons.

Chapter Two outlines the methods used in my research. These includes psychophysics, a robotic arm to deliver parameter-controlled tactile stimuli, the approach used to measure finger properties, and the process involved in manufacturing high-resolution textures. Given the complexity of these methods, I believe it is relevant and useful for other researchers to provide a detailed description of the processes involved and of the results achieved concerning the methodology involved in this work.

Chapter Three provides a literature review of some of the currently available models to simulate the response of first-order tactile neurons. This work informed the choice of the model used in Chapter Four. At the same time, this review was conceptualized to facilitate researchers in psychology, robotics, and other disciplines in choosing the appropriate model for their particular focus and to raise awareness regarding the limitations associated with each one of the presented models. This chapter also highlights the general difficulties in reproducing specific skin biomechanical properties and the associated mechanoafferent activity.

Chapter Four investigates the deterioration of tactile spatial acuity observed with ageing and the peripheral factors that might be involved. As previously shown, ageing is characterised by poorer spatial acuity than the younger counterpart together with major changes that

happen at the level of the finger. These include lower skin elasticity and stiffness, lower hydration, and partial loss of SA1 and RA1 units. However, there is little evidence that links these changes to the perceptual outcome. I employed psychophysics, measurements of finger properties, and simulation of the activity of first-order tactile neurons to assess whether skin biological elasticity, stiffness, hydration, and lower density of mechanoafferent fibres can predict the poorer spatial acuity expected for the elderly group. I also discuss the possible contribution of central in addition to peripheral factors in age-related changes in tactile discrimination including altered somatosensory representation of tactile stimuli and impairments in cortical processes linked to unbiased decision making (e.g., memory, attention).

Chapter Five continues to investigate the link between skin properties and perception. In particular, this study was aimed at improving the understanding of skin-object interactions in the presence of friction and the consequences for detection thresholds for a single microdot placed in the centre of a surface. Rather than the approach taken in Chapter 4 of taking advantage of intrinsic skin differences between young and elderly population, in Chapter 5 the skin biomechanical response is actively manipulated by moistening the finger and by changing the surface geometry. To characterise the effects of the experimental manipulations on the finger tribology, and then on perception, I recorded contact forces and analysed them in relation to participant's performance.

Chapter Six summarises the current findings and discusses them in a broader context. It also highlights the limitations of the studies presented in this thesis and provides details of planned experiments (and future directions) to improve the current understanding of the link between the characteristics and response properties of the peripheral component of the tactile system and the sense of touch.

Chapter 2

Methods for the analysis of tactile sensation

2.1 Abstract

To address the research questions of this dissertation, several methods have been developed and used. These are psychophysical approaches to study the relationship between stimuli and tactile sensitivity, the development of a device to deliver passive and controlled tactile stimuli, the approach to measure skin properties, and the manufacturing of tactile stimuli having features size in the order of microns with high resolution.
This chapter outlines the details of these methods, their advantages and caveats.

2.2 Psychophysics

The term psychophysics was introduced by Gustav Theodor Fechner. In his book Elements of Psychophysics, Fechner (1860) described the principles of psychophysical measurements and elaborated the fundamental methods for the estimation of sensory thresholds. Over the years, these methods, and the theory behind them, have been developed to take into account the observer's decision process (i.e., Signal Detection Theory) but the general goal remains the same. The main idea behind psychophysics is to determine the relationship between the physical magnitude of the stimuli and the subjective experience, or the actual perceived magnitude. That is, the goal is to determine the relationship between the performance on a psychophysical task and some characteristic of the stimulus (Kingdom and Prins, 2016). This relationship is often well described by an ogive-shaped function (e.g., logistic) which relates increases in response accuracy (i.e., percentage of correct trials) as a function of increases in stimulus intensity, x (Figure 2.1). Stimulus intensity is used here as a shorthand for "intensity along a sensory continuum" which could include the amplitude of a tactile stimulus (e.g., height of a raised dot, frequency of vibration, length or orientation of a bar), the temporal delay between two stimuli, or their spatial arrangement.

In the next section, I will introduce the main psychometric function theories developed to interpret the relationship between stimulus intensity and behavioural performance and to estimate observer's sensitivity. The information presented is not exhaustive and there are other psychophysical methods and theories, or extensions thereof, that are used in tactile research and are not discussed here (for an in-depth overview of psychophysical methods and theories see Macmillan and Creelman, 2004, and Gescheider, 2013).

2.3 Psychometric function theories: high-threshold theory and signal detection theory

To determine how the stimulus property of interest *x* relates to the performance on a psychophysical task, the common approach for forced-choice methods is to fit the data with a psychometric function (PF), typically in the shape of an ogive (e.g., Logistic, Cumulative normal). The relationship between the performance and the stimulus intensity x can be represented by Ψ(x). However, researchers are often not directly interested in the measured performance but rather in the sensitivity of the underlying sensory mechanism (Kingdom and Prins, 2016). The relationship between the sensory mechanisms and *x* is denoted by F(x; α, β). Importantly, F(x) cannot be directly measured, and it needs to be inferred from Ψ(x). The general goal of psychometric curve fitting is to estimate the two parameters α and β which determine the position of the curve along the abscissa and the slope of the curve, respectively. Researcher are interested in these parameters as they are informative of properties of the observer such as their sensitivity to changes in sensory input and bias in their decision making.

Several theories have been developed over the years to interpret the relationship between F(x) and Ψ(x). The two most popular are high-threshold theory (HTT) and signal detection theory (SDT) and these are reviewed in the next section. In the following section, I introduce

the non-parametric Spearman-Kärber method that can be used without making any assumptions about the underlying distribution.

2.3.1 HTT and SDT

The main assumption of HTT is that the sensory mechanism will detect the stimulus if the amount of sensory evidence accumulated is sufficient, or if it exceeds an internal threshold. Otherwise, it will not. This amount can vary due to internal and external noise so that a stimulus with a specific stimulus intensity may or may not be detected on a given trial. Importantly, this threshold is assumed to be high enough so that it is never exceeded when the stimulus is absent. This implies that no false alarms are generated, and the observer is left to guess when the signal is below the internal threshold. The probability of a correct guess depends on the number of alternatives embedded in the experimental design, which is 1/*m* where *m* is the number of alternatives in a forced-choice task. This is referred to as γ and determines the lower asymptote of the psychometric curve (Figure 2.1).

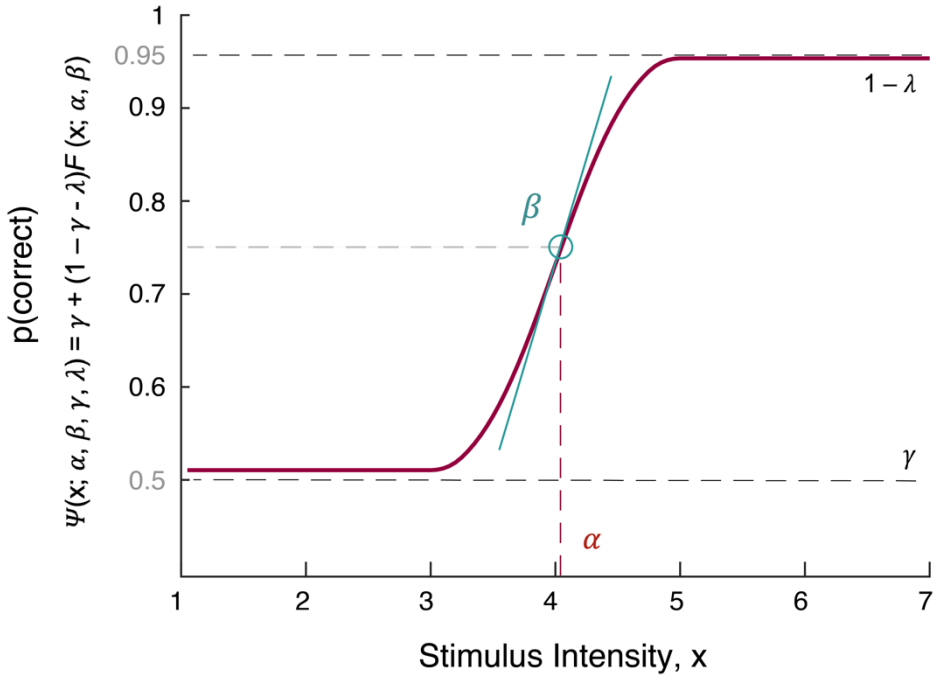

Figure 2.1. Illustrative example of psychometric curve, $\Psi(x; \alpha, \beta, \gamma, \lambda)$. F modelled as normal cumulative distribution. Function parameters are highlighted.

In the context of HTT, the two main parameters of the curve, α and β, are referred to as observer's threshold and sensitivity, respectively. α corresponds to *x* at which a given level of performance is achieved (e.g., 75% correct response rate). β is the rate of change in performance as a function of *x* (Figure 2.1). Another consideration regards the probability of an incorrect response regardless of stimulus intensity. This probability is named lapse rate, λ. Lapses are common in behavioural experiments and may occur when the observer fails to attend the stimuli or unintentionally presses the incorrect response button. The lapse rate is usually assumed to be a fixed low value (0.05) set by the researcher when fitting a PF. This value defines the upper asymptote of the psychometric curve as $1 - \lambda$ (Figure 2.1).

A second major psychophysical theory is signal detection theory. The main theoretical difference between HTT and SDT is that the latter does not assume an internal threshold at stimulus intensity *x*. The core idea behind SDT is that the sensory mechanisms will generate a graded signal for all stimulus intensities, including when x = 0, determined by the amount of sensory evidence accumulated. Similar to HTT, the degree of sensory evidence is not fixed for a given *x* but will vary due to internal and external noise. Crucially, this information is used to inform the observer's decision process which is based on the comparison between the magnitude of the sensory evidence accumulated in the intervals where the stimulus is present and in those where it is absent. Thus, the observer never guesses. Incorrect responses are generated when the sensory information in the noise interval (when the stimulus is absent) is greater than the signal in the interval where the stimulus is present. Although there are critical theoretical differences between HTT and SDT, and the assumptions of the HTT have been generally discredited (Nachmias, 1981; Swets, 1961), the equation:

$$\Psi(x; \alpha, \beta, \gamma, \lambda) = \gamma + (1 - \gamma - \lambda)F(x; \alpha, \beta)$$

where $F(x; \alpha, \beta)$ can be any sigmoidal function (e.g., Logistic, Weibull, etc)

that maps Ψ(x) to F(x) derived from HTT is consistent with the SDT framework (García-Pérez and Alcalá-Quintana, 2007). However, the interpretation of the function parameters is different. For example, SDT assumes that the observer never guesses and so γ should be interpreted as "the probability of correct or wrong answer on those trials where the signal and noise stimuli are the same" and not as guess rate. This probability is still 1/*m* which defines the lower asymptote of the psychometric curve as in HTT, where *m* is the number of alternatives in a forced-choice task. Interestingly, the impact of HTT is visible on the terminology in use. Researcher commonly and erroneously refer to α as "threshold" and γ as "guess rate", when in fact there should be no threshold or guessing. The correct terminology in the context of SDT would be "bias" for the parameter α and "noise" for β.

SDT has provided a new framework to analyse psychophysical data when the proportion of correct response is not by itself a valid measure of performance. SDT introduced the concept of d' as a measure of sensitivity or discriminability that is independent from any response bias and from the number of possible alternatives in forced-choice paradigms. Thus, d' is essential when the observer is biased towards one of the *m* alternatives in forced-choice paradigms or when one wants to compare the results from different experimental designs (e.g., 2-alternative forced-choice versus 3-alternative forced-choice).

2.3.2 Spearman-Kärber method

Psychometric function theories share the assumption that the underlying true distribution of responses has the shape of the cumulative normal distribution. This allows use of the data to estimate the parameters of the distribution and to find the relationship between stimulus intensity and observer's perception. However, there are situations in which this assumption is violated resulting in biased estimates of the curve parameters (e.g., skewed distribution), or in a poor fit.

The Spearman-Kärber method (e.g., Miller and Ulrich, 2001) is a non-parametric approach that can be used to estimate distribution parameters without making any assumption about the shape of the psychometric function except that the correct response rate is monotonically increasing with signal amplitude. Nonmonotonicity can result from a low number of trials and correction should be made to monotonize the distribution before using the Spearman-Kärber method. Ayer et al. (1955) suggested a solution to this issue. If the probability of a correct response on two or more successive stimulus levels are non-monotone (e.g., $p_i > p_{i+1}$), they can be substituted with the same value obtained by $(X_i + X_{i+1}) / (n_i + n_{i+1})$, where X is the number of correct responses for a given stimulus level and n is the total number of trials for that stimulus level.

Parameter estimation begins with subdividing the range of comparison stimuli into bins, ranging from c_{i-1} to c_i, for i = 1,...,k. Each bin is associated with response frequencies, f_i, assumed to be uniformly distributed within each associated bin, c_i. The probability densities of each bin are then estimated as $(f_i – f_{i-1}) / (c_i – c_{i-1})$, resulting in a histogram of probability densities which approximate the true distribution underlying the data (Miller and Ulrich, 2001). The most extreme stimulus values c_o and c_{k+1} must be determined so that the true values of f_0 and f_{k+1} correspond to 0 (or 0.5 in the case of a 2-alternative forced-choice) and 1, respectively. Often the psychometric function does not include these extremes because of the chosen range of stimulus intensities, lapses, or when the observer unintentionally presses the incorrect response button. In this case one can arbitrarily set stimulus values for c_o and c_{k+1} that are likely associated with $f_0 = 0$ (or 0.5) and $f_{k+1} = 1$. Importantly, the choice of these values can affect the parameters estimation and results should be interpreted carefully (Bausenhart et al., 2018).

From the raw moments of this distribution it is possible to derive estimates of mean, standard deviation, skewness, and kurtosis. Each *rth* raw moment can be calculated as (Sternberg, 1982):

$$m_r' = \frac{1}{r+1} \sum_{i=1}^{k+1} \frac{\left(f_i - f_{i-1}\right) \cdot \left(c_i^{r+1} - c_{i-1}^{r+1}\right)}{c_i - c_{i-1}}$$

The first raw moment corresponds to the arithmetic mean, or the location of the psychometric function. The standard deviation, or the spread of the underlying distribution, can be calculated as:

$$\sigma = \sqrt{m'_2 - (m'_1)^2}$$

This method is relatively efficient for estimating parameters thanks to the fact that it does not require an iterative search to do so, and it can be used in yes/no tasks (Miller and Ulrich, 2001), as well as 2-alternative force choice paradigms (Ulrich and Miler, 2004).

2.4 Psychophysical methods for sensory threshold estimation

In general, psychophysical experiments involve a large number of trials aimed at minimising the effects of experimental and behavioural noise. This can be a problem in the context of tactile perception where the stimuli are explored manually. Unconstrained tactile exploration may result in long interactions (Callier et al., 2015) when compared to the usually very brief auditory and visual stimuli used in psychophysics. Prolonged contact may result in changes of the actual properties of the stimuli such as temperature, as well as the properties of the finger, such as increased moisture following continuous occlusion which results in frictional changes (Pasumarty et al., 2011). In addition, free exploration does not allow careful control of contact dynamics, such as applied force, which might contribute to the behavioural outcome. Thus, experimental designs should be structured to minimise potential issues related to the stimuli presentation and exploration as well as ensuring a reasonable duration. Experimenters often prefer passive presentation to remove the effects of uncontrolled variation in movements reducing the achievable levels of performance. However, the risk is that the observer's engagement in the task, even the underlying processes recruited may

change fundamentally. As a result, findings obtained for passive stimulation may be of limited validity and not generalisable to the way people perceive tactile input (see *Passive exploration of tactile stimuli,* 2.2).

In the next three sections, I briefly summarise the three methods originally developed by Fechner to estimate sensory thresholds. These are the method of limits, the method of adjustment and the method of constant stimuli. In the fourth section I discuss adaptive procedures which are built on the method of limits.

2.4.1 Method of limits

This method involves the interleaved presentation of two series of stimuli with increasing (ascending method) and decreasing (descending method) magnitude along one dimension. The observer's task is to report when the stimulus seems to have changed with respect to the null or baseline stimulus (Kingdom and Prins, 2016). The experiment is stopped when the stimulus is perceived (ascending series) or when it stops being perceived (descending series). The threshold is computed by averaging the stimulus magnitudes corresponding to the transitions from a positive response (i.e., perceived) to a negative response (i.e., not perceived) or vice versa (Gescheider, 2013).

One advantage of this method is its short duration when compared to the method of constant stimuli. However, it is more prone to biases. In particular, habituation and expectation can affect the results. The former refers to the fact that participants may keep responding yes/no even when the stimulus is below/above the actual threshold. The latter refers to the participant's anticipation that the next stimulus will be perceivable, or not, based on the trial history.

2.4.2 Method of adjustment

In this method, also referred to as method of average error (Gescheider, 2013), participants are asked to self-adjust the level of the stimulus until it is detected, or until it matches the level of a reference stimulus. This procedure is repeated many times and the difference between the standard stimulus and the 'adjusted' stimulus is recorded. The threshold is calculated from the average error across all trials. As with the method of limits, the method of adjustment can generate response bias. However, this method can be useful to quickly determine the subjective sensitivity prior to the experiment, in order to adjust the intensity of the tactile stimuli in the actual experiment for each participant (Lederman et al., 1982).

2.4.3 Method of constant stimuli

This approach requires the experimenter to choose the stimulus set in advance and the range of stimuli should be defined to include the transition between not perceptible and perceptible. The range of stimulus intensity is chosen based on pilot testing, or previous research, and the number of intensity levels is usually 5 or 7. Each stimulus is presented a number of times (e.g., 10 or 20) in random order. This number is proportional to the precision of the estimates. However, there is a trade-off between the accuracy of the estimates and the length of the experiment. As suggested above, tactile exploration usually requires longer presentation time than, for example typical visual tasks. Having a large number of trials for each stimulus intensity might result in a very long session and promote lapses in participant's performance.

Ideally, the stimulus range should produce a response pattern (i.e., proportion of correct responses) that spans from chance to 100% correct. Responses are gathered with forced-choice methods in which the participant is required to choose between 2 or more alternatives for stimuli presented either simultaneously or in consecutive order. Generally, the choice can be in the form of yes/no, left/right, first/second when the task is to detect or discriminate a

target stimulus (or which interval contains the target) or rougher/smoother, harder/softer when the task is to judge a target stimulus against a standard.

The forced choice method is one of the most popular methods for estimating sensory thresholds or sensitivity and for good reasons. The data generated provide more reliable estimates of the threshold and the slope compared to other methods, such as the adaptive methods (Simpson, 1988). In addition, randomising the intensity of the stimulus allows reduction of possible biases due to habituation and expectation. The drawbacks are the high number of trials due to the fact that stimuli far below or above the perceivable range need to be included to better describe the psychometric curve, and the possibility of choosing a stimulus range that fails to include the threshold for some participants for whom the experiment was too easy or too difficult.

2.4.4 Adaptive procedure

The selection of the intensity range for the method of constant stimuli may result in a set of stimuli that does not allow estimation of the sensory threshold correctly or may result in very long testing sessions. To avoid these issues, adaptive procedures can provide a viable way to increase the efficiency of the testing procedure defined as the number of trials to reach a reliable parameter estimate that minimises its variance (Taylor and Creelman, 1967).

The major advantage of adaptive procedures is that the data points are sampled mainly around the parameter of interest. Although there are several approaches to doing this (for a review see Leek, 2001), the general idea is to adjust the intensity of the stimulus based on the response history. Usually, the first stimulus is presented at a very high, or very low intensity, in case of detection paradigm, or far below/above the intensity of the standard stimulus for discrimination. Then, the difficulty is increased or decreased based on whether the response to previous trials was correct or wrong. In one of the more common designs called the 1-Up-N-Down staircase, the task becomes more difficult when N-correct

responses are achieved in a row and becomes easier after a single wrong answer (Figure 2.2).

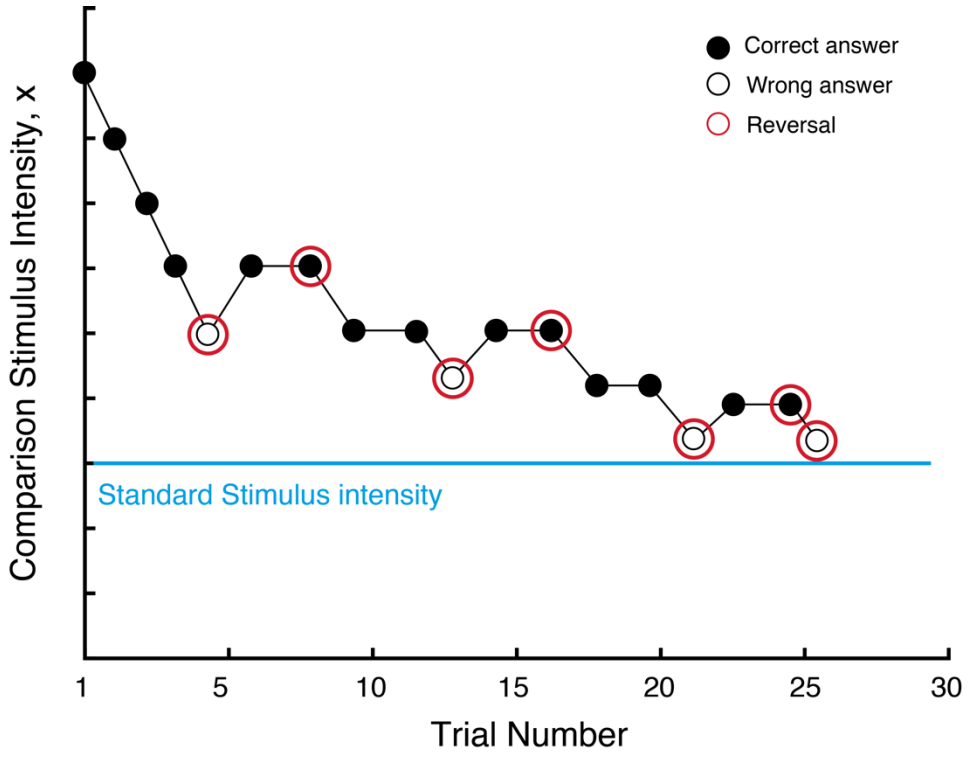

Figure 2.2. Schematic plot of data obtained with 1-Up-2-Down staircase procedure for a discrimination task between standard and comparison stimulus. Stimulus intensity is adjusted according to the response to previous trials. Task difficulty is increased following two correct answers and decreased following a single wrong answer. At the beginning of the experiment an intensity far from the standard stimulus (i.e., easy to discriminate), is chosen which then decreases with every correct answer to reduce testing time. Also, the magnitude of the intensity change may be set larger in the beginning of the testing session. Threshold is estimated by averaging the intensity of the comparison stimulus, x, at the last n reversals (e.g., 6).

The change in direction of stimulus intensity is called a reversal and the threshold can be estimated by averaging the stimulus values corresponding to the last few reversals (e.g., 6). This approach allows targeting of different threshold levels. The 1-up-2-Down procedure will converge towards the 70%, the 1-up-3-Down targets the 79%, and the 1-Up-4-Down 84% of correct responses (Karmali et al., 2016).

As with the method of limits, adaptive procedures provide a quick way to measure tactile sensitivity in those contexts where time constraints are present as in clinical settings, or where there is concern that the participant will fatigue and start to produce unreliable data.

2.5 Controlled Presentation of Tactile Stimuli

Tactile exploration of experimental stimuli is highly variable in terms of the specific exploratory patterns employed when sensing the object. For example, we can slide our finger at different speeds to judge the roughness of a surface or press with more or less force to determine the coarse spatial configuration of the surface. The specific exploratory parameters, and in general the skin-object interaction, affect the way skin deforms and mechanoreceptors are activated as described in Chapter 1. Interestingly, some tactile features are perceived consistently regardless of the exploratory parameters. For example, perceptual constancy is achieved for roughness perception across different scanning speeds and contact forces (Lederman and Taylor, 1972) as long as proprioceptive feedback is available as shown by Yoshioka et al. (2011). On the other hand, changing the contact parameters may result in a different perceptual outcome. For example, as noted in the previous chapter, Yokota et al. (2020) found in 2-point discrimination, indentation speeds of 5 mm/s and 10 mm/s resulted in better performance compared to slower (1 mm/s) and faster (20 mm/s) indentations.

Accordingly, careful considerations should be made in preparation of the experimental design and the selection of stimulus parameters. Furthermore, given the impact of mechanical aspects of stimulus presentation, it is important to control the contact dynamics and a robotic system affords this possibility. In the experiment presented in Chapter 4, I used a robotic system capable of delivering repeatable stimuli. The system (Figure 2.3) employs: i) a three-degree-of freedom robot arm, the Force Dimension Delta 3; ii) a six-channel force-torque sensor (Nano17, ATI Industrial Automation); iii) a stepper motor controlled with a microcontroller (Arduino Uno). The control of the robotic arm and the force-torque sensor is

achieved with a software framework, Golem, developed by Zito and collaborators (Zito, 2016; Zito et al., 2019). The framework allows accurate control and planning of the robotic arm motions as well as the processing of the force-torque sensor data.

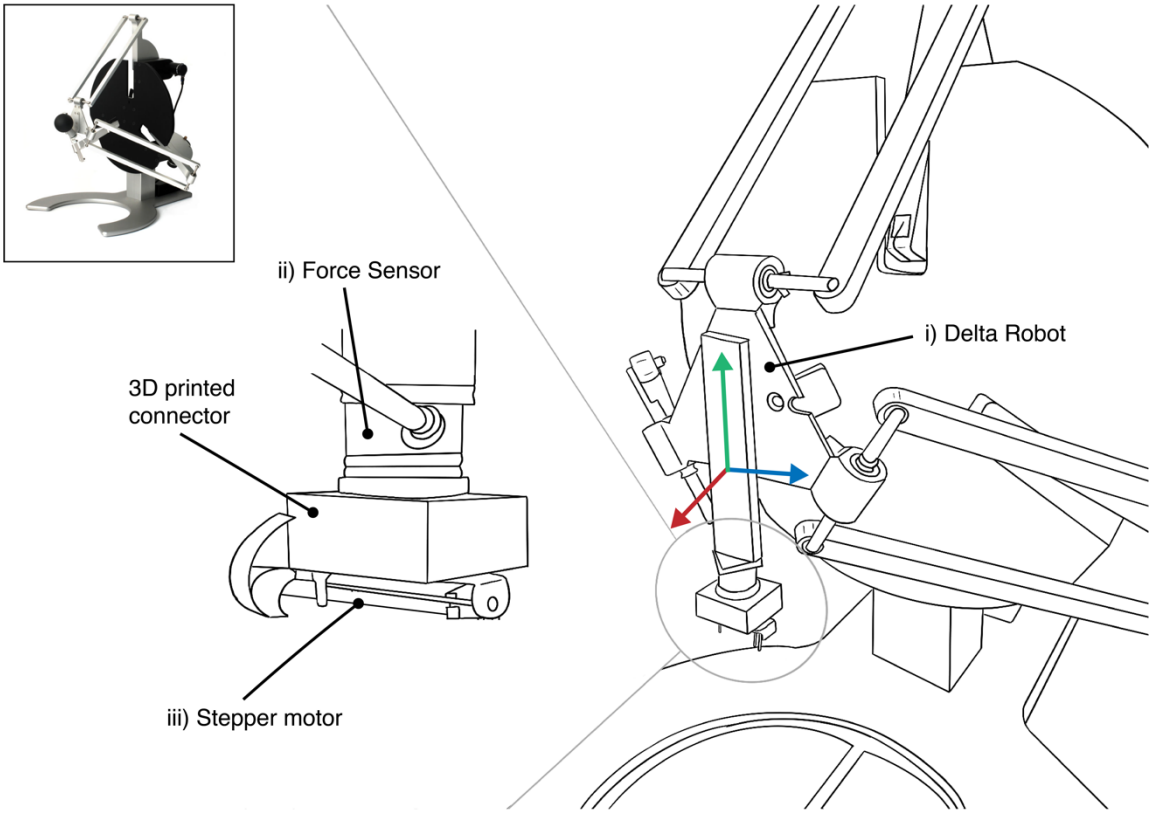

Figure 2.3. Line drawing of the Delta 3 system used to deliver controlled stimuli: i) Delta 3 with three degree-of-freedom highlighted by the colored arrows; ii) six degree-of-freedom force-torque sensor; iii) stepper motor connected to force-torque sensor through a custom-made 3D printed part. Top left image shows a real picture of Force Dimension Delta 3.

Having the possibility of controlling the robot along three dimensions allows the programming of several trajectories relevant in the context of tactile perception. For example, the robotic end effector can move laterally to reach a specified position above the subject's finger held in a fixed position, and then move down orthogonally to make controlled static contact with the skin. It also allows sliding after contact with the finger and then moving tangentially with controlled normal force and speed. A six-channel force-torque sensor attached to the front plate provides information on the contact onset/offset and it is used to

control the applied load. Importantly, the sensor needs to be calibrated to account for gravity and the marginal effect of acceleration on the force sensor readings. It is also possible to set the duration of the contact and the interval between two stimuli presented in the same trial, although the manipulation of these parameters may be limited by hardware constraints, such as the speed at which the robot can be moved.

When controlled presentation of tactile stimuli is not possible, it is important to record the stimulus presentation parameters (whether passive presented by experimenter or explored actively by the participant) and then condition the analysis on trials using regression or sorting (e.g., by similar indentation properties).

2.6 Skin measurements

Research on low-level tactile perception, such as the evaluation of spatial acuity, should take account of the skin's mechanical properties and possible interactions with the experimental stimuli. Skin is a highly complex medium with anisotropic behaviour and viscoelastic properties. In addition, these properties are highly variable across individuals depending on sex, gender, occupation, etc. Given such individual differences, it is interesting to relate subject-specific finger characteristics to the behavioural outcome to fully understand the neurophysiological and cognitive mechanisms underlying tactile perception.

There are several techniques to evaluate the skin mechanical properties in a non-invasive manner including magnetic resonance and ultrasound elastography, indentation, torsion, ballistometry and suction measurements. A commonly used technique in dermatology and cosmetics research is the suction method, which applies a negative pressure on the skin through a probe with a specific opening size and measures the resulting deformation over time. An example of a commercial suction device is the Cutometer (Courage & Khazaka), which offers a quick and easy way to measure different aspects of the skin response. It allows visualisation of the skin deformation in two ways: pressure-elevation curve and

elevation-time curve (Figure 2.2). The former shows pressure as a function of skin deformation. The latter represents skin deformation as a function of time.

From the temporal evolution of the skin deformation, it is possible to estimate absolute and relative parameters related to the viscoelastic response of the skin. Absolute parameters include immediate distension (Ue), delayed distension (Uv), immediate retraction (Ur), and final distension (Uf). Ue represents the initial elastic response while Uv shows the viscoelastic part of the deformation. The relative parameters are Uv/Ue or the ratio between the viscoelastic and elastic response; Ur/Uf which is the biological elasticity, or the ability of the skin to return to its original position following deformation; Ur/Ue, the net elasticity without the viscous part; and Ua/Uf, the gross elasticity.

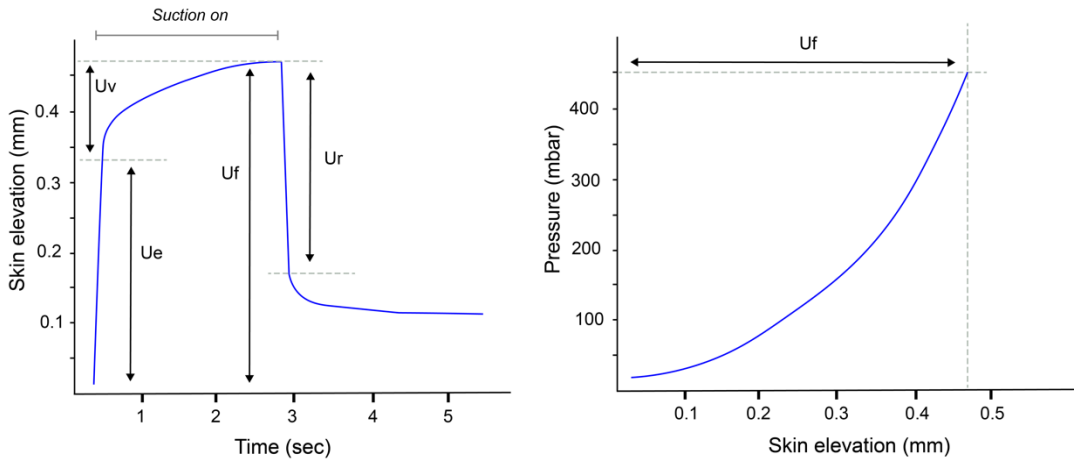

Figure 2.2. Left. Elevation-time curve. **Right.** Pressure-elevation curve.

Another important property of the skin is hydration which can have consequences on the specific interaction between the finger and the object. There are several tools used to measure it which differ in terms of measurement principle and usability. One of the most commonly used devices is the Corneometer (Courage & Khazaka). Based on capacitance measurement of the stratum corneum, it measures the change in the dielectric constant caused by skin hydration and allows quick assessment of the hydration of the outermost

layer of the skin. A major advantage of this device is that the measurement protocol is simple and does not require further processing of raw data.

Other techniques for measuring hydration include optical coherence tomography (Knüttel and Boehlau-Godau, 2000), high-frequency ultrasound (Gniadecka et al., 1996), and near-infrared spectroscopy (Martin, 1993) (for a comprehensive review of different techniques see Qassem and Kyriacou, 2019).

In the experiments presented in this thesis, the Cutometer was used to characterise the skin biological elasticity of our pool of participants. However, some considerations should be given to highlight the limitations of this approach. In particular, there are two main concerns regarding its reliability. The first is related to the measurement protocol which consists of holding the probe and manually making contact with the skin site. The contact force between the probe and the tissue can vary resulting in measurement uncertainty, especially for high loads (Bonaparte et al., 2013). For the same reason, relative movements between the experimenter and the participant can result in biased readings. Accordingly, the researcher should use the probe carefully, for example by ensuring that no movement happens during recordings, and consider limitations when analysing data and drawing conclusions. To improve the reliability of the measurements, the probe used for the Cutometer is spring loaded to try and maintain a more consistent contact force. Recently, another suction device has been developed to address this issue which features a light-weight design, called Nimble (Müller et al., 2018). The second concern is related to the fact that the absolute parameters of the Cutometer are a function of skin thickness. Thus, they should not be compared between participants or body area (Wilhelm et al., 1993), unless corrections for skin thickness can be made (Escoffier et al., 1989).

To conclude, it is worth mentioning that different methodologies can provide contradictory results due to the skin being non-homogenous with anisotropic behaviour, and It being

susceptible to effects of factors such as gender, body region, exposure to environmental factors, etc. For example, research on aging skin has shown lower stiffness (i.e., increased extensibility) in a stretching study (Berardesca et al., 1985) and more recently with an indentation test (Boyer et al., 2009), as well as higher stiffness (i.e., decreased extensibility) when torsion is used (Agache et al., 1980). A summary of the findings on aging skin in regard to its elastic properties is provided in Table 2.1.

Reference	Participants	Methodology	Results
Sanders, 1973	N = 38; 6 to 61 years old (male and female)	Torsion test (applied stress parallel to the skin) on the volar forearm	Extensibility increases with age
Agache et al., 1980	N = 138; 8 to 89 years old (male and female)	Torsion (applied stress parallel to the skin) dorsal side of the forearm	Extensibility decreases after 30 years
Escoffier et al., 1989	N = 123; 9 age-groups from 0-10 to > 90 years (male and female)	Torsion test (applied stress parallel to the skin) on the volar forearm	Extensibility constant up to the seventh decade, then decrease. Net elasticity (Ur/Ue) decreases with age.
Cua et al., 1990	N = 33; mean age young = 27 years, mean age elderly group = 74.9 years (male and female)	Suction test on 11 body regions (finger pad not included)	Extensibility increases with age. Biological elasticity (Ur/Uf) decreases with age
Dridillou et al., 2001	N = 206; 9 age-groups from 0-10 to > 90 years (male and female)	Suction test on the volar forearm	Extensibility and biological elasticity decrease with age
Boyer et al., 2009	N = 46; 3 age-groups: 18-30, 3-.50, 51-70 years	Suction and dynamic indentation on the forearm	Skin stiffness decreases with age (Indentation test). Biological elasticity decreases with age (suction test). Significant linear relationship between the two measures.
Amaied et al., 2015	Not reported	Air flow system test on the finger pad	Skin stiffness lower in elderly participants
Yang et al., 2018	N = 90; 3 age-groups: 3-19, 20-50, >50 years (male and female)	Ultrasound elastography on the finger pad	Lower stiffness in age-groups 3-19 and >50 years compared to 20-50 years age-group

Table 2.1. Summary of the findings on skin elastic properties with aging.

2.7 Manufacturing fine-textured tactile stimuli with high resolution

Research on tactile perception of surface texture has mainly focused on relatively coarse features at millimetre scale while less is known about how humans perceive fine-grained textures. This is due to the fact that experimental stimuli with features at sub-millimetre scale are difficult to reproduce, although some attempts have been put forward. For example, LaMotte and colleagues (LaMotte and Srinivasan, 1991; Johansson and LaMotte, 1983) used contact photolithography and etching to create surfaces featuring a single raised dot or a fine texture (ridges or dot patterns) to determine perceptual thresholds in humans. Notably, this technique allows creation of surface features at micron scale with an error of 0.1 μm. In brief, the process consists of exposing a photosensitive material to light to create a pattern (e.g., dot) by covering the material with a photomask resistant to light. The light will degrade only the exposed photosensitive material, leaving behind the desired shape.

Skedung et al. (2013) employed wrinkled surfaces with wavelengths from 0.27 μm to 90 μm. This type of pattern is created by mechanical in-plane compression of polyethylene thin sheets (or other materials, e.g., polydimethylsiloxane) that are eventually used as moulds to obtain the actual objects (Schweikart and Fery, 2009). However, these methods are slow and limited in the number of different geometries that can be reproduced. They also require expensive machinery and specialized personnel to operate it. On the other hand, recent advances in 3D printing technology hold promise for a relatively fast, cheap and easy way to create highly customizable objects.

There has been an increasing number of studies that have used 3D printing to create surfaces for psychological testing. Tymms et al. (2018) created high-resolution 3D textures to assess the contribution of different parameters to roughness perception (i.e., element spacing, shape, arrangements). The stimulus set consisted of surfaces featuring truncated cones with flat or rounded top with a diameter ranging from 0.1 to 0.5 mm, spaced from 0.6 to 1.4 mm, and aligned in an anisotropic or isotropic manner. Similarly, Drewing (2016)

investigated roughness judgments for low-amplitude (0.3 mm height) square-wave and 1D or 2D sine-wave 3D printed gratings.

The current state-of-the art desktop machinery (i.e., 3D printer available on the market for general users) offering the highest resolution exploit photosensitive resin to build objects by incrementally curing layers of resin and in general terms is referred to as VAT polymerization. This process can be achieved in several ways and different 3D printing methods have been developed. The most commonly found are stereolithography (SLA), masked stereolithography (MSLA), digital light processing (DLP), and low force stereolithography (LFS).

One big limitation of current commercial 3D printers is that they do not allow the production of objects with high accuracy when the minimum feature size is less than 100 microns at relatively low cost. Another issue related to 3D printing and its use in research is the biocompatibility of the resin. Currently, few of the resins available assure the absence of biohazards, such as the presence of cytotoxic residuals, and require specific tests to assess the effectiveness of the curing process and to rule out any risk. To overcome the above-mentioned issues related to 3D printing, laser micro-machining represents a useful tool to create etched surfaces with a precision down to micrometres on safe materials such as stainless steel and polymethyl methacrylate (plexiglas).

In the following paragraphs, I provide an overview of different types of 3D printers and limitations of print quality and safety considerations. Then, I will describe the laser micro-machining process, used to manufacture the tactile stimuli for the experiment on microdot detection presented in Chapter 5.

2.7.1 Type of 3d printing

Stereolithography is one of the most common and affordable technology available on the market. It is the first patented 3D printing technology, invented by Chuck Hull in 1986 who

founded the company 3D Systems Inc. It uses an ultraviolet laser beam to cure (i.e., solidify) the resin contained in the vat in order to build individual layers of the 3D model one after the other. For each layer, the laser beam is directed to different spots on the X- and Y- axis to cover the desired area by using a moving galvanometer. Then, the cured resin is detached from the bottom of the vat, as the building platform moves upwards along the Z-axis. This process is similar to suction and is referred to as peeling step**.** Parts printed by SLA have smooth finish and can render features at sub-millimetre scale. However, resolution and print quality of every resin-based 3D printing method discussed here depends on many factors including the quality of the components of the specific printer (see Resolution and Print Quality section).

Digital light processing method is very similar to SLA but DLP uses a digital light projector to form a single image of each layer all at once. This is achieved by directing a UV light source to the building platform by an array of micro-mirrors through an LCD screen that can control how the light is projected. Similarly, the light source in masked stereolithography is an LED array that displays a single layer slice as a mask through an LCD screen. Accordingly, in both DLP and MSLA the projected image is made of square pixels and each layer is composed of voxels. One advantage of DLP and MSLA over SLA is the faster printing time as the light does not have to cover the desired area point by point.

Low-force stereolithography is the next generation of SLA technology. The main updates are a flexible tank and a different optics engine (Light Processing Unit, LPU). The flexible tank allows the forces exerted on parts to be reduced during the peeling step. In addition, it allows for lighter support structures that can be easily removed. This is achieved by a flexible film which bends gradually as the part is built. The LPU can direct the laser beam always perpendicular to the building platform with high precision thanks to a new system of a single galvanometer and two mirrors (fold and parabolic). As a result, the parts will be more accurate and repeatable.

2.7.2 Resolution and Print Quality

The above methods are powerful enough to create objects' features ranging from micron to millimetre scale. However, defining spatial resolution in 3D printing is not as straightforward as for 2D printing where resolution is defined in dot per inch and it is easy to understand. Instead, to understand spatial resolution in 3D space one needs to consider two different variables: the XY resolution (horizontal resolution) and the achievable layer thickness (Z- or vertical resolution). The former is affected by a combination of the laser spot size and the increments by which the laser beam can be controlled, or for MSLA and DLP, the LCD screen resolution. Importantly, the minimum feature size will never be lower than the laser spot size (or pixel size), which is around 100 microns for the commercially available 3D printers. The latter controls the thickness of each layer which is not directly related to the resolution of the printing. In fact, layer thickness must be chosen according to what one is trying to print, meaning that a smaller layer thickness does not always result in better prints. Thinner layers are associated with smoother transitions on diagonals, which leads many users to generalize and push Z resolution to the limits. At the same time, more layers mean more time and more susceptibility to artefacts and errors. Accordingly, if the model consists mostly of vertical and horizontal edges, with 90-degree angles and few diagonals, additional layers won't improve the print quality. However, it is useful to set the layer thickness to its minimum if the aim is to print very fine features and to orient the object on the building platform so as to build the smallest feature along the z-axis, although the chances of failure or errors increase. In addition, the orientation can affect the finishing or print quality by determining how slices are layered on top of each other with respect to the overall shape of the sample. For example, when printing a rectangular surface oriented horizontally to the building platform, the top surface will have a smoother finish while the layers will be visible on the side surface. The ideal orientation depends on what we are trying to print and printing time.

Another important aspect is the print slicing parameters such as individual layer curation time (e.g., hardening of the resin). Curation time is usually suggested by the manufacturer of the resin and different monomers and colours will require different curation times (see Resin section). The colour of the resin may also have an impact on resolution and print quality because different pigmentations are more or less penetrable by the light. This is particularly noticeable, when comparing regular resins with plant-based resin since the plant-based resin tends to be cloudy and opaque as opposed to clear and transparent. Slight differences can be noticed even when using a clear resin or dark colour. The placement of the object on the building platform is sometimes important too. For example, when printing with SLA if the object is placed on the side of the platform the laser beam will be projected diagonally and its efficacy is reduced compared to an orthogonal projection which occurs around the centre of the platform. The software itself can also affect print quality as some software packages will provide full control over the slicing process while others are more limited. Eventually, resolution is also affected by the quality of the optics and other components such as the trail that moves the building platform along the Z-axis, the resin, the overall stability of the machine (anti-vibration system) and so forth. Thus, testing is always suggested when using a 3D printer as the specifications reported by the manufacturing companies are only partially informative.

2.7.3 Resin

Nowadays, there is a variety of photosensitive resin formulations featuring different optical (e.g., clear, matte), mechanical (e.g., high tensile strength, flexible) and thermal properties (i.e., ceramic) that make resin-based 3D printing suitable for a wide range of purposes. As briefly mentioned above, M/SLA, DLP and LFS exploit photopolymerization of monomers and oligomers in a liquid state that when irradiated by a specific light wavelength form thermosets. In order for the reaction to happen, a photoinitiator is needed which usually features high molar extinction coefficients at short wavelength, i.e. ultraviolet ~ 400 nm. (Mondschein et al., 2017). Alternatively, photoinitiators use visible or near-infrared light. The

most common resin formulations contain (meth)acrylate monomer and oligomers (for a comprehensive review of photopolymerization techniques, mechanisms and resin composition see Bagher and Jin, 2019). While this class of chemicals present some advantages (e.g., mechanical strength when cured into polymers, long shelf life), they come with some limitations of which the most relevant is their poor biocompatibility. In fact, acrylate monomers and oligomers have been shown to be highly irritant or even cytotoxic (Andrews et al., 1986). Thus, when in direct contact with the human body, it is necessary to assure that they are fully converted into safe polymers. In addition, it is important that there is no leakage or presence of degradation on the printed part which would cause the exposure of harmful chemicals. Although some biocompatible formulations have been approved by the FDA and used for clinical applications (e.g., polycaprolactone, polylactic acid), their use is limited to dedicated printers and further investigation is needed to improve their diversity and applicability. Recently, several companies are producing bio-compatible resins which are used, for example, for dental implants. However, they still contain potentially harmful chemicals and still need to be tested to verify the rate of conversion and the presence of any uncured residual. This type of testing requires specific tools, such as Fourier Transform Infrared Spectroscopy.

2.7.4 Laser micro-machining

For a set of tactile stimuli to be of interest for research and clinical applications, there is a need for safety, high resolution, reliability, and relatively short production time. Laser macro-machining have all the characteristics to be preferred over other methods when the goal is to produce very fine-textured stimuli with micron precision. Laser micro-machining is an advanced subtractive machining process that uses a collimated, monochromatic and coherent laser light beam to remove portions of material substrate (Penchev, 2016). Material removal is possible thanks to the absorption of the high energy density laser beam into the workpiece. This interaction generates highly localised heating of the material which can melt, vaporise, or chemically change, and removed from the substrate (Slatineanu et al., 2010).

The machining process depends on the characteristic of the laser source (e.g. pulse duration) as well as of the material properties (e.g., thermal conductivity, thermal diffusivity) (Parandoush and Hossain, 2014). In fact, a distinction can be made between photothermal and photochemical processes. The former refers to the interaction between a laser with short pulse durations (nanoseconds and longer) and a material with thermalization time (material characteristic time for electrons and phonons to reach equilibrium) shorter than the pulse duration. As a result, the material is first melted and then is evaporated from liquid state (Yao et al., 2005). The latter involves a laser with ultrashort pulse durations (picoseconds to femtoseconds) and a material thermalization time longer than the pulse duration (Chichkov et al.,1996). This process allows the direct transition from solid phase to gaseous phase (i.e., phase explosion) without melting the material (Yao et al., 2005). Laser processing with short pulse can result in excessive heating over the surrounding material producing heat-affected zones, the formation of recast layer, and micro cracks (Figure 2.3a) (Parandoush and Hossain, 2014; Petkov 2011). Instead, the photochemical process has minimal heat transfer within the near region. As a result, the ablation process is more precise and clean with limited thermal damage and highly localised material removal (Bäuerle, 2000)(Figure 2.3b).

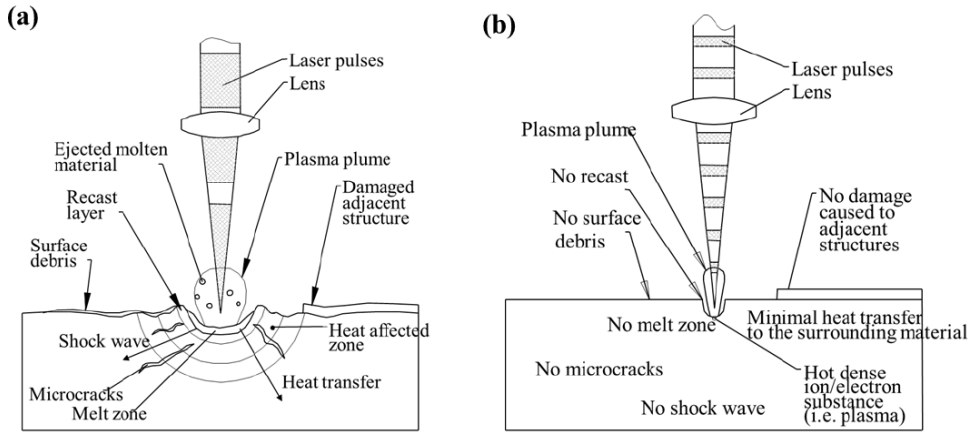

Figure 2.3. Schematic view of **a)** short-pulse, and **b)** ultrashort-pulse laser ablation. Image from Penchev, 2016, modified from Petkov, 2011.

2.7.5 Manufacturing of fine-textured stimuli

The production of fine-textured stimuli for the experiment presented in Chapter 5 required a series of attempts aimed at characterizing the photochemical process in terms of cost, production time, durability, accuracy and safety for the production of tactile stimuli for psychophysical research. The goal was to establish whether this was a viable approach and how it compared to 3D printing. The stimulus set was to be used in a 2-alternative forced-choice detection task carried out with the method of constant stimuli. The set consisted of square shaped plates (25 x 40 mm) featuring either a single dot in the centre of the surface or a matrix of dots (for more details see Chapter 5). The single dot is also square shaped with fixed side length of 300 µm and variable height from 2 to 12 µm, increasing in steps of 2 µm.

Before investing time and resources in more advanced tools, the first attempt to reproduce the stimuli was done with the 3D printer Anycubic Photon S which was available in our lab and it is easy use with low cost. However, several trials resulted in failed prints (i.e., flat surface with no dot) or produced surfaces with dot size not even close to the designed one (e.g., 60 µm height instead of 10 µm). In addition, it was almost impossible to obtain a completely flat surface top due to hardware issues which generated smooth but to some extent wavy surface top.

To further evaluate the potential of 3D printing when dealing with such fine features, a print sample was requested from Formlabs which manufactures printers with slightly better build quality and more capabilities than Anycubic Photon S. The model consisted of a series of dots with fixed diameter of 200 µm and variable height from 20 to 180 in steps of 20 µm, placed on the same surface. The step size was 10 times larger than for the desired samples. This was done to facilitate the printing task for a first attempt before moving to 2 µm increments. The samples were printed with Formlabs Form 3 and inspected with Alicona G4

InfiniteFocus Optical 3D Microscope at Advanced Manufacturing Centre, University of Birmingham. The measurements of 4 dots are shown in Figure 2.4.

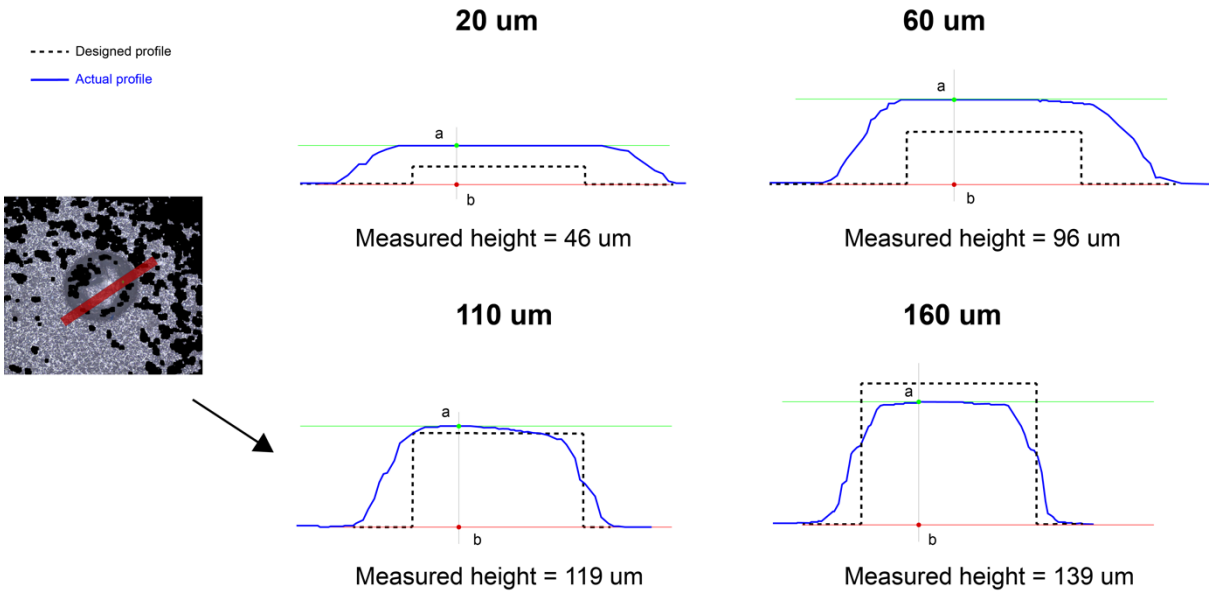

Figure 2.4. Left. Top view of a dot with 110 µm height and 200 µm diameter. **Right.** Black dotted lines show the designed dot profile. Blue traces show the profile of the 3D printed dot. The headers on the profile graph represent the height of each dot. The actual height is measured as the distance from point a (green) to b (red). Dots diamater is 200 µm.

When the goal is to create a feature with incremental steps of the order of a few microns, results showed that the accuracy (how close the measurement is to the true value being measured) is highly variable even across different features printed on the same object. Also, resolution is poor (the smallest change that can be printed) as the printer failed to render the small increasing in height in the original design. Furthermore, some of the dots on the same surface were absent or almost completely damaged.

With this in mind, the first attempt was made with flat polymethyl methacrylate surfaces (i.e., plexiglass). The samples were produced with photochemical process with a multi-axis laser micro machining platform. As mentioned above, the outcome of the ablation process depends on both the laser source and the material properties. In this case, plexiglass proved

not too be ideal as it was not possible to resolve features below 5 µm and in incremental steps smaller than 5 µm. Next, stainless steel plates were used to manufacture the surfaces which are slightly more expensive than plexiglass but offer more advantageous thermal properties. This time the production process was successful. It was possible to obtain very accurate features with submicron accuracy, 2 µm increments, and highly consistent results. Measurements of the 2 µm and 8 µm dots are shown in Figure 2.5. These measurements show that both the height and the side length are faithfully created on the stainless-steel samples with minimal roughness (0.1 µm) on the surrounding area.

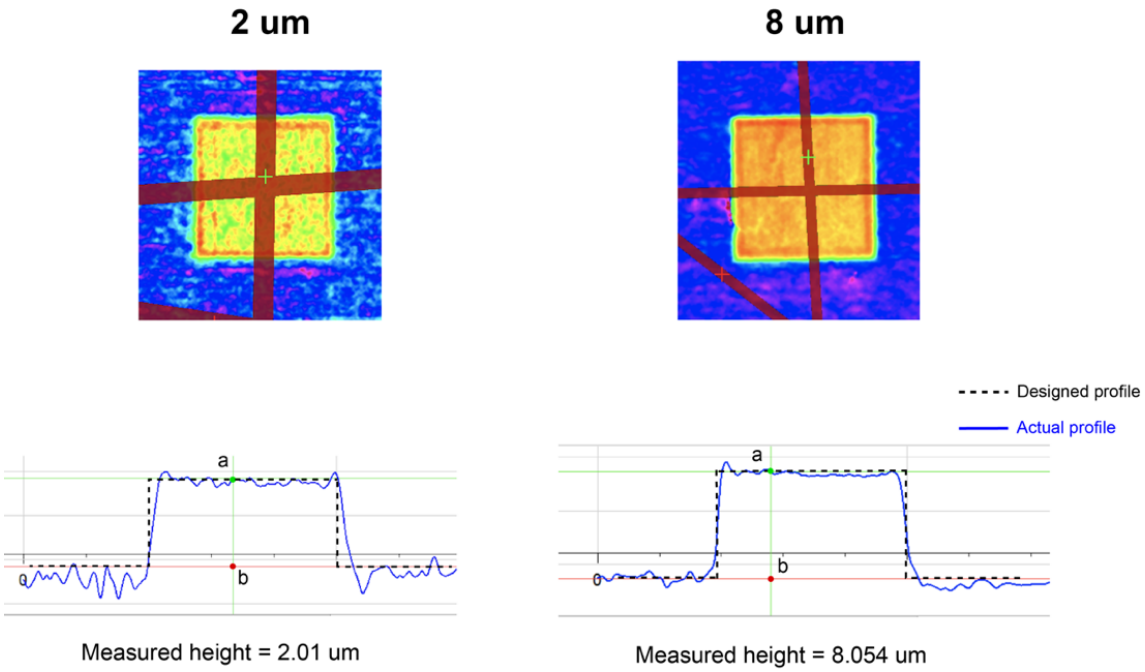

Figure 2.5. Top. Top view heatmap of a 2 µm dot (left) and 8 µm dot (right). **Bottom.** Profile of the same two dots. Black dotted line shows the profile of the designed dot. Blue traces showed the dot profile produced with ultrashort laser. The actual height is measured as the distance from point a (green) to b (red). Diameter is 300 µm.

As described, laser ablation is a subtractive process. Although this method can be time-consuming and expensive, the production time and cost for our set of stimuli was limited by the small sample and feature size. Time, and hence cost, depends on the size of the feature, the overall surface area, the material, and the desired accuracy. For example, the larger the feature (or area) to machine, the longer the time required and hence the higher the cost.

Chapter 3

Skin and Mechanoreceptor contribution to tactile input for perception: a review of simulation models

3.1 Abstract

We review four current computational models that simulate the response of mechanoreceptors in the glabrous skin to tactile stimulation. The aim is to inform researchers in psychology, sensorimotor science and robotics who may want to implement this type of quantitative model in their research. The modelling approach taken is relevant to understanding the interaction between skin response and neural activity and avoids some of the limitations of traditional measurement methods of tribology, for the skin, and neurophysiology, for tactile neurons. This, in turn, affords new ways of looking at the combined effects of skin properties on the activity of a population of tactile neurons, and allows examination of different forms of coding by tactile neurons. The models reviewed range over stimulus application to neuronal spiking response, and their evaluation covers existing data, and their implications for human tactile perception.

3.2 Introduction

The sense of touch is fundamental to our everyday life. It enables us to discriminate material properties, to identify objects, and to act on and interact with the external world, including affective and social exchange. It is the first sense to develop in the womb, at eight weeks embryos respond to tactile stimulation (Bradley and Mistretta, 1975), and works via the largest organ of the body, the skin. The lack of tactile perception undermines safe and successful interaction with the environment and to some extent impacts independent living as is the case with people affected by peripheral neuropathy (Cole, 2016).

Understanding how touch sensory signals arise at the periphery and are processed at the central level is important for research and applications in many fields, such as neuroprosthetics and neurorehabilitation, service robots to assist the elderly or robotics applied to industry, and haptic devices to assist surgery or visually impaired people. For example, implementing biomimetic sensory feedback based on the known properties of mechanoreceptors and the way in which tactile features are extracted (e.g., spike timing versus mean firing rate) has helped to improve the quality of neural prostheses in delivering tactile sensations (George et al., 2019).

There are several issues concerning research on the sense of touch ranging from the peripheral acquisition of sensory information to the transformation of this signal into a meaningful percept. Here, we consider two main questions related to the early stages of sensory processing. The first is how do the mechanical properties of the skin affect the activation of the receptive organs? The second is what are the relevant features of the signal sent to the central nervous system by the large number of mechanoreceptors that work together to create the sense of touch? The skin is composed of different layers that have complex, nonlinear mechanical properties. As a consequence, it is difficult to characterise and predict how skin stretches and deforms under different stimulations. Tactile signals are also complex and highly variable as they are generated by a large number of mechanoreceptors, hundreds in the finger pad alone, which respond to mechanical deformation in a variety of ways.

Skin behaviour and mechanoreceptor response are intertwined and should be concurrently addressed when investigating the sensory mechanisms of tactile perception. Yet, because of their complexity, it can be especially challenging to study them together, and various simplifying assumptions have been adopted to allow this.

A common approach to investigate the mechanics of the skin is to use video recordings, displacement sensors such as vibrometers, accelerometers, ultrasound scanners, or suction and indentation devices (Greenspoon et al., 2020; Delhaye et al., 2016; Diridollou et al., 2001), to measure the stresses and strains at the level of the skin. However, in practice, it is difficult to use these methods while recording the activity of a population of tactile neurons with microneurography, which allows direct observation of peripheral nerve activity in vivo with a high temporal resolution. These recordings are even more challenging when combined with the constraints of psychophysical testing.

Microneurography recordings are performed by inserting a very fine needle electrode through the skin and into an underlying nerve fibre to register the potential across the afferent fibre membrane. The experimenter has to place the electrodes by hand through a process of trial and error (typically listening to the electrical discharge pattern signifying the needle tip has penetrated a nerve fibre) which makes the task difficult and requires fine manual dexterity and takes a lot of time and patience. In addition, only a single fibre or a small number of fibres can be recorded at a time. Thus, recording the response of a high number of fibres would require multiple sessions on the same task.

Notwithstanding these limitations, animal and human studies have provided enough knowledge for the development of computational models to predict skin behaviour under specific circumstances (e.g., Pawluk and Howe, 1999) as well as to simulate the activity of tactile neurons in response to a variety of stimuli (e.g., Sripati et al., 2006b). Having functional quantitative models that can reproduce the behaviour of the skin and the response of tactile neurons is helping to overcome the limitations of classical recording techniques and address the two questions mentioned above. In particular, models allow the running of computer simulations that can be a viable way to study the relation between skin properties and neuron population response and to assess differences in tactile neural coding. However, it is important to keep in mind that this approach comes with limitations and still requires

validation with real data, especially when the simulations are performed on stimuli that differ from the ones used to build the original model.

The aim of this chapter is to inform researchers in psychology, sensorimotor science and robotics who seek to implement quantitative models in their research. The focus is: (i) to provide an overview of the available models of the transduction process from stimulus application to neuronal spiking response; (ii) to evaluate the models in relation to existing data; and (iii) to determine their applicability in relation to human tactile perception.
In the first Chapter, I outlined the most important properties of the glabrous skin of the finger and the skin behaviour that make modelling touch difficult (i.e., complex structure, viscoelastic properties). In the second and third section of Chapter 1, I summarised how the mechanoreceptors work and what is currently understood about the link between peripheral activity (i.e., skin and mechanoreceptors) and human tactile perception, to highlight why it is important to study the population activity of tactile fibres. The information presented in Chapter 1 was not intended to make an exhaustive description of the biological origins of the mechanical properties of the skin or of first-order tactile neurons, but rather to provide a summary of the most prominent requirements that a simulation model should consider. The goal was to highlight that the theoretical and computational requirements need to be carefully considered before undertaking a quantitative modelling effort.

In the remaining sections of this chapter, I present a selection of models that simulate the activity of tactile fibres and describe the advantages, limitations, and applications of each model. I do not consider models that address the processing of tactile information at the cerebral cortex or decision-making processes but rather the characteristics of the information that is sent to the brain.

3.3 Modelling the skin

The complexity and variability of skin biomechanics poses a challenge to the development of realistic and computationally efficient models. One way to capture the deformation and reproduce the behaviour of the skin is to employ continuum mechanics and finite element techniques. Continuum mechanical modelling involves a simplified characterisation of the skin to predict its deformation and simulate the mechanoreceptors response properties accurately. The skin is often assumed to be homogenous, isotropic and linearly elastic. On the other hand, finite element modelling aims to provide a more realistic description of the different layers of the skin having different thickness and mechanical properties (i.e., viscoelasticity) as well as being influenced by adjacent bones and nails. Typically, finite element modelling is focused more on quantifying the exact relationship between specific loads applied to the skin and the resulting deformation, and less on the neural response. However, finite element modelling can be demanding as it requires the construction of a 2D or 3D mesh of interacting elements each with a set of parameters based on actual measurements of the finger. Thus, choosing one approach or the other will depend on the scope of the model. For example, applications in neuroprosthetics and robotics require fast computations to be carried out in real-time. As such, a simplification of the skin mechanics may be advantageous in this kind of scenario.

A further issue is related to the transformation of the skin response into neural activity. A common approach is to derive the stresses and strains resulting from contact with a specific stimulus at the level of the receptor of interest and to transform them into spike trains and/or firing rates. The question is then which of the several measures of stress and strain that have been successfully tested is preferable, including strain energy density, maximum compressive stress and strain, von Mises stress, change in the receptor area, and combinations of these measures (Gerling et al., 2014; Sripati et al., 2006b; Dandekar et al., 2003; Connor and Johnson, 1992: Phillips and Johnson, 1981b). In addition, there are other mechanical cues that can be exploited by the peripheral nervous system. For example, the

strain fluctuation variation, defined as the mean absolute difference of the maximum compressive strain between pairs of sample points in the skin, has been recently used to successfully predict the perceptual roughness of 3D printed objects (Tymms et al., 2018). Similarly, the variations in tangential force generated when sliding the finger on a regular texture reflects the interaction between the skin and the geometry of the surface and has been used to predict the subjective estimation of the surface roughness (Smith et al., 2002), or the performance in a roughness discrimination task (Roberts et al., 2020).

3.4 Open questions

Several studies support the idea that coarse features (> 0.1- 0,2 mm) are mainly encoded in a spatial manner mediated by SA1 fibres, while fine feature (< 0.1- 0.2 mm) perception relies on the vibratory activity generated by stroking movement which mainly activates RA fibres (Blake et al., 1997; Hollins and Risner, 2000; Hollins et al., 2001). However, the prevalence of a spatial variation code over a temporal variation code might not be as evident in texture perception (e.g., Connor and Johnson, 1992), and the contribution of SA and RA may not be so distinct (Weber et al., 2013).

Furthermore, it is worth mentioning that although passive and active touch generate similar responses in the population of receptors and fibres, they differ in the extent to which the contact dynamics, and hence, the activation of tactile units can be controlled. Proprioceptive feedback and motor control allow exploratory patterns to be adjusted to optimise the sensory input (Kaim and Drewing, 2011), and can provide additional cues. For example, the applied force and speed alone can affect the signal in several ways. Higher force may result in greater contact area between the finger pad and the surface, generate stronger vibrations, and provide more reliable auditory cues when sliding.

Another question is how the state of the peripheral components affects the information encoded in the response of afferent fibres and transmitted to the central nervous system. As

mentioned previously, skin and mechanoreceptors properties depend on the individual characteristics such as occupation, gender, age. People differ in terms of skin stiffness due, for instance, to the thickness of stratum corneum. Or, the afferent density which is inversely related to the finger pad area and decreases with ageing.

In order to extend the understanding of the relationship between neural activation and tactile perception, it becomes clear that models should account for the presence of all fibre types at population level, their properties, and a realistic definition of the skin. Yet, modelling the four afferent types together or each one at a time as well as the extent to which the modelled skin reproduces the complexity of the real skin requires a different range of skills and resources. Thus, in order to improve efficiency, the amount of details that are included in a model should be related to the type of stimuli simulated (e.g. static indentation vs vibrations), type of skin contact (e.g. pressing vs sliding, active vs passive), and the task that is being analysed.

3.5 Models of tactile neurons

The challenge of recording the population activity of the afferent fibres in combination with psychophysical testing, makes it difficult to understand how the information is encoded from behavioural or neurophysiological data alone. In order to further characterize the low-level mechanisms of tactile perception and to extend the knowledge of the underlying cognitive mechanisms, it is necessary to study the response of the four afferent populations working together, and the effects of skin properties on the neural activation. In this regard, computational modelling holds promise to bridge the gap between neurophysiological, psychophysical and neuroimaging studies. Although a model is built on the limited data from neurophysiology, it can provide further insights into how tactile features are extracted at population level and link the neural activation to perception. It allows examination of the recorded data from a different perspective and to make and test predictions faster by simply changing one or more parameters (e.g., skin stiffness, number of receptors). However, this

approach carries the limitations embedded in the data on which it is built, such as the type of task used during the recordings.

3.5.1 Introduction to simulation models

The most common approach to build and validate a model is to rely on neurophysiological data recorded on monkeys. Although they are devoid of SA2 fibres, monkeys' tactile systems are very similar to the human tactile system (Parè at al. 2002). The literature on these types of studies provides more data when compared to those from recordings in humans but tends to be limited in the psychophysical tasks used.

Generally, a computational model aimed at simulating the activity of afferent fibres comprises three major components: the stimulus (i.e. which stimuli can be simulated and how), the skin mechanics (i.e. how the finger is shaped and how the skin moves leading to mechanical stimulation of the receptors, mostly involving a continuum mechanics approach or a Finite Element Method of analysis), and the neural model (i.e. afferent type and response properties, how the neural dynamics are generated, usually on an integrate and fire basis). These components may be characterised from an engineering and mathematical perspective in terms of a stimulus transformation into a neural response by means of a series of functions and equations (Figure 3.1).

The goal of a model is to tractably implement the properties of each afferent type so as to produce an output when stimulated by a specific input. This normally includes the four types of fibres, and their properties, such as receptive field characteristics (e.g., small and large, single and multiple hotspots), firing rates, spike timing, frequency tuning, adaptation, edge enhancement, and surround suppression. In addition, the model should have a realistic definition of the finger shape and its mechanics (i.e., 3D shape, presence of hard structure like bones and nails, viscoelasticity), with the possibility of simulating both static and sliding stimuli, and a faithful mechanotransduction process for a wide range of stimuli. In reality, all

of this is not possible yet, mainly because of the computational demand and the lack of knowledge in some domains such as skin mechanics. Accordingly, all the models available focus on one or few aspects, come with limitations, and are far from exhaustive.

The next few paragraphs outline the main characteristics of a few selected models presented in Gerling et al. (2014), Saal et al. (2017), Ouyang et al. (2020), and Hay and Pruszynski (2020). The selection of these models was based on the fact that each successfully reproduces a small set of properties (e.g. slow versus fast adapting units, viscoelasticity of the skin) and is more or less suited for specific tasks as illustrated in the Application section. The models differ from one other with respect to the stimuli that are simulated, how they resolve skin mechanics and which afferents are included, the response properties of the simulated fibres, and their applications (for a summary see Table 3.1).

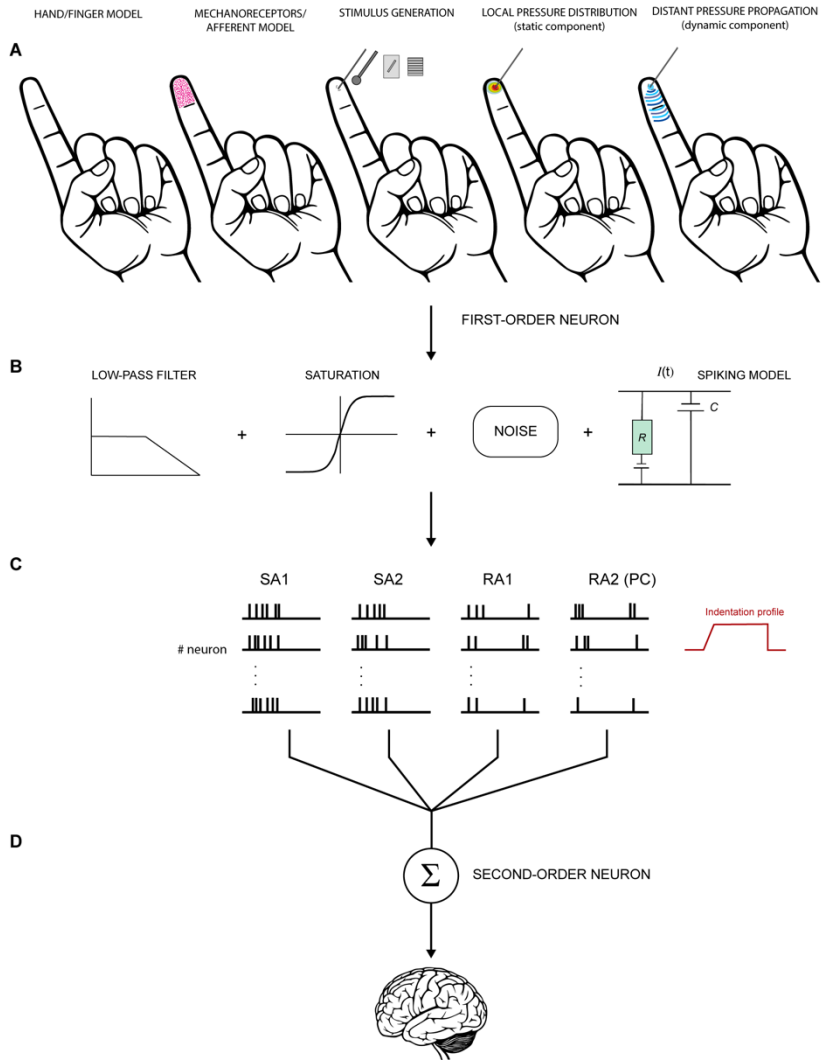

Figure 3.1. Schematic view of a hypothetical model to simulate the activity of tactile units of the hand. **A.** First step involves the definition of the hand/finger model (shape, geometry, mechanics), the depth and density of receptors/fibres, and the stimulus generation. Then, these factors are used to compute local and distant pressure distribution and derive the stresses acting at the receptors' depth. **B.** The mechanical output is fed into a neural model to generate spiking responses. The signal can be transformed through a series of functions to resemble the biological properties of the neurons. For example, low-pass filter is often used to account for the fact the tactile units do not respond above certain frequencies. Saturation reproduces the tendency of the neurons to saturate at high intensities. Eventually, noise is introduced to account for the random occurrence of the spikes in some conditions. **C.** Spikes are generated for each receptor or each tactile unit (receptors and fibres together, first-order neurons). The activity of each receptor must be integrated to account for innervation branching observed in SA1 and RA1 but not in RA2 (PC) and SA2. **D.** Subsequently, the output of first-order neurons is combined at the level of second-order neurons for further processing before is transmitted upstream. The last step is often overlooked in this kind of models but is fundamental to understand the nature of the information that is sent to the brain.

3.5.2 Stimuli

Tactile inputs are of many different sorts as they depend on specific object characteristics, properties of the finger, and their interaction. Lederman and Klatzky (1987) identified two major classes of object properties: substance-related (i.e., roughness, slipperiness, hardness, weight) and structure-related properties (i.e., weight, volume, shape). In fact, real-world objects comprise a variety of these properties which, in combination with the different exploratory procedures that can be employed, generate a variety of possible tactile inputs. Accordingly, it would be difficult to replicate the full range of inputs that we deal with in real life, and researchers have to select the most relevant stimuli according to the scope of their model (Table 3.1).

Gerling et al. (2014) used cylinder, bar and sphere indenters of different but fixed size to validate their model of the finger and the resulting units' response. These inputs were always simulated to be statically indented and no vibratory stimuli were considered. Saal and colleagues (2017) tried to extend the set of virtual stimuli by defining the input for their model as a single cylindrical pin or a set of pins that indent the skin orthogonally with spatiotemporal variations. Each pin is independent from the others with regards to location and indentation depth. As a result, it is possible to approximate different shapes from a single dot of a desired diameter to gratings, textures, curved lines, or other spatial patterns. In addition, their model allows the manipulation of the dynamics of the indentation including static stimuli with controlled onset and offset (i.e., ramp-and-hold) and vibratory stimuli (e.g., sinusoidal, diharmonic, etc.). Similarly, Ouyang et al. (2020) defined their stimulus as a single or a set of probes, with fixed diameter, indented orthogonally into the skin. Here, the probes can have different heights (i.e., indentation depth) that can be combined to produce many different spatial configurations. Their approach also allows direct creation of tactile input from a visual image. It is sufficient to extract height information from a grayscale 2D image and input it to the model. Similar to Saal et al. (2017), this model can be used to simulate static and vibratory stimuli but not sliding contacts.

MODEL	Gerling et al. 2014	Saal et al., 2017	Ouyang et al., 2020	Hay and Pruszynski, 2020
DATA	Monkeys	Monkeys	Monkeys	Humans
AFFERENT POPULATION TYPE	SA1	SA1, RA1, RA2	SA1, RA1, RA2	RA1, second-order neurons
RECEPTIVE FIELD	Simple, no multiple hotspots	Simple, no multiple hotspots	Simple, no multiple hotspots	Complex with multiple hotspots
RESPONSE PROPERTIES	Firing rate Spike timing Response adaptation	Firing rate Spike timing Frequency tuning Response adaptation Edge enhancement	Firing rate Spike timing Frequency tuning Response adaptation Edge enhancement	Firing rate Spike timing Response adaptation Edge enhancement
MODELS OF SKIN MECHANICS	3D Finite Element Model resembling different layers and viscoelastic properties	Skin treated as a flat surface – continuum mechanics to derive deformation	Skin treated as a resistance network	No, skin is only represented by a grid as reference for receptors location
NEURAL DYNAMICS	Leaky Integrate and Fire	Leaky Integrate and Fire	Leaky Integrate and Fire	No
STIMULI	Static indentation of cylinders, bars, and spheres	Static spatiotemporal indentation of single pins that can be combined to form complex shapes	Static spatiotemporal indentation of single pins that can be combined to form complex shapes	Static indentation of edges and dots
APPLICATIONS	Predicting behavioural response from simulated neural response Assessing the effects of realistic skin properties (e.g. viscoelasticity) on the skin response with static indentation of cylinders, bars, spheres. Evaluating potential mechanisms of peripheral sensory processing at the level of first-order neurons	Predicting behavioural response from simulated neural response Assessing the effects of finger properties (e.g. skin elasticity, afferent density) on the neural population response to static and vibratory stimuli having a wide range of shapes Real-time generation of spike trains for robotics and neuroprosthetics Evaluating potential mechanisms of peripheral sensory processing at the level of first-order neurons	Predicting behavioural response from simulated neural response Simulating the neural population response to static and vibratory stimuli having a wide range of shapes Real-time generation of spike trains for robotics and neuroprosthetics Evaluating potential mechanisms of peripheral sensory processing at the level of first-order neurons	Predicting behavioural response from simulated neural response Assessing the role of complex receptive fields on the neural population response to statically indented edges and dots Evaluating potential mechanisms of peripheral sensory processing at the level of second-order neurons
CODE	n/a	bensmaialab.github.io/software/	github.com/ouyangqq	senselab.med.yale.edu/modeldb
DOCUMENTATION	n/a	Yes	Limited	Limited

Table 3.1. Summary table of the main features of selected models.

Hay and Pruzinsky (2020) built their model on neurophysiological data recorded in response to embossed dots and oriented bars sliding over the finger pad with specified velocity (Pruszynski and Johansson, 2014). The sliding movement was chosen to finely characterise the spatial layout of the recorded afferent's receptive field and to investigate how the distribution of highly sensitive zones within each receptive field affects the neural response.

3.5.3 Properties of the virtual skin

The implementation of skin mechanics and different types of afferents is subject to a trade-off between realism and computational efficiency. As a result, modelers have to make a choice about what elements to include and how to implement them (Table 3.1).

Gerling et al. (2014) used finite element modelling to create a 3D model of the human distal phalange consisting of about 276.000 elements and 232.000 nodes (Figure 3.2, left). They included the different layers of the skin and their properties such as viscoelasticity, but not anisotropy. Then, in order to derive the response of SA1 fibres, they used strain energy density as the input for their leaky integrate-and-fire neural model. This solution originated in the work of Phillips and Johnson (1981b) who found that SA1 firing rates closely correlate to maximum compressive strain and strain energy density generated in the skin. Subsequently, Sripati and colleagues (2006b) developed the model of Phillips and Johnson (1981b) by implementing the RA1 fibres and testing how well different measures of stresses and strains can predict the neural response. They showed that maximum compressive strain and stress, maximum deformative strain and stress, maximum tensile strain, and relative change in receptor area are all good candidates to drive the response of both RA1 and SA1 afferent fibres.

Although computationally demanding, the realistic 3D shape and a subject-specific definition of the finger of a finite element model can provide a good understanding of the relationship between skin properties, neural activity, and tactile perception. In fact, individual differences

in skin elasticity, finger size, and shape are likely to affect the skin mechanical response, the resulting contact area, pressure, friction, and mechanoreceptor activation. This is especially relevant in the presence of tangential loading, such as during object manipulation.

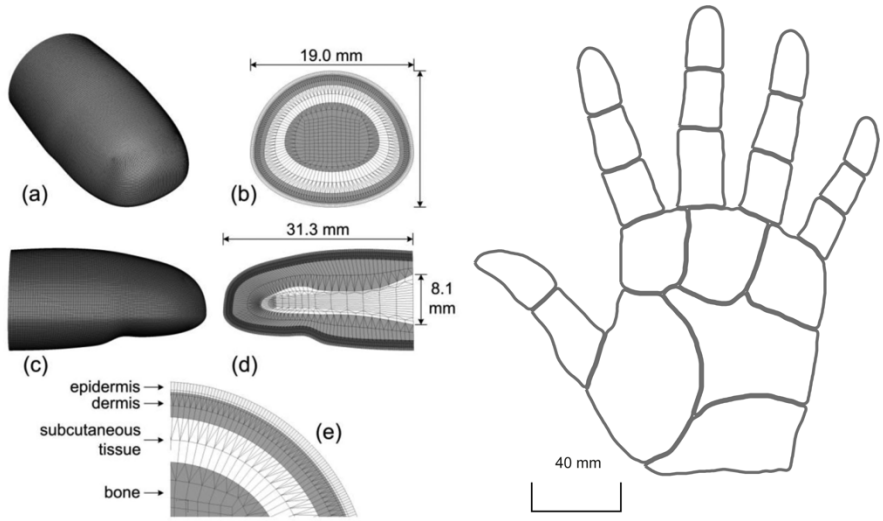

Figure 3.2. Left. 3D mesh of human distal phalange in Gerling et al. (2014). **(a)** overall mesh, **(b)** cross section of the mesh near the interconnect with the middle phalange, **(c – d)** longitudinal section for both the outer surface and inner mesh, and **(e)** four layers of microstructures. In (e) the epidermis is 0.471 mm thick (0.371 mm stratum corneum and 0.1 mm living epidermis) and the dermis is 1.153 mm thick. **Right.** 2D reconstruction of the virtual hand in Saal et al. (2017). Here, the skin is treated as a flat surface. Left figure republished with permission of The Institute of Electrical and Electronics Engineers,Incorporated (IEEE), from IEEE transactions on haptics, Gerling GJ et al, Vol 216, 2013; permission conveyed through Copyright Clearance Center, Inc.

In contrast to finite element models, continuum mechanics simplifies the analysis allowing the skin response to be resolved more efficiently (Figure 3.2, right). In this approach, the skin is considered as a flat surface with homogenous elasticity, with isotropic and elastic behaviour, and devoid of any underlying hard structures. This method allows fast computation and produces characteristic responses in both slowly and rapidly adapting fibres. With this approach, Saal et al. (2017) were able to simulate the activity of multiple SA1, RA1, and RA2 fibres. This model was focused on the whole hand and allows the manipulation of the location and density of the units. Saal et al. exploited continuum mechanics to derive the stresses at the depth of receptor that are then used as input to a

leaky integrate-and-fire neural model to generate trains of action potentials. The stresses are estimated for two different aspects of the indentation: a (quasi)static and a dynamic component. The former represents the resulting distribution of pressure over the skin close to the contact point, the latter accounts for the variations of pressure that propagates through the skin which cause the afferents to respond to vibrations far from the contact point.

Although simple, this approach is relatively cumbersome when dealing with complex stimuli because the resulting deformation is computed individually for each of the pins that form the stimulus. In order to increase the efficiency and reach real-time simulation of afferent response, Ouyang et al. (2020) went further to simplify the definition of the skin mechanics. The authors built the virtual skin as a resistance network made out of multiple connected nodes each representing a tactile unit. The units have fixed locations and are distributed only on the fingertip. Here, the assumption is that the actual pattern of indentation can be represented by a pattern of node voltages. The input currents for each node (i.e. afferent) are computed solely from the indentation depth of the stimulus image. The resulting voltages are processed by a two-channel filter in which low-pass and band pass filters mimic the static and dynamic aspect of the indentation. Then, an integrate and fire model is used to generate the action potentials. The advantage of this method is that the input currents are fast and easy to compute compared to the skin deformation and resulting stresses at receptor depth as in Saal et al.'s or Gerling et al.'s approaches. This makes this method more suitable for real-world applications such as neural prostheses and robotics where speed and accuracy may be crucial.

Importantly, all the skin models shown so far are limited to responses to stimuli indented orthogonally into the skin and do not include lateral sliding, the tangential forces, the friction between the skin and the stimulus nor the onset of slip which are relevant factors when simulating a sliding or a grasping movement. A further approach is to omit any consideration of skin mechanics. Obviously, this prevents understanding of the link between skin

properties and neural response, but it represents a viable solution to focus the efforts on the neural elements. For example, Hay and Pruszynski (2020) set up the virtual skin as a 12x12 mm grid uniquely designed for the arrangement of a set of modelled RA1 mechanoreceptors. They focused their modelling on an accurate definition of the relationship between mechanoreceptors, first-order neurons (i.e., afferent fibres), and second-order neurons (i.e., spinal cord and cuneate nucleus).

3.5.4 Tactile units of the virtual hand

Tactile neurons respond to stimuli in a specific manner. The response features include a receptive field which may be of varying size with single (SA2 and RA2) or multiple hotspots (SA1 and RA1), adaptation to constant stimuli, timing of individual action potentials, frequency tuning, and spatiotemporal sensitivity. For a model to be useful in aiding research about how tactile features are extracted, it is important that it is able to reproduce the response properties of interest (Table 3.1). For example, if we were to look at how vibratory stimuli are reflected in the spike timing, the model would have to simulate this feature accurately.

The finite element model of Gerling et al. (2014) focused on simulating a realistic skin response and the resulting activity of the population of simulated SA1 fibres. They showed that their model matches the proximal (< 0.5 mm) and distal (0.5 to 5 mm) skin deflection observed in the work of Srinivasan (1989) in humans. Here, the skin deflection is simulated in response to a 50 microns line load and a 3.17 mm cylinder with 1 mm indentation depth, consisting of a dynamic ramp and a static hold. Interestingly, the spike timing and firing rate during the ramp and static phases, which closely matched the data on monkeys recorded by Phillips and Johnson (1981a), showed a faithful representation of the SA1 adaptation rate to statically indented stimuli. Although, this model does not implement vibratory stimuli, it outperforms the model of Ouyang et al. (2020) in reproducing the trend and the intensity of the response to indented stimuli (Figure 3.3) during the static phase of indentation.

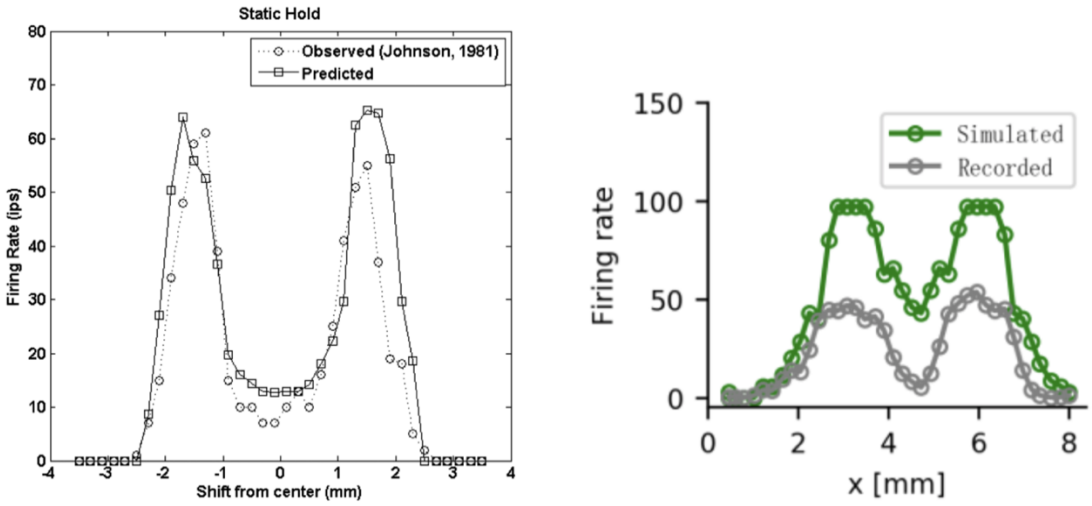

Figure 3.3. Firing rates during the static phase of the response to a 3 mm wide edge indented 1 mm. **Left.** Recorded (dotted line, Phillips and Johnson, 1981a) and predicted (solid line, Gerling et al., 2014) SA1 firing rates as a function of the location with respect to the stimulus. Note the x-axis is different in the two graphs. **Right.** Recorded (gray, Ouyang et al. 2020) and predicted (green, Phillips and Johnson, 1981a) SA1 firing rates as a function of the location with respect to the stimulus. Left image republished with permission of The Institute of Electrical and Electronics Engineers, Incorporated (IEEE), from IEEE transactions on haptics, Gerling GJ et al, Vol 216, 2013; permission conveyed through Copyright Clearance Center, Inc. Right image republished with permission of The Institute of Electrical and Electronics Engineers, Incorporated (IEEE), from IEEE transactions on biomedical engineering, Ouyang Q et al, pp556-567, 2020; permission conveyed through Copyright Clearance Center, Inc.

A more systematic attempt to reproduce the response properties of tactile neurons has been made by Saal et al. (2017). Their model was fitted to data recorded from rhesus macaques (Muniak et al., 2007) when presented with sinusoidal and bandpass noise vibrations (frequency range 1 to 1000 Hz) and tested with diharmonic stimuli of different frequency.

Four main points emerge from their simulation. First, the simulated firing rate and the spike timing correlated well with the actual data. The model can simulate the response of each afferent type to a static ramp-and-hold indentation that results in a different pattern of firing rate (i.e. adaptation, slow versus fast). In addition, the model is able to simulate the timing of spikes with a temporal precision from 3 to 8 millisecond for SA1 and RA1, and sub-millisecond precision for RA2. Although not entirely accurate, this range of values is

acceptable as it has been shown that the stimulus information (i.e., vibratory frequency, texture) can be best decoded when spike trains are compared to one another with a temporal resolution of around 5 milliseconds for RA1, 10 milliseconds for SA1, and 2 milliseconds for RA2 (Weber et al., 2013; Mackevicius et al., 2012). Second, the simulated receptive fields have similar features to the actual ones, including size, susceptibility to indentation depth (e.g., RA1 RFs increase with increasing indentation, but not SA1), and increased threshold amplitude with increasing distance from the RF centre. However, the innervation pattern, and hence, the receptive field shape does not match the real characteristics. In the human hand, SA1 and RA1 are connected to multiple receptor organs and each receptor is innervated by multiple fibres. Instead, the mapping between the modelled receptors and fibres is 1 to 1. Accordingly, one must keep in mind that the nature of these virtual receptive fields might affect the activation of the simulated tactile fibres. Third, tactile neurons are sensitive to different frequency ranges. Here, the simulated response of each class of fibre to sinusoidal vibration mirrors the actual sensitivity profile with respect to the minimum amplitude to elicit a single spike (i.e., absolute threshold), and the minimum amplitude to generate at least one spike per cycle (i.e. tuning threshold). Fourth, the simulated SA1 and RA1 fibres reflect the spatial layout of the applied stimulus which is achieved by a combination of edge enhancement and surround suppression, which is more evident for SA1.

The work of Ouyang et al. (2020) has a number of similarities with Saal et al. (2017). The authors used the same dataset as in Saal et al. (2017) for fitting their model (Muniak et al. 2007), and despite a different solution to reproduce the interaction between the skin and the stimulus, they obtained similar results with regards to the precision of the firing rate and spike timing when compared to real data. In particular, the simulated firing rates reproduce the trend observed when a probe with a diameter of 1 millimetre is indented with different frequencies and depths. The rate increases with depth as expected, although the number of spikes does not match the actual measurements perfectly. On the other hand, spike timing

has a temporal precision slightly higher than in Saal et al. (2017) for SA1 and RA2 (3 to 6 milliseconds versus 3 to 8 milliseconds), and similar for RA2. Using a resistance network to model the skin mechanics proves an interesting solution when dealing with receptive field characteristics. This model provides a viable way to characterise the receptive field size and the changes that occur in response to different indentation depths. Also, it can generate the characteristic edge enhancement and surround suppression, prominent in SA1 and less in RA1, observed in response to statically indented texture, form and shape.

It is worth noting that none of the above models included a realistic definition of the innervation branching that characterises SA1 and RA1 units. In this regard, Pruszynski et al. (2018) proposed a model that takes into account the complexity of the receptive field of first-order tactile neurons having multiple subfields. They compare this model to a second version in which all units had uniform sensitivity in the context of edge orientation discrimination. In both versions, the first-order neurons have the same receptive field size but are connected to either a single receptor that covers the entire area for the simple model or multiple receptors that form random subfields of sensitivity (Figure 3.4a). The activation of each first-order neuron in the two models can only be either 0 or 1 based on whether the virtual edge falls on the receptor area. As a result, the population response of complex receptive fields shows more variability (Figure 3.4b) and can better account for the behavioural results (Figure 3.4c).

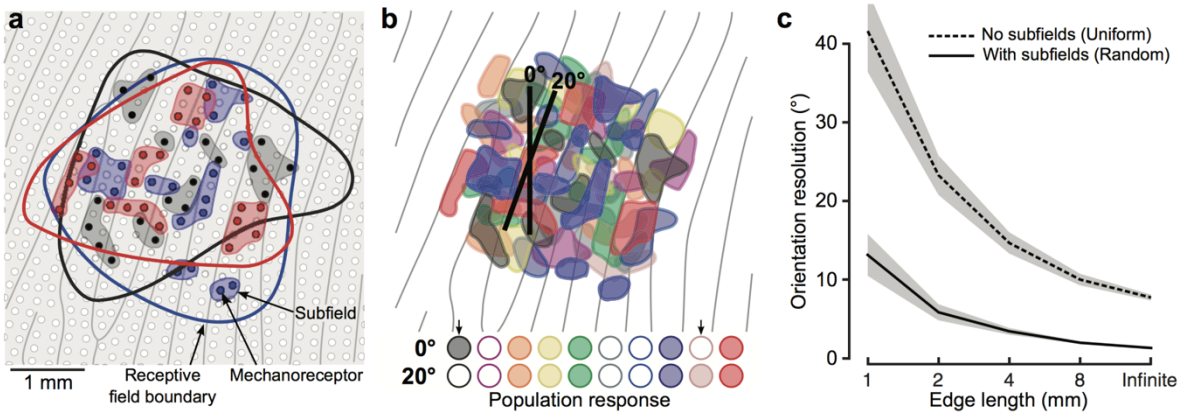

Figure 3.4. a. Schematic of skin patch with papillary ridges (grey lines) and mechanoreceptors (white and colored dots). Blue, black and red dots represent receptors innervated by one of three first-order tactile neurons. Colored contour represents first-order neurons receptive field, while shaded area behind the colored dot represents subfields. **b.** Color-coded subfields for 10 first-order tactile neurons. Representation of 10 first-order tactile neurons with overlapping receptive field and subfields (color-coded). First-order neurons are activated if the edge falls on one subfield. Here, the activation response is shown for 10 neurons and 2 edges of 2 mm with different orientation (0° and 20°). Colored circles are filled if the neuron is active and empty otherwise. **c.** Output of the two tested models (subfields vs uniform sensitivity). The lines indicate the mean and the shaded areas represent the 95% confidence interval. Image from Pruszynski et al., 2018, reproduced under the terms of a Creative Commons Attribution License

Recently, Hay and Pruszynski (2020) extended these findings with a model built on data from microneurography recordings in humans presented with embossed dots and bars of different orientations (Pruszynski and Johansson, 2014). Here, the individual RA1 afferents are designed to be connected to multiple mechanoreceptors arranged on a 12 x 12 mm grid and spaced 0.1 mm. The location and the weight (i.e., output) of the mechanoreceptors as well as the maximal firing rate of the first-order neuron were free parameters determined by a genetic algorithm. Locations were searched within the area of responsivity of the recorded neurons and different numbers of innervated mechanoreceptors were used for optimisation runs. The best fit model was obtained at around 20 mechanoreceptors, each having different weights representing the different degree of sensitivity within the same receptive field, in line with empirical findings (Nolano et al., 2003). Also, this model predicted the spike timing and firing rate with high accuracy in response to edges with different orientation. In addition, the

authors included a model for input integration at the level of second-order neurons and tested whether the output can discriminate between different oriented stimuli. First, they simulated the response of 330 RA1 units and convolved it with two post-synaptic waveforms having short or long decay representing two types of synapses, AMPA and NMDA respectively. Then, the weighted sum of the convolved outputs is computed to simulate the integration of the signal mediated by second-order neurons.

3.5.5 Applications

One of the main goals of modelling the activity of tactile afferent fibres is to clarify the nature of the inputs the central nervous system receives and to help explain how individual differences (e.g., skin properties in the ageing population) contribute to shape the tactile signals at early stages. In this review, the focus has been on how modelling can be employed to better understand the basic sensory mechanisms that underlie and enable tactile perception, and how it can be used in combination with behavioural experimentation. In this section we highlight the applicability of each selected model.

Finite element 2D and 3D models can be built with different level of detail, including macrostructures (e.g. finger shape, skin layers) as well as microstructures (e.g. fingerprint, dermal papillae, etc.). Although the main strength of finite element modelling is the realistic definition of the finger properties to accurately estimate the deformation of the skin and the stresses acting on the mechanoreceptors, it can certainly be used in combination with psychophysics to assess potential mechanisms of peripheral sensory processing. For example, Gerling et al. (2014) showed that the simulated firing rate in response to spherical indenters with different radii can predict the behavioural performance in a previous psychophysical experiment on curvature discrimination (i.e., Goodwin et al., 1991). Interestingly, they tested two potential encoding strategies based on first spike latencies and the firing rate in the dynamic and static hold, separately. These two coding schemes are Gradient Sum Method and Euclidean Distance Method (see Gerling et al. 2014 for details).

They found that the firing rate during the static phase of indentation produced a better fit to the behavioural data for both methods. Notwithstanding this finding, the first spike latencies and the firing rate in the dynamic phase were still good predictors suggesting that these two measures may carry information about the stimulus as early as the initial phase of the stimulation. However, this model does not include RA1 fibres, which have good spatial resolution, and may contribute to the encoding of stimulus information. Also, only static stimuli are included while vibrations and dynamic contacts are not.

Continuum mechanics models can provide further insights into the mechanisms underlying tactile perception and offer a more efficient way to simulate the spiking response. A good example of this is a study of Delhaye and colleagues (2019) on edge orientation. They used the model of Saal and colleagues (2017) to simulate the activity of the entire population of SA1 and RA1 fibres of the finger pad in response to indented edges with different orientation. They sought to determine how the information about the geometric feature (e.g. orientation) in contact with the skin can be extracted so efficiently as to enable rapid object manipulation. Although previous studies show that shape can be extracted from the spatial variation of the response of the tactile fibres (e.g., Phillips and Johnson, 1981a), the focus was on the mean firing rates over long time intervals and only for a few recorded afferents. As a result, it is not clear whether such a spatial code can be accurate and fast enough. Delhaye and colleagues (2019) used a classification approach to show that the spatial pattern of activation of simulated SA1 and RA1 fibres contains accurate information about edge orientation and that it can be decoded starting from the early phase of the indentation. In particular, they found that edge orientation can be decoded within 10 milliseconds, when most afferents have produced only a single spike, with an error of 5°, and within 50 milliseconds with an error of 1° to 3°. In addition, they found that taking spike timing into account did not improve performance. These results suggest that a spatial variation code is a better candidate for how peripheral neurons encode geometric features. This work has some limitations too. For example, the model output does not faithfully reproduce the trial-to-

trial variability observed in real neurons which may boost the orientation decoding performance. The authors tried to overcome this issue by jittering the stimulus position on each trial to resemble this variability. Most importantly, the model does not provide an accurate picture of neuronal receptive fields. Real SA1 and FA1 neurons have multiple hotspots of sensitivity, not implemented in Saal's model, which may affect how a stimulus activates the population of afferents.

The role of the complex structure of receptive fields is highlighted in the results of Hay and Pruszynski (2020). Their model of RA1 units shows that such complexity enables the discrimination of fine orientations (e.g. -1° vs +1°) under different level of stimulus noise and outperforms a similar model with uniform receptive fields. In addition, they implemented the population response of second-order neurons, connected to first-order neurons with both AMPA- and NMDA-like connections. Using different stimulus presentation time windows (from 5 ms to unlimited time) revealed that AMPA- and NMDA-like synapses are more robust to noise within short and long-time windows, respectively. These results suggest that AMPA-like connections may allow the computations that underlie fast object manipulations while NMDA-like connections may be involved in object discrimination. Overall, this work supports the possibility of peripheral sensory processing of geometric features as opposed to the traditional view of central processing (Bensmaia et al., 2008b) and can be used to assess similar questions related to shape or texture. Similar to other models, these results provide only a partial picture due to the lack of SA1 neurons which are known to have very fine spatial resolution. In addition, Hay and Pruszynski (2020) implemented sliding stimuli with no consideration of skin mechanics. The sliding movement produces a complex mechanical response that may result in a rearrangement of the receptive fields depending on scanning direction (Jarocka et al. 2021).

The model of Saal and colleagues has also been used to investigate the activity of RA2 units in contexts where vibrations are the only source for tactile information. Miller et al. (2018)

simulated the response of RA2 fibers to corroborate their neurophysiological findings in a tool sensing task. First, the authors showed that the primary somatosensory cortex can rapidly and efficiently access the information relative to where a rod, hold in the hand, is hit (close vs far). This is reflected by the repetition suppression effect on EEG traces between 44 and 140 ms. This finding suggests that mapping touch on an external tool is achieved similarly to somatosensation in terms of temporal dynamics and brain area involved. Then, they used the experimental acceleration recordings, collected by hitting the rod at close or far locations, as the signal to stimulate the virtual RA2. They showed that the simulated spiking patterns carry information about location as early as 20 ms, a time-course compatible with their neurophysiological findings.

An additional example of how Saal's et al model can be used to investigate the peripheral mechanism of tactile perception is presented in Chapter 4. The focus of this work is on the effects of skin properties and afferent density on the encoding of stimulus infomation and tactile sensitivity. It is known that these factors change with ageing (Yang et al., 2018, Garcia-Piqueras et al., 2019) which is also characterised by a deterioration of tactile spatial sensitivity. However, there is no evidence to support a link between these age-related anatomical and morphological changes and poorer performance. To address this question, Saal's model was used to simulate the neural activity for young and elderly group in response to 2-point discrimination task and estimate the perceptual performance based on the virtual response. This model allowed the two groups to be defined by setting lower Young's modulus and lower afferent density for the elderly and generate the virtual response to a single pin and two-pins at different separation levels for each group. The model output was then be used as input for an LDA classifier trained to discriminate between the single pin and the two-pins at each separation level, separately, and estimate the perceptual thresholds by fitting a logistic function to the classifier output.

In summary, modelling can be used to investigate the sensory mechanisms of tactile perception including potential coding strategies and the extent to which each afferent type contributes to the encoding of the stimulus, and to assess the effects of skin properties.

3.6 Discussion

Somatosensory processing begins at the periphery with the transformation of the mechanical stimulation into neural activity. The components involved in processing tactile signals enable the multifaceted aspects of touch, which include object and body perception, social and affective interaction, and they provide the basis for action control. Tactile information is transmitted from the skin to the upper spinal cord, and on to the thalamus, the primary and secondary somatosensory areas, which are the ending point of a hierarchical organisation with various overlapping networks involved in different functions (de Haan and Dijkerman, 2020). Simulating the activity of tactile neurons and estimating the information conveyed by their activation pattern under different circumstances is crucial to assess the mechanisms acting at lower levels of the somatosensory system and to predict the impact of different skin and peripheral neuron properties.

The state of the art of this type of models has enabled research to focus on the basic sensory mechanisms underlying tactile perception without the need for challenging microneurography recordings. Research in different fields can benefit from this approach as it can provide additional evidence to test experimental hypotheses. However, it is important to be aware of the limitations of the model being used and to interpret results with caution. Models are built on real data recorded from a limited number of tactile fibres when stimulated with specific stimuli (e.g., vibration, edge indentation, etc.), and only some of the properties of the skin and neurons can be currently reproduced. Although these limitations prevent complete reliance on modelling for hypothesis testing, this approach can provide useful insight into open questions that cannot still be addressed with microneurography. For

example, it can help address the effects of contact dynamics and the state of the peripheral sensory components on the information subserving tactile perception.

Interestingly, Saal et al.'s model allows some factors to be manipulated with ease. It is possible to change the density and distribution of the simulated fibres, the stiffness of the skin, the position of the indentation, or its depth on each trial. Having the possibility to manipulate these properties may help address questions related to the decay in spatial sensitivity observed in the elderly, a group which typically has stiffer skin and fewer mechanoreceptors, as described in the previous sections. One advantage of this model over the others is its ease of use. The available bundle of functions for MATLAB and Python, supported with usage examples, makes it accessible even to users that are not familiar with modelling (for code and documentation availability of all models see Table 3.1). Ouyang et al. (2020) and Hay and Pruszynski (2020) also provided the code for their model but only very limited documentation to help the users running the scripts. Gerling and colleagues (2014), instead, did not release their code but explained the framework in detail on their original publication.

Another limitation of all the models presented in this review is that none of them implement skin mechanics and neural dynamics in the presence of tangential loading. In fact, an important aspect of tactile perception is the dynamic behaviour of the skin during object manipulation and sliding movement in which normal and tangential forces are concurrently acting and covarying together. In these contexts, the friction between the finger and the surfaces well as the 3D geometry of the finger are extremely important and their absence is a relevant limitation of the models presented here. In particular, a realistic 3D definition of the finger geometry is crucial to understand its effects on the bulk and local deformation of the skin, and hence on resulting neural response.

Finally, the models discussed in this review cannot directly account for whether and how the information coming from peripheral neurons is used at higher level. For example, the fact

that two different stimuli are discriminable based on a spatial code does not imply that the brain can directly extract this information. Similarly, faster sliding movement on the same texture will produce higher frequency vibrations in the skin and higher firing rates in the peripheral neurons (Greenspoon et al., 2020) posing the problem of understanding how perceptual constancy is achieved for the same tactile stimulus under different conditions. In this regard, a recent study on intracortical recordings of rhesus macaques S1 area by Lieber and Bensmaia (2020) provides some insights. The authors showed that scanning the same texture at different speeds generates higher variability in the afferent fibers compared to the cortical neurons in S1. These results suggest that perceptual constancy for the same texture explored at different speed stem from the property of S1 neurons which can represent texture and speed in a relatively independent fashion.

Accordingly, further models are needed to establish how the cortical representations are formed, maintained, and reorganized (e.g., Detorakis and Rougier, 2012), and perceptual judgment are made by taking into account additional factors such as memory decay and perceptual noise (e.g., Metzger and Drewing, 2021).

Future work should be aimed at improving the understanding of the dynamic behaviour of the skin and in general of its mechanics as well as of the mechanotransduction process and the individual differences. The goal is to develop models that implement realistic 3D finger geometry, skin and mechanoreceptors properties, includes SA2 fibres, and is able to reproduce the dynamic aspect of touch. Improving the accuracy, generalizability and efficiency of these models will help research in other related fields such as cognitive neuroscience, psychology, and neurorehabilitation.

Chapter 4

Finger properties and afferent density in the deterioration of tactile spatial acuity with age

4.1 Abstract

Tactile sensitivity is affected by age, as shown by the deterioration of spatial acuity assessed with the 2-point discrimination task. This is thought to be partly due to age-related changes of the peripheral somatosensory system. In particular, in the elderly the density of mechanoreceptive afferents decreases with age and the skin tends to become drier, less elastic, and less stiff. To assess to what degree mechanoreceptor density, skin hydration, elasticity, and stiffness can account for the deterioration of tactile spatial sensitivity observed in the elderly, several approaches were combined including psychophysics, measurements of finger properties, modelling, and simulation of the response of first-order tactile neurons.

Psychophysics confirmed that the Elderly group has lower tactile acuity than the Young group. Correlation and commonality analysis showed that age was the most important factor in explaining decreases in behavioural performance. Biological elasticity, hydration and finger pad area were also involved. These results were consistent with the outcome of simulations showing that lower afferent density and lower Young's modulus (i.e., lower stiffness) negatively affected the tactile encoding of stimulus information. Simulations revealed that these changes resulted in a lower build-up of task-relevant stimulus information. Importantly, the reduction in discrimination performance with age in the simulation was less than the one observed in the psychophysical testing, indicating that there are additional peripheral as well as central factors responsible for age-related changes in tactile discrimination.

4.2 Introduction

Ageing is characterized by progressive impairments of vision, hearing, taste, and smell (Peelle, 2020). The sense of touch is no exception in this decline, as it is affected by age in several ways including decreasing pressure sensitivity (Bowden and McNutty, 2013), vibrotactile sensitivity (Gescheider et al., 1994) and spatial acuity. The latter has been extensively studied in a variety of tasks. Stevens and Cruz (1996) showed higher thresholds for elderly participants than their younger counterparts (mean age 77.5 vs 22.7 years) in three different tasks: two-point gap detection, line orientation and line length discrimination. Similarly, Goldreich and Kanics (2003) observed a linear decrease of sensitivity in a grating orientation discrimination task with age for both sighted and blind participants ranging from 19.7 to 71.6 years. Furthermore, age-related impairment of tactile spatial acuity has also been reported for the 2-point discrimination paradigm (Woodward, 1993; Bowden and McNutty, 2013). This deterioration seems to be more evident at the toes and fingers as shown by Stevens and Choo (1996) who tested the sensitivity of different body parts across participants between 8 and 87 years of age by means of the gap detection task.

There are several anatomical and morphological changes that affect the glabrous skin of the finger that might contribute to this decline in tactile performance. (a) With age, the skin tends to lose its biological elasticity – the ability to recover its original shape following deformation – and, for some individuals, it become less stiff – it shows an increased displacement for a given indentation force (Boyer et al., 2009). Yang et al. (2018) used real-time shear wave elastography to measure Young's modulus (YM) in participants from three different age groups. YM determines the stiffness of the initial indentation of the skin, i.e. when the force applied is small and the amount of indentation is *quasi* linearly-proportional to the force applied. Stiffness was lowest (low YM, which means softer skin) in participants aged 3-19 years (mean 25.2 kPa). Stiffness was highest in the age group of 20-50 years (mean 36.1 kPa) and then it decreased for and older participants >50 years old (mean 29.6 kPa), indicating a softening of the skin. (b) Ageing glabrous skin becomes drier, as observed by

Skedung et al. (2018) who showed that skin hydration was significantly lower in elderly compared to young participants, mean age (SD) 73 (4.5) vs 22 (1.5) years. (c) Mechanoafferents exhibit significant change with age. Myelination of axons deteriorate (Peters, 2002), size and morphology of neurons change, the number of some of the mechanoreceptors is reduced (Garcia-Piqueras et al., 2019). Garcia-Piqueras et al., (2019) employed immunohistochemistry and immunofluorescence to measure the number of Merkel, Meissner and Pacinian receptors on post-mortem samples in three age-groups (20-39, 40-59, 60-90 years). Results showed that the number of Merkel and Meissner cells was four to five times lower in the 60-90 year age-group when compared to the 20-39 year age-group. In addition, the size of receptive organs was reduced, and morphology compromised. However, no difference in terms of number, size, and morphology was observed for the Pacinian corpuscles between the three age groups. Importantly, the age-related effect of lower number of receptors might be compounded by increases in finger width (Dequeker and Vadakethala, 1979) resulting in reductions in receptor density with age.

These skin properties determine how a tactile stimulus activates the population of mechanoreceptors and are likely to affect the encoding of the sensory information that is transmitted downstream. However, there is little evidence that links these changes to the decline of tactile perception. The present study combines psychophysics of tactile discrimination (2-point threshold) and measurements of finger properties to investigate the degree to which peripheral factors (biological elasticity, hydration, finger pad area) might drive the deterioration of tactile spatial sensitivity observed in the elderly in the index finger.

To interpret the behavioural findings, the spiking activity of a population of type 1 slowly adapting fibres (SA1) and type 1 rapidly adapting fibres (RA1) was simulated in response to stimuli modelled on those employed in the behavioural experiment. The simulation was based on the model of Saal et al. (2017) which allows the creation of a flexible representation of afferent fibres (i.e., density, location), and implements a simplified basic

skin mechanics that can be manipulated in terms of YM to account for differences in skin properties.

The focus was on determining whether the spatial layout of our stimuli can be decoded based solely on the firing rate variations of the virtual neurons (i.e., rate coding) and how the decoding performance is affected by lower YM (Yang et al., 2018) and lower mechanoafferent density (Garcia-Piqueras et al., 2019). A spatial code was chosen as it has been previously shown to be a viable mechanism through which stimulus shape, or stimulus spatial layout, can be extracted under naturalistic condition in the presence of noise (e.g., shift in location of the indentation). Other potential mechanisms subserving the extraction of shape information, such as first spike latency (Johansson and Birznieks, 2004), are considered in the Discussion section.

Model simulations were run separately for Young and Elderly groups with the goal of predicting behavioral performance. The two virtual groups differed in terms of skin stiffness and mechanoreceptor density. The simulated neurophysiological data were also used to examine how stimulus information unfolds over time in the two age-groups and which afferent type might be more closely tuned to the fine spatial details of the stimulus employed.

4.3 Methods

4.3.1 Ethical approval

The study was approved by the STEM Ethical Committee at University of Birmingham (ERN_09-528AP24) and conformed to the standards set by the Declaration of Helsinki, apart from registration in a database. All participants gave their written informed consent before the beginning of the experiment. Both Young and Elderly participants were reimbursed for taking part in the experiment.

4.3.2 Participants

Fourteen young participants (9 females, age range 18-32 years, mean age (SD) = 23.85 (3.25) years) and fourteen elderly participants (6 female, age range 60-86 years, mean age (SD) = 72.36 (8.39) years) were recruited for this study. There were 13 right-handed participants in the Young group and 11 in the Elderly group. One of the authors (DD) was tested and the data included in the Young group. Eligibility criteria for both groups were normal or corrected-to-normal vision, independence in activities of daily living, absence of physical hand injury, absence of motor and sensory impairment due to arthritis or other causes (e.g., carpal tunnel syndrome, diabetes) based on self-report. Furthermore, participants confirmed they were not taking any medication with central nervous system effects.

Testing of participants involved first measuring skin elasticity, hydration, and fingertip size in this specific order, followed by psychophysical testing. All testing was carried out with the index finger of the right hand as previous studies showed no difference in sensitivity between hands for the 2-point discrimination task (e.g., Kalisch et al., 2009).

4.3.3 Psychophysical task and stimulation setup

Blindfolded participants were tested on a spatial 2-point discrimination task to determine sensitivity thresholds for each individual. The threshold was defined as the 2-point distance at which participants could respond correctly on 75% of trials and here referred to as the Just Noticeable Difference (JND). We used a 2IFC procedure (two intervals forced choice), in which a single flat-ended brass pin and a pair of brass pins were moved, first one then the other, vertically down onto the supported index finger pad in random order. The finger was positioned, finger pad facing up, at the beginning of the experiment so that the pins made contact with the central portion of the finger pad and did not touch the outer edges or the tip of the finger. The position was monitored throughout the experiment and re-adjusted when needed (e.g., after a break or in case of any small movement of the hand). Participants

were instructed to verbally report which interval contained the two-point stimulus (i.e., first or second) and to give their best guess when they were not sure about the answer. We tested 7 different separation levels for the pair of pins which differed between the two age-group based on a pilot study. For the Young group the separations were 0.1, 0.3, 0.6, 1, 1.3, 1.6, 2 mm. For the Elderly group the separations were 1, 1.5, 2, 2.5, 3, 3.5, 4 mm. Each separation distance was presented 10 times for a total of 70 trials. To control the contact area, we chose the single pin to have a diameter of 0.6 mm and each of the pins in the pair a diameter of 0.4 mm. The resulting contact area was 0.28 mm^2 for the single and 0.25 mm^2 for the two pins together. All the pins were levelled and inspected with microscope and micrometre to ensure they all had the same length.

The pins used as tactile stimuli were attached to a stepper motor to automatically and accurately control the separation distance through Arduino custom software. The single pin was fixed on one end of the stepper motor. Similarly, one pin of the pair was attached to the other end, and the other pin of the pair was attached to a screw-and-slider actuator (Figure 4.1).

While the participant's right index finger rested on a support (Figure 4.1), at each trial it was passively stimulated by either one or two pins. In order to control the timing, force and location of the application of the tactile stimulus, and especially the velocity of indentation which has been shown to affect discrimination in this kind of task (Yokota et al. 2020), we employed a custom-built apparatus based on a Force Dimension Delta 3 device. At each trial, the Delta lowered and raised the tactile stimulus on the participant's finger. The payload of the Delta comprised the single pin and two pins in the pair whose distance was controlled by mounting one of the pins on a slider so that its position could be adjustable by a stepper motor. The Delta delivered either the single or the two pins to the participant's finger by moving sideways and lowering on a random location of the participant's fingertip. The force applied by the pins on the finger was limited using an ATI Nano17 force sensor. The Delta

was programmed to move and indent the skin at 4 mm/s. The force sensor was calibrated to account for gravity and the marginal effect of acceleration on the force sensor readings. The target force level was set to 0.25 N. The resulting indentation depth ranged between 1 and 2.5 mm. The duration of each indentation was about 3 seconds from the initial contact to the release. The interval between the first and second stimulus was approximately 5 seconds due to hardware repositioning constraints and to allow the skin to fully recover between the first and second contact.

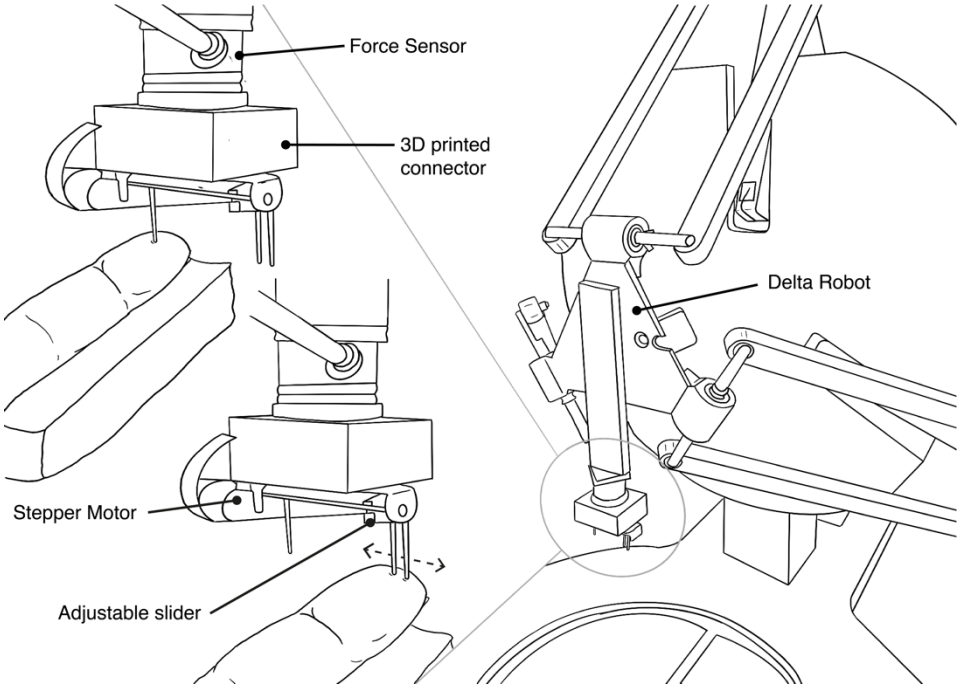

Figure 4.1. Line drawing of the experimental setup used for the passive presentation of stimuli for the 2-point discrimination task. **Right.** Force Dimension Delta 3 robot. **Left.** Details of the robotic arm. The drawing shows the force sensors attached to a custom-made 3D printed part used to mount the stepper motor on the force sensor. The distance between the two pins was controlled with an adjustable slider.

4.3.4 Finger measurements

Skin elasticity and hydration measurements were carried out with a Cutometer dual MPA 580 (Courage and Khazaka Electronic GmbH). Elasticity was measured with the aspiration probe which was placed in contact with the right index finger resting on the table. The probe

was set to apply a negative pressure of 450 mbar and to record the skin deformation during the aspiration and the release phase. Each measurement consisted of 3 suctions with on-time of 2 s, off-time of 5 s, for a total of 21 seconds. Biological elasticity (Ur/Uf) was computed by the Cutometer software as the ratio between the amount of immediate skin retraction (Ur) during the release phase and the maximum elongation of the skin during the aspiration phase (Uf).

The hydration level of the stratum corneum was measured with a Corneometer CM 825 (Courage and Khazaka Electronic GmbH) which expresses changes in water content in arbitrary units. We repeated the hydration measurement five times and computed the average value. Finger pad size was manually measured with a digital calliper having a resolution of 10 microns. We measured the length and width of the index finger pad and calculated its area (finger pad area = width x length). The length was measured by aligning one tip of the calliper with the joint connecting the distal phalanges with the intermediate phalanges, and the other tip of the calliper with the tip of the finger. The width was measured by aligning the two tips of the calliper on the left and right side of the finger pad.

4.3.5 Overview of TouchSim model

To simulate the response of the tactile fibres that innervate the tip of the index finger, an existing model (TouchSim, Saal et al. 2017) was used to generate our specific stimuli and manipulate the parameters characterising the two groups (see *Simulation of neurophysiological data*).

In the Saal et al. model (2017), several assumptions were made to create an efficient framework suitable for real-time applications. Saal et al. (2017) modelled the virtual skin with continuum mechanics to estimate the stresses acting on the receptors that serve as input to a leaky integrate-and-fire neural model. Thus, the skin is assumed to be flat, homogenous and elastic, with isotropic behaviour and does not include any hard structures (e.g., bone),

nor the fingerprints. We argue that these assumptions are not a major concern in the present work for the reasons outlined in the Discussion section.

Importantly, this model allows direct manipulation of several parameters, such as the density and distribution of the virtual mechanoafferents, the YM of the skin, the location and depth of the indentation. Being able to assess the effects of these parameters on the response of afferent population makes it possible to address open questions related to aging. In particular, we employed this model to understand whether lower YM and lower afferent density, as observed in the elderly population, have an impact on the very first stage of tactile perception.

In this work, the simulated population response in the Elderly group depends exclusively on the stiffness of the virtual skin and the number of mechanoreceptive afferents, while the effects of altered morphology and size of the receptors are not included. This approach was aimed at gauging the extent to which changes in skin properties such as lower YM and lower mechanoafferent density limit the amount of information in the spatial activation of mechanoafferent units, assuming no other difference in the response properties of first-order neurons between young and elderly.

4.3.6 Simulation of neurophysiological data

Virtual Young and Elderly groups were defined based on the YM of the virtual skin and the afferent density. We set the YM to 50 kPa for the Young group (default value in the original model) and to 35 kPa for the Elderly group. The choice of a lower value for the Elderly group was informed by the findings of Yang et al., (2018) and Boyer et al. (2009). In particular, Boyer et al. (2009) showed that biological elasticity measured with the Cutometer (Ur/Uf), and skin stiffness measured with an indentation device, both decrease with age and show a significant positive correlation. In the Saal et al. model, YM is used to define the stiffness of

the skin, so that lower values will determine a larger deformation for the same indenting force.

In both the virtual groups, the simulations included the response of SA1 and RA1 fibres which are known to have small receptive fields and are both potentially involved in fine spatial sensitivity. Type 2 rapidly adapting afferents (PC) were not included because their low density and large receptive fields make them not tuned to fine spatial details, as previously shown by Saal et al. 2017. Type 2 slowly adapting fibres (SA2) were not included because they are not available in the model.

Virtual afferents were arranged on a square grid covering an area 1 cm^2 around the centre of the virtual index fingertip. To make the afferent distribution more biologically relevant, x and y coordinates of each fibre were jittered by adding a random value taken from a normal distribution with mean 0 and standard deviation = afferent spacing x 1/5 (Figure 4.2). The afferent spacing was 1.1 mm for SA1 and 0.8 mm for RA1 units in the Young group; and 1.2 for SA1 and 1.8 for RA1 units in the elderly group. For the Young group, the modelled density of virtual afferents was in line with the observations of Johansson and Vallbo (1979) resulting in 121 SA1 units and 196 RA units. For the Elderly group, the number of SA1 and RA1 was 49 and 100, respectively (Figure 4.2). This choice was informed by the work of Garcia-Piqueras et al. (2019) who observed a progressive reduction of receptors in the finger pad across the lifespan.

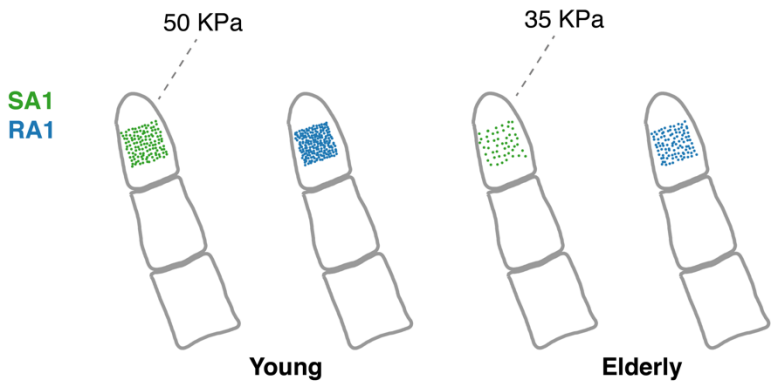

Figure 4.2. Virtual SA1 in green and RA1 in blue for Young (left) and Elderly (right) virtual groups modelled with TouchSim (Saal et al. 2017). The numbers at the top of the virtual finger show the modelled skin stiffness in KPa for each group.

The set of simulated stimuli applied to the fingertip reproduced the pins used in the behavioural experiment (i.e., single pin versus pair of pins) in terms of contact area and separation distance. Importantly, the set of separation distances was the same in the two simulations (i.e., from 0.1 to 2 mm for both). This was done to determine the impact of our manipulations over the same range of stimuli and to facilitate the comparison between Young and Elderly groups.

The virtual stimuli were orthogonally indented into the centre of the modelled index finger. To make the simulated conditions similar to the actual indentations, a trial-to-trial jittering of the position of the virtual stimulus was added to mimic small variations in the actual stimulus presentations due to small movements of the finger during the psychophysical experiment. Forty different positions were generated by applying a random value in the two directions obtained from a normal distribution with mean 0 and standard deviation 0.5 mm.

The indentation pattern was simulated as a ramp-and-hold function with a ramp-on phase of 100 ms, a sustained hold of 300 ms, and a ramp-off phase of 100 ms. Such timings result in a shorter duration than the one used in the human experiment, but it was necessary to not saturate the probability of a correct response in some of the conditions. We used 5

indentation depths ranging from 1 mm to 2.5 mm in steps of 0.375 mm. The number of simulations for each stimulus level was 200: 40 random locations x 5 indentation depths. This adds up to 1600 simulated indentations for each of the two groups (7 levels of separation + 1 single pin x 40 random locations x 5 indentation depths).

To systematically assess the contribution of skin elasticity and afferent density, the simulations were run four times for: i) the Young group; ii) the Elderly group having lower YM but same afferent density as the Young group; iii) the Elderly group having lower afferent density but same YM as the Young group; iv) the Elderly group with both lower afferent density and lower YM.

4.3.7 Analysis of behavioural data and finger measurements

The aim was to determine whether skin biological elasticity, hydration, and finger pad area are related to the performance obtained in the psychophysical task. First, the detection thresholds in the two groups were defined as the two-point distance at which the correct response rate was 75% (JNDs). To estimate this value, a Logistic function was fitted to individual data for each age group using MATLAB (Mathworks Inc.) and Palamedes Toolbox (version 1.10.4). Second, the presence of a significant difference was assessed between the two age-groups in terms of finger properties, and the presence of correlation between each of the measured finger properties and the discrimination thresholds. Due to the presence of multicollinearity, commonality analysis was employed to gain a better understanding of the contribution of biological elasticity, hydration, finger pad area and age, or of all the possible combinations of these factors, to the variance observed in the 2-point discrimination JNDs.

4.3.8 Analysis of simulated neurophysiological data

A classification approach was used to discriminate between the simulated response to single pin and two pins at each separation level, separately. An LDA classifier was built with a 10-fold cross-validation measure using MATLAB built-in function *fitcdisc* with pseudolinear

discrimination type to deal with predictors having zero within-class variance (e.g., first time-window when no spikes are elicited). Each classification was repeated 50 times to address the variability of the output due to the jittering of the stimulus location and the different indentation depths. The train-test split was randomised in each of the 50 iterations. The feature vector employed by the classifier consisted of the simulated spike count for each afferent. Due to the high dimensionality of the feature space, we used principal component analysis to transform the original data and selected the first n-components that accounted for 95% of the explained variance. Principal component analysis was performed on the training set first and the obtained n-principal component coefficients (i.e., loadings) were used to transform the data in the test set. This procedure was repeated for each train-test split.

Based on the classifier output, the aim was to determine: i) whether lower YM and lower afferent density negatively affects the encoding of stimulus information; ii) the accumulation of stimulus information throughout the indentation phase; iii) the contribution of the individual population of afferent fibres (SA1 and RA1) to the encoding of stimulus information, i.e. which afferent type is more closely tuned to fine spatial details. To allow direct comparison with behavioural data, estimates of the stimulus level at which the classifier accuracy rate was 75% (referred to as JND) were obtained by fitting a Logistic function to the accuracy values of the different classifications.

4.4 Results

4.4.1 Psychophysics

The estimated JNDs revealed higher sensitivity for the Young group (mean (SD) = 0.69 (0.33) mm) compared to the Elderly group (mean (SD) = 2.49 (0.58) mm). For one young participant, it was not possible to estimate the psychometric curve parameters as the performance was above 75% even at 0.1 mm. The JND for this participant was set to 0 mm. A two-tailed independent sample t-test showed a significant difference between the two age-

groups (t(26) = 10.081, p < .001; Cohen's d = 3.81) (Figure 4.3). The difference in the average JNDs between the Elderly and the Young group was 1.79 mm, 95% CI [1.43, 2.16].

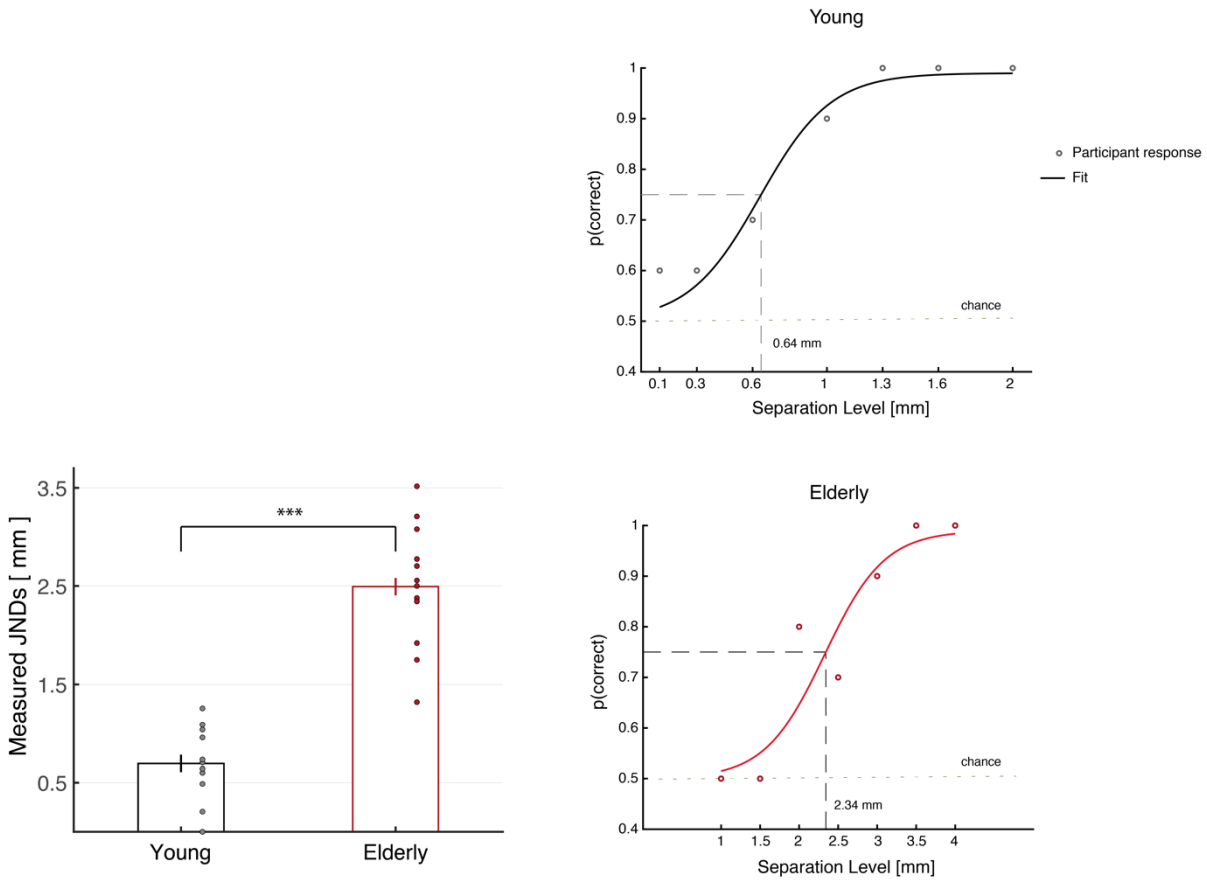

Figure 4.3. Left. Measured 2-point discrimination JNDs for Young, N = 14 (black), mean (SD) = 0.69 (0.33) mm, and Elderly, N = 14 (red), mean (SD) = 2.49 (0.58) mm. Young participants have significantly lower JNDs than the Elderly participants (p < .001). Error bars show SEM. **Right.** Example of psychometric curve fitted to the proportion of correct responses for young participant number 2 **(top)** and elderly participant number 11 **(bottom).** Dots shows the actual proportion of correct responses. Figures also show the estimated JNDs for the young (0.64 mm) and elderly participant (2.34 mm).

4.4.2 Finger measurements

Mean and standard deviation of biological elasticity, hydration, and finger pad area are shown in Table 4.1. Three two-tailed independent sample t-test showed that there was a statistically significant difference between Young and Elderly in biological elasticity ($t(26) = 2.985$, $p = .0061$; Cohen's $d = 1.13$), mean difference from Young to Elderly: 0.09, 95% CI [0.03, 0.15]; a significant difference in hydration level ($t(26) = 3.798$, $p = .00079$, Cohen's $d = 1.43$), mean difference from Young to Elderly: 30.08 a.u., 95% CI [13.80, 46.37]; and a significant difference in finger pad area ($t(26) = 2.712$, $p = .0117$; Cohen's $d = 1.025$), mean difference from Elderly to Young: 80.1 mm^2, 95% CI [19.38, 140.81].

	Young	**Elderly**
Biological elasticity [Ur/Uf] **	0.29 (0.10)	0.19 (0.05)
Hydration [a.u.] ***	76.9 (23.5)	46.8 (18.2)
Finger pad area [mm^2] **	392.9 (70.3)	473.0 (85.3)

Table 4.1. Summary table of finger measurements. ** $p < .01$, *** $p < .001$.

A summary of the correlation analysis between each pair of finger properties and age is shown in Figure 4.4. Results showed that all the three variables were significantly correlated with age. Specifically, a negative relationship was found between hydration and age (Pearson's r = -0.59, p = .00086, 95% CI [-0.79 -0.28]), a negative relationship between biological elasticity and age (Pearson's r = -0.46, p = .0129, 95% CI [-0.71 -0.11]), and a positive relationship between finger pad area and age (Pearson's r = 0.53, p = .0038, 95% CI [0.19 0.75]). In addition, biological elasticity was positively correlated with hydration (Pearson's r = 0.58, p = .0012, 95% CI [0.26 0.78]), hydration was negatively correlated with finger pad area (Pearson's r = - 0.38, p = .0467, 95% CI [-0.66 -0.007]). No significant correlation was found between biological elasticity and finger pad area (Pearson's r = -0.06, p = .74, 95% CI [-0.43 0.31]).

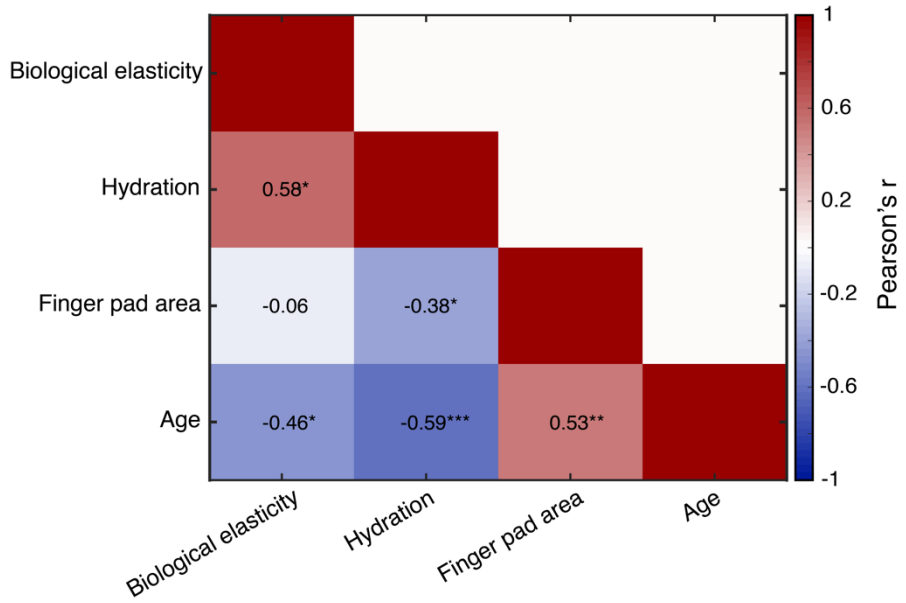

Figure 4.4. Matrix showing the correlation results between each pair of the measured finger properties and between finger properties and age of participants. * p < .05, ** p < .01, *** p < .001.

4.4.3 Influence of finger properties and age on behavioural task

Results of a correlation analysis performed between each of the measured finger properties and the estimated 2-point discrimination JNDs showed a significant relationship for every pair (Figure 4.5). In particular, there was a negative correlation between biological elasticity

and the JNDs (Pearson's r = -0.42, p = .02, 95% CI [-0.68 -0.06]), as well as between skin hydration and the JNDs (Pearson's r = -0.61, p = .0005, 95% CI [-0.80 -0.30]). A positive correlation was found between finger pad area and the JNDs (Pearson's r = 0.56, p = .002, 95% CI [0.24 0.77]). A significant correlation was also found between age and the JNDs (Pearson's r = 0.94, p < .001, 95% CI [0.87 0.97]).

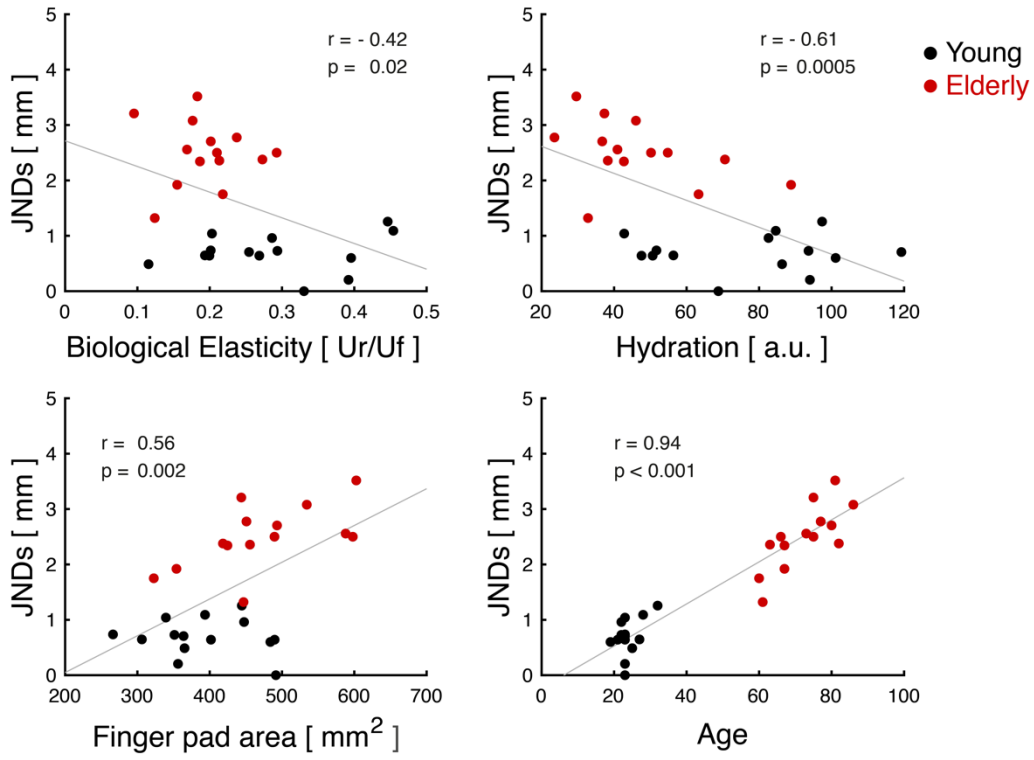

Figure 4.5. Scatter plots showing the correlation between the 2-point discrimination JNDs and each of the finger properties as well as age. Black dots represent values obtained from the participants in the Young group and red dots the ones from the Elderly group. Pearson's r and p-value for each correlation are shown in the respective quadrant.

A commonality analysis performed on the various measures (Table 4.2) showed that biological elasticity, hydration, finger pad area and age explained 89.8% of the variance (R^2) in the behavioural performance measured through the 2-point JND values. Examination of unique effects revealed that age was the best unique predictor of JNDs, accounted for 37.34% of the variance in the dependent variable. Finger pad area, hydration, and biological elasticity explained 0.35%, 0.33%, and 0.1% of the variance, respectively.

Although unique effects suggest that elasticity, hydration, and finger pad area are not strongly related to JNDs, the analysis of common effects provide a more complete picture. In particular, the ratio between total effects for each predictor (i.e., unique and total of common effects combined) and the overall variance explained in the behavioural performance was used to determine the amount of variance shared with regression effect by each independent variable. This calculation revealed that elasticity was involved with (0.1 + 17.79) / 89.8 = 19.9% of the explained variance, finger pad area was involved with (0.35 + 36.65) / 89.8 = 41%, hydration was involved with (0.33 + 31.25) / 89.8 = 35%, and age contributed (37.34 + 51.55) / 89.8 = 98.9%.

These results showed that biological elasticity, hydration and finger pad area shared a significant amount of variance with the regression effect despite the major contribution of age.

				Unique and Common effects (%)	Total of Common effects (%)
age				37.34	51.55
age	**hydration**			14.4	
age	**hydration**	**area**		13.7	
age		**area**	**elasticity**	12.4	
age		**area**		5.6	
age	**hydration**	**area**	**elasticity**	4.9	
age			**elasticity**	2.6	
		area		0.35	36.65
	hydration			0.33	31.25
	hydration	**area**		0.2	
	hydration		**elasticity**	0.2	
			elasticity	0.1	17.79
		area	**elasticity**	-0.1	
	hydration	**area**	**elasticity**	-0.1	
age	**hydration**		**elasticity**	-2.1	
Total variance explained (%)				89.8	

Table 4.2. Summary table of the commonality analysis results. Values in the coefficient column show the explained variance in the measured JNDs by each unique factor (unique effects, white) and all possible combinations of factors (common effects, shades of grey). Total of common effects column shows the total explained variance by all combinations of each factor with the others. % Total shows the proportion of the total variance explained in y by each factor and all possible combinations of factors. Unique and common effects are listed in decreasing order.

4.4.4 Simulated neurophysiological data

The spiking activity of SA1 and RA1 in response to the stimulus set used in the psychophysical task was simulated with three goals in mind: (1) determining whether and to what extent lower YM and lower afferent density affect the amount of information encoded in the afferents' response; (2) assessing how stimulus information accumulates over time for the Young group versus the Elderly group; and (3) determining which afferent type is more tuned to fine spatial details, again comparing Young and Elderly group. An example of the simulated spiking response of SA1 and RA1 fibres is shown in Figure 4.8b. As expected, the response pattern differs between the two types of fibres. SA1 showed a strong activity at the onset of the stimuli and some sustained response during the hold phase, while RA1 were active only during the onset and offset of the indentation.

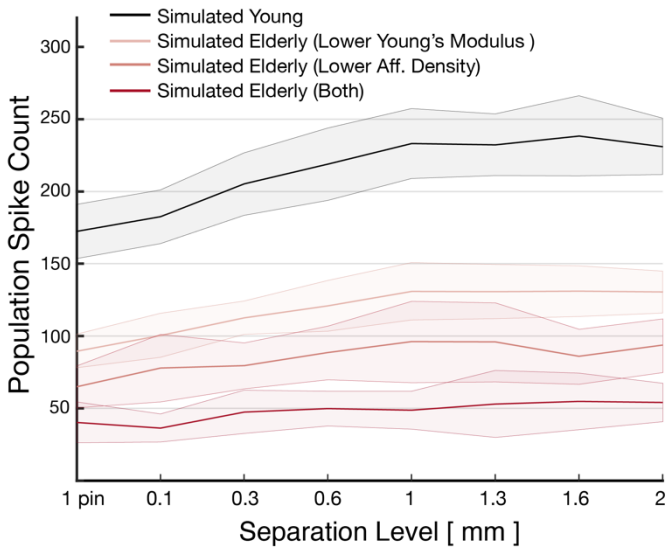

Figure 4.6. Population spike count for all the simulated groups at each stimulus level for 2.5 mm indentation depth collapsed across the 40 randomised contact points. Shaded area shows one standard deviation. The variability within the same stimulus level is mainly driven by the jittering of stimulus location.

Figure 4.6 shows the population spike count for each simulated group at each stimulus level, including the single pin, at a fixed indentation depth of 2.5 mm and collapsed across the randomised contact points. Increasing separation level between the 2-pins produced an

overall increase in spike count for all groups. However, the variability of the spike count across stimuli depended on the simulated group. For Young group, the number of spikes generated in response to the single pin is similar to the one obtained for the two-pins separated by 0.1 and 0.3 mm (i.e., black line and shaded area in Figure 4.6), while it differs substantially from the spike count in response to the two-pins separated by 1 mm or more. Instead, it can be noticed that for the Elderly group with both manipulations this is not the case and there is a great overlapping in terms of population spike count between all stimulus levels.

In brief, the highest variability was observed for the Young group, followed by the Elderly group with lower YM, the Elderly group with lower afferent density, and last the Elderly group with both manipulations.

With this in mind, the simulated response over the entire 500 ms stimulation window was used to generate the classification output for the simulated Young group and each of the three manipulations for the Elderly group to test (1). This analysis was performed by using the response of SA1 and RA1 together to discriminate between the single pin and two pins at each separation level, separately. Then, a logistic curve was fitted to the classifier accuracy results in order to estimate the simulated 2-point discrimination JNDs (75% correct response rate) for each virtual group. The mean (SD) estimated JNDs for the Young group was 0.87 (0.04) mm, the mean (SD) JNDs for the Elderly group having lower YM and same afferent density as the Young group was 0.99 (0.04) mm, the mean (SD) JNDs for the Elderly group having lower afferent density and same YM as the Young group was 1.25 (0.04) mm, and finally the mean (SD) JNDs for the Elderly group with both lower YM and lower afferent density was 1.35 (0.07) mm (Figure 4.7a). A one-way ANOVA was performed to compare the effect of our manipulations on the virtual JNDs.

Results showed that there was a statistically significant difference between at least two of the simulated JNDs ($F(3,196) = 1045.63$, $p < 0.001$; $\eta^2 = 0.94$). Tukey's HSD test for multiple

comparison revealed that the virtual JNDs were significantly smaller for the Young group than each of the three Elderly groups ($p < 0.001$). The estimated mean difference in JND between the Young group and the Elderly group with lower YM was 0.12 mm (95% CI [0.15, 0.10], Cohen's d = 3.11). The estimated mean difference in JND between the Young group and the Elderly group with lower afferent density was 0.38 mm (95% CI [0.41, 0.36], Cohen's d = 9.61). The estimated mean difference between the Young group and the Elderly group with both lower YM and lower afferent density was 0.48 mm (95% CI [0.51, 0.45], Cohen's d = 8.39). In addition, the JNDs for the Elderly group with both manipulations was significantly higher than the JNDs for the Elderly group with lower afferent density ($p < 0.001$, estimated mean difference of 0.10 mm, 95% CI [0.12 0.07), and the JNDs for the Elderly group with lower YM ($p < 0.001$, estimated mean difference 0.36 mm, 95% CI [0.38 0.33]). Finally, the JNDs for the Elderly group with lower afferent density were significantly higher than the JNDs for the Elderly group with lower YM ($p < 0.001$, estimated mean difference 0.26 mm, 95% CI [0.28 0.23]). These results showed an additive effect of each of our manipulations with a stronger contribution of afferent density.

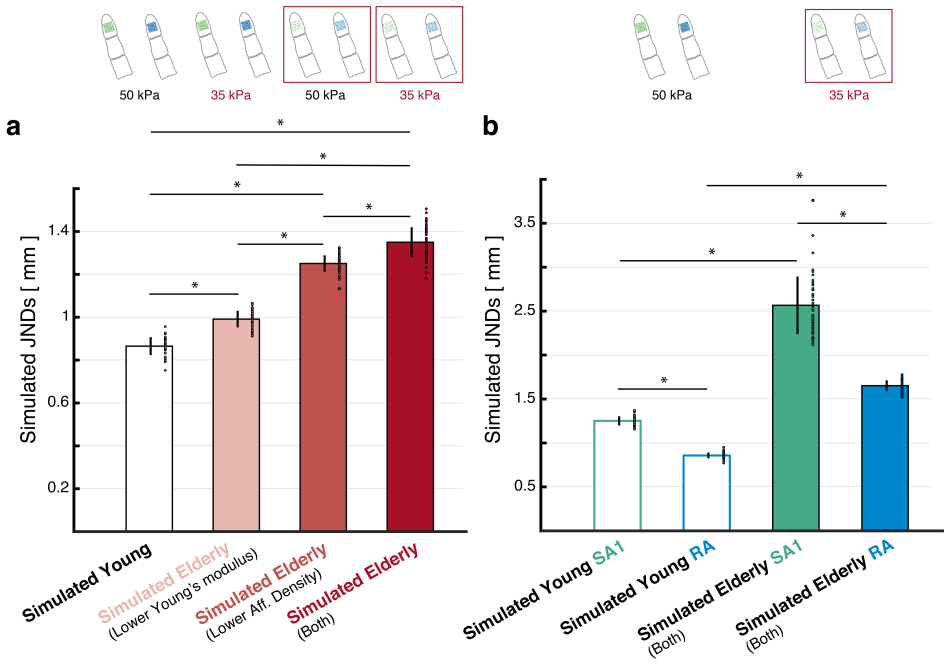

Figure 4.7. Simulated JNDs based on accuracy values obtained from classification of the simulated response to the 2-point discrimination task using parameters to capture the Young and Elderly groups. Classifier built on the entire indentation window (i.e., 500 ms). **a)** JNDs estimated from the response of SA1 and RA combined for Young (black), Elderly with lower Young's modulus (pink), Elderly with lower afferent density (light red), Elderly with both lower Young's modulus and lower afferent density (red). Error bars represent the standard deviation of the JNDs obtained for each of the 50 runs of classification. Coloured dots show the values obtained for each of the 50 runs of classification. * $p < .001$. **b)** JNDs estimated from the response of SA1 (green) and RA1 (blue), separately. Void bars show results for the virtual Young group. Filled bars for the virtual Elderly group with both lower Young's modulus and lower afferent density. Coloured dots represent the estimates from each of the 50 classification runs. Error bars represent the standard deviation of the JNDs obtained for each of the 50 runs of classification. * $p < .001$, Bonferroni-corrected.

To establish how the stimulus information accumulates throughout the indentation period (2), classification analysis was performed over 15 logarithmically spaced cumulative time windows, ranging from 1 ms to 500 ms. The response of SA1 and RA1 together was used to discriminate between the single pin and two pins at each separation level, separately. This analysis was run on each separation level for the Young group and the Elderly group. Similar to the previous analysis, the virtual JNDs (75% correct response rate) were estimated based on classification results by fitting a Logistic curve to the accuracy values of the decoder. Figure 4.8a shows the evolution of the virtual JNDs for young and elderly over time.

For the Young group, the spatial activation across afferents was informative enough to discriminate between the single pin and the two pins as early as 20 ms after the onset of indentation, when only a few spikes have been elicited. Results for the Elderly group showed, not only a poorer classification performance, as previously shown, but also a slower information build-up with the neural response only becoming informative at around 35 ms (red line, Figure 4.8a). A further difference between simulated young and elderly data is the variability of results, indicated by the standard deviation (shaded area, Figure 4.8a). In particular, we observed that results from the young were more consistent than the elderly counterpart.

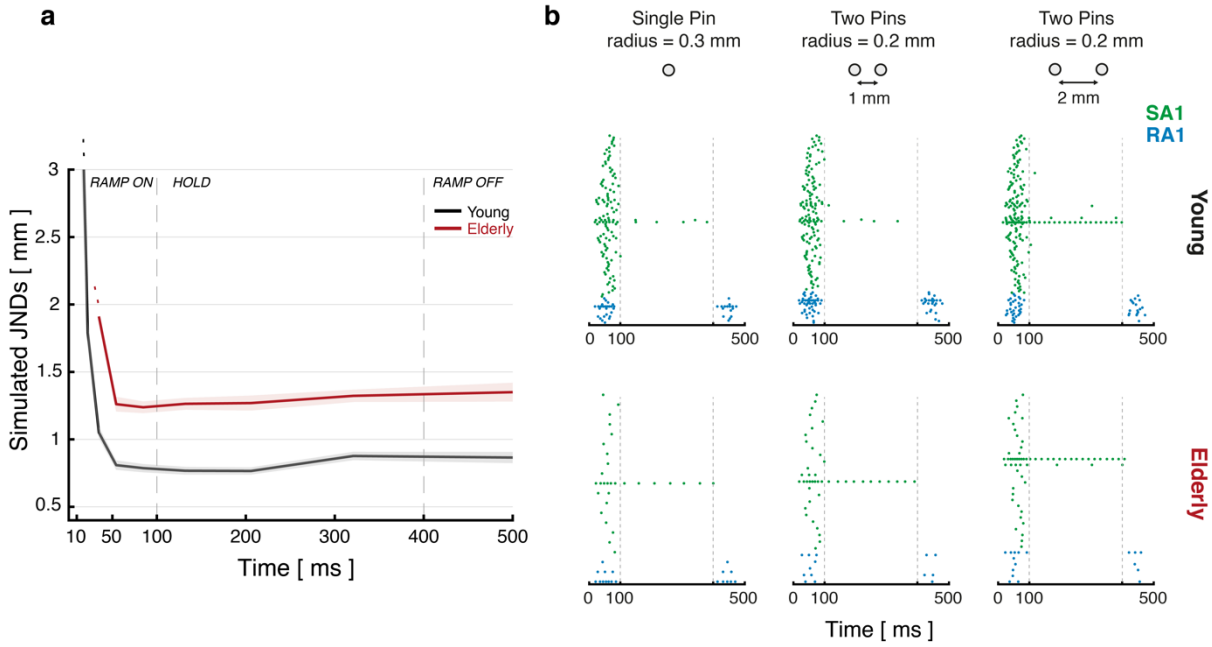

Figure 4.8. a) Time-course estimation of virtual JNDs based on simulated neurophysiological data for the Young group (black lines, SA1 and RA1 units combined), and for the Elderly group (red line, SA1 and RA1 units combined). Shaded area represents standard deviation of the estimated JNDs based on each of the 50 classification runs. JND values at 500 ms correspond to the performance shown in figure 7a for the Young group (black) and the Elderly group with both manipulations (dark red). **b)** Simulated population response of SA1 (green) and RA1 (blue) tactile fibres for Young (top row) and Elderly group (bottom row) to a subset of virtual stimuli indented 2.5 mm. From left to right the raster plots show the neural response to a single pin with a radius of 0.3 mm, two pins with a radius of 0.2 mm each separated by 1 mm, and two pins with a radius of 0.2 mm each separated by 2 mm. Only the active fibers (at least 1 spike) were plotted. Vertical gray dotted lines indicate the start and the end of the hold phase of the trace.

Finally, we set out to determine which afferent type is more tuned to the fine spatial layout of the virtual stimuli. The simulated response over the entire 500 ms stimulation window was used to generate the classification output for the simulated Young and Elderly group, built on SA1 data and RA1 data separately. Then, the JNDs (75% correct response rate) were estimated for both group and each afferent type (Figure 4.7b). Two dependent sample t-test were performed to compare the simulated JNDs based on SA1 against RA1 data in each age group, and two independent sample t-test to compare the simulated JNDs based on SA1 and RA1 response of the Young group against the respective JNDs obtained for the Elderly group. p-values were corrected with Bonferroni method. Results showed that in both age groups there was a significant difference between the JNDs estimated from the response of SA1 and those estimated from the response of RA1. For the Young group (SA1-RA, $t(49) = 43.7661$, $p_{corrected} = 2.44e\text{-}40$; Cohen's $d = 8.91$), the estimated mean difference was 0.39 mm, 95% CI [0.37, 0.41]. For the Elderly group (SA1-RA, $t(49) = 19.7842$, $p_{corrected} = 2.07e\text{-}24$; Cohen's $d = 3.88$), the estimated mean difference was 0.91 mm, 95% CI [0.82, 1.00]. As expected, a significant difference was found between the JNDs estimated on SA1 response of Young and Elderly group ($SA1_{young}$ -$SA1_{elderly}$, $t(98) = -28.03$, $p_{corrected} = 5.41e\text{-}48$; Cohen's $d = 5.61$), the estimated mean difference was -1.31 mm, 95% CI [-1.40, -1.22]; and between the JNDs estimated on RA response of Young and Elderly group (RA_{young} -$RA_{elderly}$, $t(98) = -80.77$, $p_{corrected} = 7.09e\text{-}91$; Cohen's $d = 16.15$), the estimated mean difference was -0.79 mm, 95% CI [-0.81 -0.77].

4.5 Discussion

A combination of psychophysics with measurements of finger properties, and computational modelling was employed to evaluate some of the potential factors underlying the deterioration of tactile spatial sensitivity observed with ageing. Results from the previous literature on 2-point threshold showing a decrease in performance in the elderly population for statically indented tactile stimuli (Stevens, 1992; Woodward, 1993; Kalisch et al., 2009)

were replicated by using passive stimulation with computer-controlled speed, force and contact duration. The Elderly group 2-point discrimination threshold was over three times larger than for the Young group. Importantly, new evidence was provided on which factors might drive the observed difference in the psychophysical task between the two groups. Commonality analysis showed that age was the best unique predictor of the sensitivity to our set of stimuli, followed by hydration, finger pad area, and biological elasticity. Although the unique contribution of skin properties to the regression effect was minimal, biological elasticity, hydration and finger pad area definitely contributed to the regression effect as they were involved with 19.9%, 35% and 41% of the total explained variance in the measured 2-point JNDs, respectively.

The relevance of age in predicting the behavioural performance is not surprising as ageing is accompanied not only by a decline of peripheral sensory systems but an alteration of cortical representations of sensory information as well as cognitive processes. Previous studies showed that impaired tactile acuity in the elderly is reflected in increased excitability of the primary somatosensory area S1 (Lenz et al., 2012), and enlargement of hand representation (Kalisch et al., 2009). This might be due to a reduction of intracortical inhibition which results in the spread of activity from the stimulated cortical RFs to nearby regions (Kalisch et al., 2009) and may elicit less sharp neural representations. Memory decay and sustained attention might also have played a role in this kind of paradigm. Our 2IFC task involved short term memory to store the sensory information about the first stimulus and compare it to the second one a few seconds later. Similarly, the repetitive nature of task could make attending to the sensory inputs more challenging for the older participants. The cognitive demand might have been exacerbated in the elderly by the poorer sensory inputs. Ageing effects on central mechanisms might also explain the difference observed between the behavioural

thresholds in which more than a three-fold increase of threshold for the Elderly group was recorded and the simulated thresholds where a two-fold increase was found.

The contribution of finger pad area to the perceptual performance can be linked to the fact that the number of at least one type of mechanoreceptor, Meissner's corpuscles, does not vary much across individuals and is inversely correlated with finger pad area (Dillon et al., 2001; Nolano et al., 2003). The Elderly group had a larger finger pad area than young participants. One possible reason for this difference might be the enlargement of bone epiphysis observed in both males and females with age (Kalichman et al., 2008), This in itself could contribute to reducing density of receptors with age. However, ageing is also characterized by a reduction in the number and also changes in the morphology and depth of receptors (García-Piqueras et al., 2019), as well as slower conduction velocities of peripheral nerves due to demyelination (Peters, 2002) which might also degrade tactile input and raise 2-point discrimination thresholds with age. Importantly, the loss of Meissner's corpuscles varies across elderly individuals and likely contributes to the extent to which tactile sensitivity is reduced with age (Skedung et al., 2018)

The role of finger pad area and age was consistent with the results from the simulation based on Saal et al. (2017). Model-generated JNDs were negatively influenced mainly by lower afferent density which relates to either factor. In fact, the density of the virtual afferents had a greater impact on the simulation results than the manipulation of YM. This is not surprising according to the traditional view that tactile spatial resolution is limited by the afferent density and the centre-to-centre spacing of the receptive fields (Friedman et al., 2002; Dodson et al., 1998). However, the extent to which these factors can affect spatial acuity is still not clear.

SA1 and RA1 fibres are characterised by innervation branching which generate receptive fields with a complex sensitivity map with multiple hotspots (Johansson, 1978). In the model of Saal et al., (2017) the receptive field of these neurons are circular with a single sensitive zone. However, they have similar features to the actual ones including overall size, sensitivity to indentation depth, and lower threshold in the centre of the receptive field compared to the periphery. Some insights on the contribution of the complex structure of receptive fields to a different measure of spatial acuity come from the work of Hay and Pruszynski (2020). They compared a model of RA1 units having such complex receptive field with a similar model of RA1 having uniform receptive fields. They found that the multiple hotspots slightly improved the discrimination of fine orientations (e.g., -1° vs +1°) when compared to a similar model of receptive fields with uniform sensitivity. However, the classification was largely above chance for both uniform and complex receptive fields. In addition, the modelling work of Hay and Pruszynski (2020) does not include any consideration of skin mechanical response and the stresses acting on the receptors.

In regard to skin elasticity and hydration, results suggested that they also contributed to the discrimination performance. Simulation results also showed a small effect of YM which is related to biological elasticity. In particular, lower YM significantly increased the estimated JNDs by only 0.12 mm compared to the virtual Young group. The significant results in the presence of a small effect could have been driven by the relatively high number of observations generated with simulations that were needed for the classification of the stimuli and the low variability of the model output. In addition, this minimal difference might not be meaningful at behavioural level (e.g., discriminating or manipulating objects).

It is worth mentioning that attempts to measure YM of skin have provided contrasting results. In a recent review paper, Kalra and Lowe (2016) showed that the estimated YM depends on

the methods used to measure it as well as other factors. It seems that indentation and torsion tests result in estimates of YM that reduce with age (e.g., Boyer et al., 2009) while suction tests sometimes provide increasing estimates with age (e.g., Dridillou et al., 2001). As this experiment involved indentation of the stimuli, a lower value for the Elderly group was chosen from the literature. Although skin elasticity was measured with a suction device, the obtained measurements across age groups were similar to those of Boyer et al. (2009) who found lower elasticity, measured in the elderly with a suction device, was associated with lower stiffness (i.e., Young's modulus), measured with an indentation protocol. This choice was also supported by the work of Yang et al. (2018) who used ultrasound to measure YM and found that it was significantly lower in the over 50 year olds compared to the 20-50 year old group. Yang et al. (2018) also observed that the age related difference in YM was greater at the finger pad than at other body sites.

The analysis of the simulated neurophysiological data over time provided evidence for effects of YM and afferent density not only on the asymptotic level of performance but also on how the stimulus information unfolds over time. Classification output showed that stimulus information is available as early as 20 ms from the initial contact for the Young group. This finding is consistent with Delhaye et al (2019) who showed a similar unfolding of information in an edge orientation task. As the authors noted, having such a rapid response is crucial for object manipulation and fine manual dexterity tasks, although the precise temporal dynamics are dependent on the indentation parameters and can happen at slightly different temporal scales. Importantly, comparing these results with those obtained for the Elderly group revealed that our manipulations delayed the way stimulus information builds up. This might interact and further reduce elderly performance compared to young if, for example, the contact with the stimuli is very brief.

In regard to the individual contribution of SA1 and RA1 units in conveying the shape of the statically indented stimuli, there is still an open debate about whether the functions of different units' type are segregated (Johnson et al., 2000; Johnson, 2001) or partially overlapping (Saal and Bensmaia, 2014). Results for both the Young and the Elderly virtual groups suggest that the spatial activation and firing rates of both SA1 and RA1 fibres carry information about the stimulus spatial layout. These findings support the rate coding hypothesis by which geometric features are encoded in the firing rate intensity and variations across afferents. It has been shown that the firing rate of SA1 and to a less extent RA1 for both static and dynamic touch might convey the shape of a step (i.e., steepness) indented either vertically or stroked across the skin (Srinivisan and LaMotte, 1987), the curvature of corrugated surfaces (LaMotte and Srinivisan, 1996), the orientation of cylinders (Dodson et al., 1998), and the configuration of raised dots (Connor and Johnson, 1992). Overall, results support the idea that these types of fibre are of an equal importance which is in contrast with the traditional segregation model (Johnson et al., 2000; Johnson, 2001). The latter assigns an exclusive role for shape perception to the SA1. However, recent studies are in line with our findings supporting a convergence of functions across the different afferent types (e.g., Weber et al., 2013). In order to address this question, it will be necessary to study the population activity of real tactile neurons as this may reveal emergent properties that are not present in the response of individual units.

The model of Saal et al. (2017) has been built on several assumptions to simplify the computations to generate the neural response. The skin is modelled as flat, homogenous and elastic, with isotropic behaviour and does not include any hard structures (e.g., bone), nor the fingerprints. Having a realistic 3D shape and layered structure of the finger is definitely important for large deformations when the applied force and contact area would cause the skin to protrude from both sides of the finger pad activating receptors in that area.

The stimuli in this experiment were flat-ended pins with small diameter (0.2 mm and 0.3 mm) indented to small depths (1 mm to 2.5 mm) in the centre of the virtual finger and the assumed flat structure of the skin in the model does well in reproducing the response properties of the simulated afferents to this type of stimuli as shown in Saal et al, 2017. In particular, the firing rate and the spike timing correlate well with actual data showing several response properties of real first-order neurons including slow versus fast adaptation, frequency tuning, and edge enhancement/surround suppression.

The lack of fingerprint geometry, anisotropic behaviour and viscoelastic response would be a major concern for dynamic stimuli in the presence of friction (e.g., sliding movement). For example, the skin deforms to a different extent if a scanning movement occurs in lateral versus proximo-distal direction or when making contact with a sticky or slippery texture. In fact, in this model the virtual stimuli are defined as a single cylindrical pin or a set of pins that can be indented only orthogonally which makes it suitable to simulate the classical 2-point discrimination task in which the skin is stimulated with static stimuli in vertical direction without the presence of any major shear component. Nonetheless, the contribution of the realistic 3D shape of the finger and the hard structures (i.e., bones, nails) to the informativeness of the neural activation cannot be assessed with this model.

PC units were not included in the simulations as their large receptive fields and sparse distribution makes them unsuited for resolving the fine spatial layout of tactile stimuli. This is highlighted in the seminal work of Phillips and colleagues (1988) who showed that the PC afferent response used to construct a spatial event plot result in a blurred image. Nonetheless, PC sensitivity to vibratory stimuli across a wide range of frequency and very small amplitude skin deformation is important for the perception of textures and vibrations

acting on objects held in the hand (Kandel et al., 2021), as well as the contact onset and offset of static stimuli.

In this work, simulations results were based on the spatial activation of the afferent populations, or the population firing rate (i.e., rate coding). This does not imply that this information can be directly used by the central nervous system. Other potential coding strategies have been proposed as mechanism to extract shape information. These include the spike timings of individual afferents for edge orientation (Pruszynski and Johansson, 2014) and the variations across afferents of the first spike latency for curvature (Johansson and Birznieks, 2004). However, the temporal aspect of the neural response has been shown to be highly susceptible to differences in other stimulus parameters (Suresh et al., 2016), and taking into account precise spike timings to classify statically indented edges with different orientation might make the signal less informative if these differences are present (Delhaye et al., 2019) compared to the population firing rates. Certainly, spike timing is essential in the coding of texture and vibrations (Weber et al., 2013; Mackevicius et al., 2012) and the present findings do not exclude the possibility that the stimulus spatial layout can also be extracted from the timing of individual spikes. In addition, the neural response evolves as it moves through the different stages of the hierarchy (i.e., spinal cord, brainstem, thalamus, cortex). An open question is where the integration and transformation of the signals coming from the four types of afferent units begins (for a review see Abraira and Ginty, 2012). For example, the integration of the signal from a population of neurons at the level of the cuneate nucleus is compatible with a coincidence detection mechanism based on the timing of individual spikes (Pruszynski and Johansson, 2014). Future work should aim at elucidating the contribution of precise spike timings with a focus on aging touch including skin properties, the response properties of aging neurons, and the integration of the afferent signal starting at the level of the cuneate nucleus.

4.6 Conclusion

Spatial tactile sensitivity decreases throughout the lifespan. Previous research has mainly focused on cognitive mechanisms and changes that happen at central level. Although the role of peripheral sensory components, such as skin and mechanoreceptors properties, has been pointed out, there is little evidence that link these factors to the deterioration of tactile perception. This experiment showed that elderly people, in fact, have lower sensitivity than their younger counterparts. Importantly, this difference was linked to finger pad area, which was found to be higher in the Elderly group, and afferent density, lower in the Elderly group as previously shown. There were also contributions of reducing biological elasticity and hydration to aging reductions in tactile sensitivity, but these were appreciably less than for the finger pad area and afferent density. The present findings also highlight the contribution of impaired cognitive processes that it is suggested might have contributed to the difference between behavioural and simulations results.

Chapter 5

Surface geometry and moistened finger affect friction and detection threshold for a single microdot

5.1 Abstract

With sliding contact people are able to perceive tactile features at the micron scale, such as a single dot raised only few microns when placed on a smooth surface. Frictional effects are important in determining the tactile cues available in sliding. However, little is known about the effects of fluid environments and surface geometry on the detection of microfeatures. This study investigated how detection sensitivity to a single micro dot is affected when the dot is placed on a smooth versus rough surface, and when the stimuli are sensed with dry finger, moistened finger with water, or with a solution of water and soap. These manipulations were chosen to alter the skin-surface interaction and the resulting forces acting on the skin.

The results showed that detection threshold was 6-fold higher for the rough surfaces when compared to smooth surfaces. Moistening the finger with water or water and soap reduced the friction as well as the magnitude of tangential force variations when compared to dry finger, regardless of the surface geometry. However, detection sensitivity improved for the 'smooth' surfaces but worsened for the 'rough' ones with moistened finger. It is suggested that this is due to the different nature of neural noise generated when making contact with smooth or rough background surfaces, and the extent to which different fluid environments modulated friction and the forces acting on the skin with consequences for the neural response.

5.2 Introduction

Human tactile perception is very fine-tuned. When we visually spot irregularities on a surface, such as a line on our car body or food particles on a dish, we are able to determine the nature and the extent of those irregularities by moving our fingers across it. These features can be in the order of microns (and sub-micron as well) and touch often proves necessary to discriminate and detect this sort of stimuli. Research on tactile perception has only partially focused on these fine features at sub-millimetre scale but some insights come from a series of studies by LaMotte and colleagues (LaMotte and Srinivasan, 1991; LaMotte and Whitehouse, 1986; Johansson and LaMotte, 1983). They used contact photolithography and etching to create surfaces featuring a single raised dot or a fine texture (ridges or dot patterns) to investigate perceptual thresholds in humans and the related peripheral neural events in monkeys. They showed that people can detect very small dots, on an otherwise smooth surface, of only 1 micron height with a diameter of ~600 microns (3 microns with ~230 microns diameter and 6 microns height with a diameter of ~40 microns) and very fine textures (parallel bars 45 microns wide and spaced ~100 microns) of only 0.1 microns height, when compared against a 'blank' surface in a 2AFC task. They found that lateral sliding is essential for these fine features to be perceived as no sensitivity to the same set of stimuli was found with static touch.

Neurophysiological recordings in monkeys showed that rapidly adapting mechanoreceptors (RA1 and RA2/PC) have a primary role in the detection of these types of microfeature (LaMotte and Srinivasan, 1991). This is consistent with more recent evidence regarding the existence of two different codes for tactile perception (Duplex theory – Katz, 1925). Several studies support the idea that coarse features (> 100-200 micron) are mainly encoded in a spatial manner, while fine feature perception (< 100-200 micron) relies on skin vibratory response, generated by stroking movement (Blake et al., 1997; Hollins and Risner, 2000; Hollins et al., 2001).

Skin response results from the complex interaction of surface and skin properties in the presence of friction. It has been shown that skin vibration characteristics reflect the texture of the sensed surface (Hollins and Bensmaia, 2003), and the variation of tangential forces acting on the skin, observed when sliding the finger over a texture, have been used to predict roughness magnitude estimation (Smith et al., 2002) and the performance on a roughness discrimination task (Roberts et al., 2020). Interestingly, Smith et al. (2002) also showed that these variations are less prominent when friction is actively reduced by the addition of liquid soap and this change is followed by a reduction of roughness magnitude estimates.

In fact, the tribological properties of the skin can affect perception and depend on a variety of factors including surface geometry (e.g., rough/smooth), material molecular properties (e.g., hydrophobic/hydrophilic material), the exploratory pattern (e.g., applied normal force), finger properties (e.g., hydration), and environmental conditions (e.g., relative humidity, use of moisturiser). For example, Skedung et al. (2018) found that the application of humectant increased the friction between the finger and wrinkled surfaces in the elderly population with improvement in discrimination judgments. Aktar et al. (2017) observed that the ability to discriminate surface roughness is reduced when the objects are placed in a high-viscosity lubricant in young participants. Recently, Zhou et al. (2022) performed a similar study suggesting that this change in perception might be due to the fact that different fluid environments affect friction and the interfacial film thickness. However, little is known about the extent to which manipulations of finger tactile friction can affect detection sensitivity for a single microfeature.

The aim of this experiment is to extend the knowledge of how human sensitivity to micro features is affect by surface geometry and moistening of the finger with active exploration. We measured psychophysical thresholds for a microdot placed on a smooth, or rough surface. And we evaluated how participants' sensitivity is affected when the task is

performed with dry finger, after wetting the finger in water, or in a solution of water and liquid soap. Measurements of skin hydration and contact forces were carried out to characterise the interaction between skin tribology and perception.

The two surface geometries and the addition of water and liquid soap were chosen to alter the contact dynamics between the finger and the sensed surface. It was expected that the smooth surfaces explored with dry finger will produce higher friction than the rough ones (Derler and Gerhardt, 2012). Also, dipping the finger in water or the solution of water and soap was expected to reduce friction and the tangential force variations when compared to the dry condition for the same surface geometry as shown for high moisture content of the skin (Andrè et al., 2009).

In terms of detection sensitivity, the reduction of friction on smooth surface was anticipated to potentially improve performance. This is because with moistened finger the sliding movement should be easier to perform and possibly results in a reduction of stick-to-slip transitions that produce irrelevant vibrations detrimental for the detection of the microdot. For the rough surfaces, predictions are unclear as the effects of a reduction of friction will be concurrently acting on the target microdot as well as the surrounding dots. This might make it difficult to uncouple the vibrations generated by the rough background and the target.

5.3 Materials and Methods

5.3.1 Participants

The study was approved by the STEM Ethical Committee at University of Birmingham (ERN_09-528AP24) and conformed to the standards set by the Declaration of Helsinki. All participants gave their written informed consent before the beginning of the experiment.

Seventeen young participants were recruited from the cohort of undergraduate psychology students at University of Birmingham who received course credits after completion (9 female, age range 18-21, mean age 19.17 ± 1.01 years). Eligibility criteria were normal or corrected-to-normal vision, independence in activities of daily living, absence of physical hand injury, absence of motor and sensory impairment. These criteria were self-reported by the participants. Participants were also asked to self-report their dominant hand (15 right-handed), but the task was always performed with the index finger of the right hand to ensure that the sliding movement was consistent across participants.

5.3.2 Psychophysical task and measurement of skin hydration

Participants were tested on a 2-AFC detection task to determine detection thresholds in six conditions. Experimental design consisted of 2 factors: Surface geometry and Finger condition. Surface geometry refers to the roughness of the surface and had two levels, i.e.: smooth and rough (for more details see *Stimuli*). Finger condition refers to the moistening of the finger and had three levels: dry, wet with water, wet with a solution of water and liquid soap. The solution of water and soap was prepared before each session for each participant by diluting 10 grams of Fairy Platinum washing up liquid (Procter & Gamble) in 90 grams of water (10% solution), measured with a precision scale. Tap water was used at room temperature for both conditions involving finger wetting.

In the dry finger condition participants performed the sliding movement without further action. In the wet conditions, participants were instructed to dip their index finger on a glass standing next to the stimuli filled with water or the solution of water and soap before the first as well as the second interval. Before making contact with the stimuli, they were also asked to use a paper tissue to dry the back of the finger (i.e., nail area) to avoid any excess liquid spilling on the electronic components.

The task was to detect a single dot placed in the centre of the target surface against a blank surface with no dot, where the intervals with dot present and dot absent were presented in a randomized order. Participants were instructed to verbally report which interval contained the target surface (i.e., first or second). Individual trials consisted of sliding the right index finger from left to right for only one continuous stroke on each surface. Participants were told to keep the fingertip at a moderate angle to the surface, avoiding the extremes of 90 or 180 degrees (i.e., orthogonal or parallel to the surface). Sliding duration, use of a single stroke and to some extent the angle of the finger during the movement were the only constraints on the exploration of the surface. Speed and contact forces were spontaneously chosen by the participants. Participants performed a short practice session before the experiment consisting of 6 trials for each surface type, during which they familiarised themselves with the stroking movement and the stimuli. At this stage, the experimenter provided feedback about the accuracy of the participant's response, but no feedback was given during the experiment.

The task was performed with "blurred" vision to avoid potential visual cues, embedded in the stimuli due to manufacturing process (i.e., specular highlights), that might be used to detect the target surface. To do so, a face shield was used to which attached one layer of bubble wrap was attached. In doing so, participants were able to locate the surface to perform the reaching and sliding movements but could not see the specular highlights reflected by the surface. This method was confirmed to be successful during a pilot study and by analysing the frequency spectrum of a picture taken through the face shield with and without the bubble wrap. Results showed that there was a significant reduction of high frequency components suggesting that the specular highlight were successfully cut-off.

The experiment was divided in three sessions of about 60 minutes each that participants attended on different days and in a randomized order to control for learning effects over the course of the study. In each session, participants performed the experiment with both

smooth and rough surfaces in one of the three Finger conditions. Before each session, participants were asked to wash their hand with water and liquid soap and waited 10 minutes which included the experimenter providing instructions.

To speed up the testing time, the experiment was carried out in blocks of 12 trials. On each block, 24 stimuli (12 target and 12 standard) were placed on two different rigid aluminium trays. Each tray contained cut-out slots to hold 12 stimuli for a total of 6 trials (Figure 5.1). Participants were informed about this and instructed to move to the next tray after completing the six trials on the first one. After the second set of six trials was completed, participants were asked to move away from the table and the experimenter swapped the stimuli for the next block. Each participant performed a total of 288 trials: 2 surface geometry x 3 finger conditions x 6 stimulus levels x 8 repetitions.

Before the beginning of the session performed with dry finger and before hand washing, the hydration of the stratum corneum was measured for each participant with the Corneometer CM 825 (Courage and Khazaka Electronic GmbH) which expresses changes in water content in arbitrary units. The measurement was performed five times to then compute the average value. This was done to assess the effects of hydration on the resulting contact forces and detection sensitivity. Hydration was not measured in the 'wet' conditions as the stratum corneum becomes saturated with water after dipping the finger in water or the solution of water and liquid soap. The temperature and relative humidity of the room was measured at the beginning of each session. The average temperature was 21.52 °C ± 0.56, and the average relative humidity was 45.74% ± 6.93.

5.3.3 Force recordings

Contact forces were recorded with a 6 degree of freedom force-torque transducer (ATI Nano17, NC, USA) at a sampling rate of 820 Hz. The sensors had a resolution of 0.003 N for the forces and 0.015 N/mm for the torques. The force-torque transducer was attached to a

3D printed part that was glued on the table on its lower side and at the bottom of the tray hosting the stimuli on its upper side (Figure 5.1). The force torque measurement setup was checked with standard weights place at a range of different positions across the tray. On each block, the force-torque transducers were calibrated to correct for any potential DC offset by taking the mean amplitude of the signal over 1 second and subtracting it from each sample.

On each trial, two beeps were played in consecutive order before the first interval as well as before the second one. The first beep was low pitch to inform participants to get ready and the second beep, played after 1.5 seconds, was high pitch to signal the beginning of force recordings. Participants were informed that the recording would last 5 seconds for each interval and the interstimulus interval was 2 seconds.

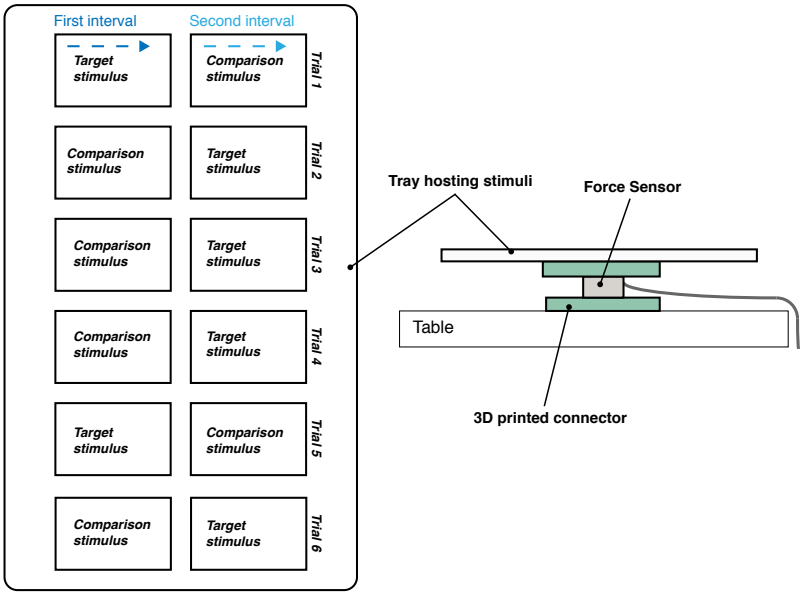

Figure 5.1. Schematic view of the experimental setup. Left. Top view of the tray used to host the stimuli. The tray consisted of 12 slots divided in six rows and two columns. Each row represents a separate trial. The position of Target and Comparison stimuli was randomised. Participants performed a single continuous sliding movement from left to right (blue and light blue arrows). **Right.** Lateral view of the apparatus used to record contact forces. The force-torque transducer (grey) is connected to a 3D printed (green) part glued on the table one side and on the tray hosting the stimuli on the other.

5.3.4 Stimuli

The stimuli comprised custom-made laser-etched stainless-steel plates with either smooth or rough geometry. This method was chosen because it allows very fine details to be resolved with high accuracy and is relatively fast (see Chapter 2, *section 2.5.3 Manufacturing of fine-textured stimuli*).

The Smooth set consisted of 6 smooth blank surfaces used as standard stimulus and 6 smooth surfaces featuring a single dot placed in the centre of the surface used as target stimulus. The single dot was designed to have a square shape with a fixed side length of 300 microns and 6 different heights: 2, 4, 6, 8, 10, 12 microns (Figure 5.2).

The Rough set consisted of 6 rough blank surfaces featuring a matrix of 19 x 35 dots initially arranged in a regular grid with an edge-to-edge separation of 700 microns. The position of each dot on the long side (i.e., 35 columns) was then shifted by adding a random number to the original coordinate taken from a uniformly distributed interval from 0 to 1 mm. The dot position on each row was shifted with the same approach but applied to the entire row. The resulting layout was checked to avoid any overlapping between dots. The arrangement of the matrix was the same across all the Rough surfaces including comparison and target stimuli. The multiple dots were designed to have a square shape with a fix side length of 300 microns and height of 100 microns. The target surfaces of the Rough set were the same as the Rough blank surfaces with the dot placed in the centre of the surface raised above the surrounding dots. The raised dot was designed to have the same side length has the surrounding dots (i.e., 300 microns) and 6 different heights protruding by 20, 30, 40, 50, 60, 70 microns (Figure 5.2).

The surfaces were inspected with an optical 3D microscope (Alicona InfiniteFocus). The surface roughness of the Smooth set was about 0.1 micron and the dot dimensions were resolved with a resolution of about 0.1 micron in both the Smooth and Rough set.

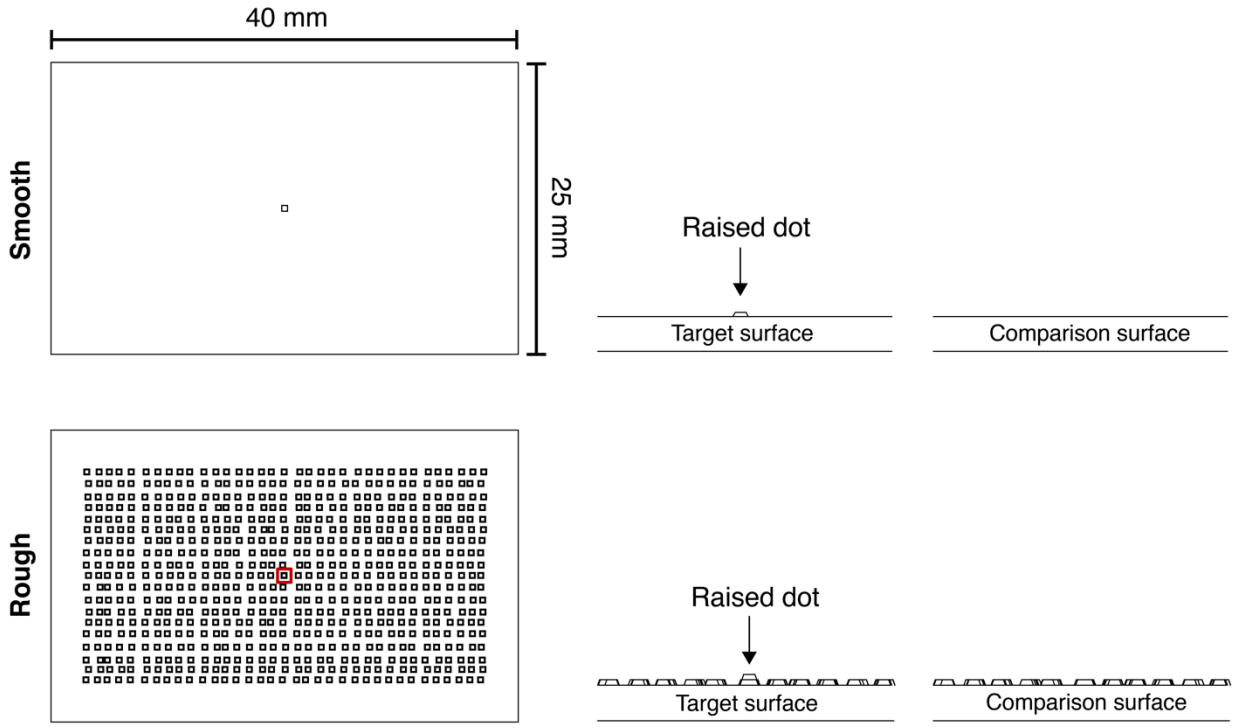

Figure 5.2. Line drawing of the stimuli. Top row. Top view (left) and lateral view (right) of Smooth surfaces. **Bottom row.** Top view (left) and lateral view (right) of Rough surfaces.

5.3.5 Analysis of behavioural data

Detection thresholds were defined as the dot height at which the correct detection rate was 75% (here referred to as the JND). To estimate this value, Spearman-Kärber method (Ulrich and Miller, 2004) was used. This approach was chosen over the classical Logit analysis due to the nature of the current dataset. A first attempt to fit the behavioural responses with the Logistic function was unsuccessful in one or two conditions for 4 participants, for a total of 6 missing JNDs out of 102 (6 conditions x 17 participants). This was due to a combination of stimulus set, relatively small number of trials, and individual variability, with some participants showing ceiling effect starting from the first stimulus level while others showing floor effect. Notwithstanding, the stimulus set was ideal for the majority of participants across the 6 conditions. To avoid excluding a high percentage of participants (4 out of 17 = 23,5%) or relying on imputation methods which can alter the real distribution of the data, Spearman-

Kärber method was successfully used to fit the entire dataset. This is a non-parametric estimate which makes no assumption about the shape of the psychometric function. The only constraint is that the correct response rate increases monotonically from the lowest to the highest stimulus level. Corrections were made to monotonise the distribution of responses when needed, following the approach described by Ayer et al. (1955) and summarised by Miller and Ulrich (2001). The proportion of responses was fitted at every two stimulus levels starting from a 50% level (i.e., guess rate) and ending at 100%.

5.3.6 Analysis of contact forces

The relationship between detection sensitivity and contact dynamics was determined using estimates of the mean normal and tangential force, the dynamic coefficient of friction, and the RMS of tangential force variations. To do so, the raw force traces were pre-processed before further analysis to remove artefacts, bad or missing trials, as well as filtering out unwanted noise. All the analyses were performed in MATLAB (Mathworks Inc.) using custom-made scripts.

First, force recordings were visually inspected to remove bad or missing trials. Sporadically, participants made contact with the wrong surface, the surface slipped out of its slot, participants touched the tray rather than the stimulus, or they tapped their finger on the table which affected the recordings. If necessary, the trial was repeated without recording the forces. Second, force traces were filtered with a sixth order lowpass Butterworth filter with a cut-off frequency of 100 Hz by using MATLAB built-in function *filtfilt*. Third, we determined the onset and offset of contact between the finger and the surface from the temporal dynamics of normal and tangential forces to trim off part of the recordings preceding and following the interaction. The onset timepoint was defined as the first value of tangential force along the scanning direction exceeding 0.02 N. The offset timepoint was defined as the first value of normal force below 0.05 N. These values were determined through a process of trial and error due to the noisy nature of the recordings especially in the Smooth/Dry

condition. The trimmed traces were then individually inspected to confirm the slicing was correct and otherwise they were excluded. At the end of the pre-processing, we excluded 15.65% of the trials (766 trials out of 4896).

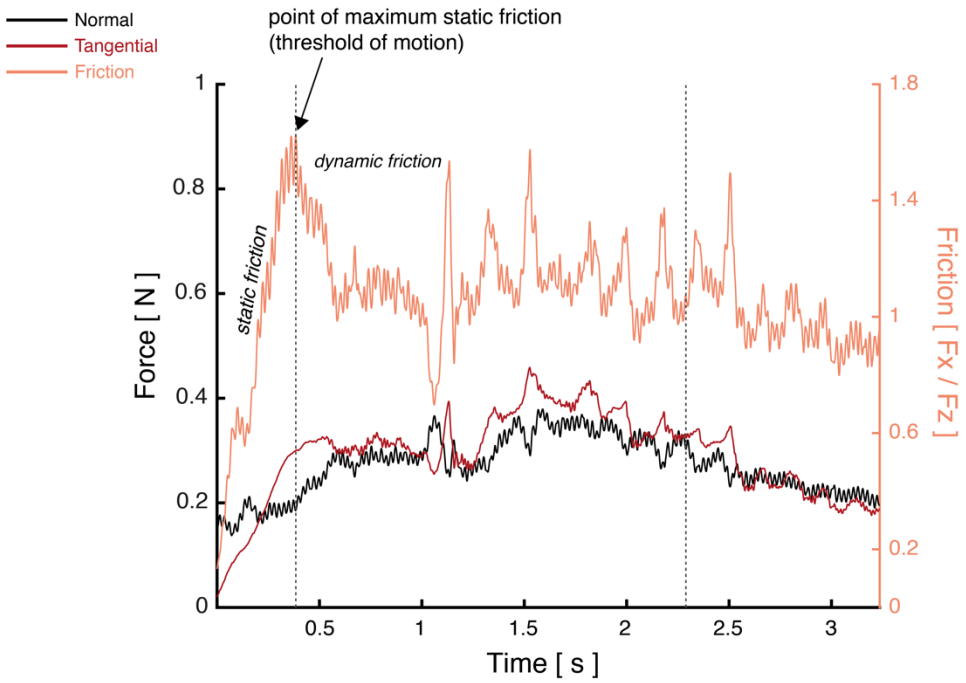

Figure 5.3. Analysis of contact forces. Example of Normal force **(black),** Tangential force **(red)**, and Friction **(orange)** obtained for participant 2 (trial 22, first interval) for a rough surface sensed with dry finger (same as top right quadrant of figure 5.5). The traces shown in the figure are trimmed and filtered following the procedure detailed in section 5.3.6 – Analysis of contact forces. Vertical dotted lines show the start and end point of the time interval of interest for statistical analysis. This interval was defined as one sample after the point of maximum static friction until two thirds of the remaining samples to ensure that the analysed traces included only the sliding movement.

Statistical analysis was performed on the mean normal and tangential force, coefficient of dynamic friction, and RMS of tangential force variations, calculated in the time interval including only the sliding movement. This interval was defined as starting from one sample after the point of maximum static friction until two thirds of the remaining samples. The point of maximum static friction was identified by taking the maximum value of friction in the first quarter of the recording (Figure 5.3).

Tangential forces were defined exclusively by the force acting in the same direction of the movement (i.e., x-axis in our setup) as movement along the orthogonal y-axis was negligible. Friction was calculated as the ratio between tangential and normal force: F_x / F_z. The coefficient of dynamic friction was calculated by averaging the obtained friction during the sliding movement. Finally, the RMS of tangential force variations was calculated by computing the first derivative of the tangential force and then its Root Mean Square value. The RMS values were normalised by dividing the individual RMS with the mean RMS collapsed across the six conditions.

5.4 Results

5.4.1 Psychophysics

The estimated JNDs in each finger conditions are shown in Figure 5.4 for Smooth and Rough surfaces, separately.

A 2x3 repeated measures ANOVA was performed in SPSS with Surface geometry (2 levels) and Finger condition (3 levels) as the two factors. Results showed a statistically significant main effect of Surface geometry on the detection thresholds ($F(1,16) = 200.784$, $p < 0.001$, $\eta_p^2 = 0.926$). It was also found a significant main effect of Finger condition ($F(2, 32) = 5.08$, $p = 0.012$, $\eta_p^2 = 0.241$), and a significant interaction between Surface geometry and Finger Condition ($F(2, 32) = 7.902$, $p = 0.002$, $\eta_p^2 = 0.331$). To reveal which pairs of means were statistically different across the levels of Finger condition, six two-tails dependent-sample t-tests (i.e., three comparisons for each Surface geometry) were performed and the significance values were corrected using the Bonferroni method. Results showed that the group average JND was significantly higher in the Smooth/Dry condition with means difference of 3.10 um ($t(16) = 4.351$, $p_{corrected} = 0.003$, Cohen's d = 1.09, 95% CI [1.593 4.622]). Similarly, the group average JND in the Smooth/Dry condition was significantly higher than in the Smooth/Liquid condition with means difference of 3.95 um ($t(16) = 4.306$, $p_{corrected} = 0.003$, Cohen's d = , 95% CI [2.004 5.89]). No statistically significant difference

was found between Smooth/Water and Smooth/Liquid condition with means difference of 0.84 um (t(16) = 1.550, $p_{corrected}$ = 0.564, 95% CI [-0.31 1.99]). For the Rough surfaces, results showed that the group average JND in the Dry condition was significantly lower than the group average JND in the Water condition with means difference of -27.95 um (t(16) = -3.168, $p_{corrected}$ = 0.023, Cohen's d = 0.994, 95% CI [-46.65 -9.25]). No statistically significant difference was found between Rough/Dry and Rough/Liquid condition having means difference of -14.375 um (t(16) = -1.758, $p_{corrected}$ = 0.586, 95% CI [-31.70 2.95]), nor between Rough/Water and Rough/Liquid (means difference = 13.578, t(16) = 2.198, $p_{corrected}$ = 0.258, 95% CI [0.480 26.675]).

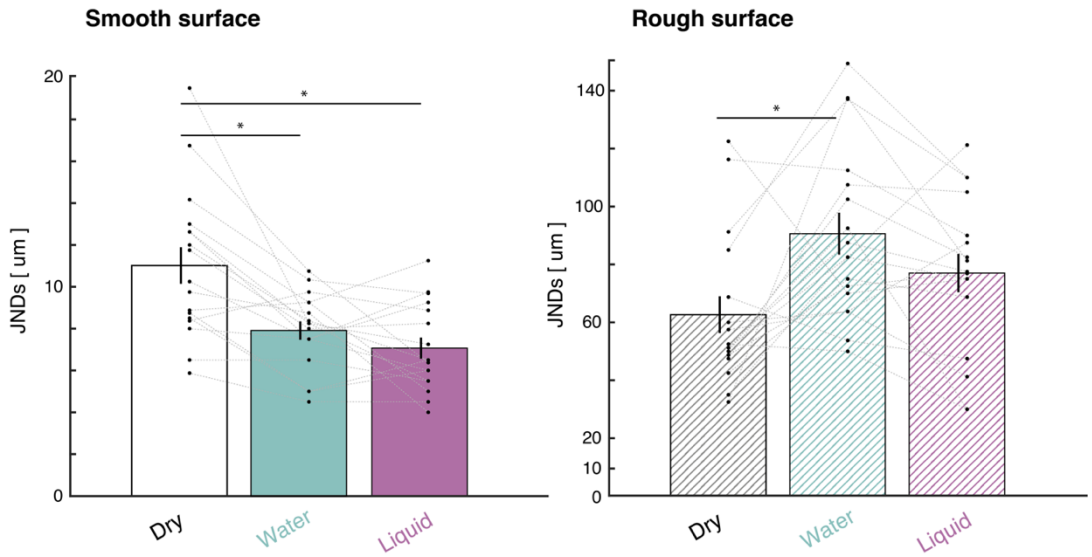

Figure 5.4. Behavioural results. Group average JNDs plotted as a function of Finger condition for Smooth surfaces (left) and Rough surfaces (right). Note the different scale of y-axis for Smooth and Rough surface. White bars show the average JNDs when the task was performed with dry finger. Light green bars show the average JNDs when the task was performed with moistened finger in water. Purple bars show the average JNDs when the task was performed with moistened finger in a solution of water and liquid soap. Error bars showed the SEM. Grey dots show individual JNDs. * p < α-Bonferroni corrected

5.4.2 Contact dynamics

To determine the effects of Surface geometry and Finger condition on the scanning speed, the mean normal and tangential forces, the coefficient of dynamic friction, and the RMS of

tangential force variations, a 2 (Surface geometry) x 3 (Finger condition) repeated measures ANOVA was performed in SPSS.

An example of the normal and tangential force traces for a single trial from participant 2 in each condition are shown in Figure 5.5. The traces show the modulation of normal and tangential forces across the different conditions. It is worth noting that the force recordings in the Smooth/Dry condition (Figure 5.5, top left quadrant) show multiple aperiodic oscillations (i.e., slow rise/sharp drop) generated by high friction and stick-to-slip transitions.

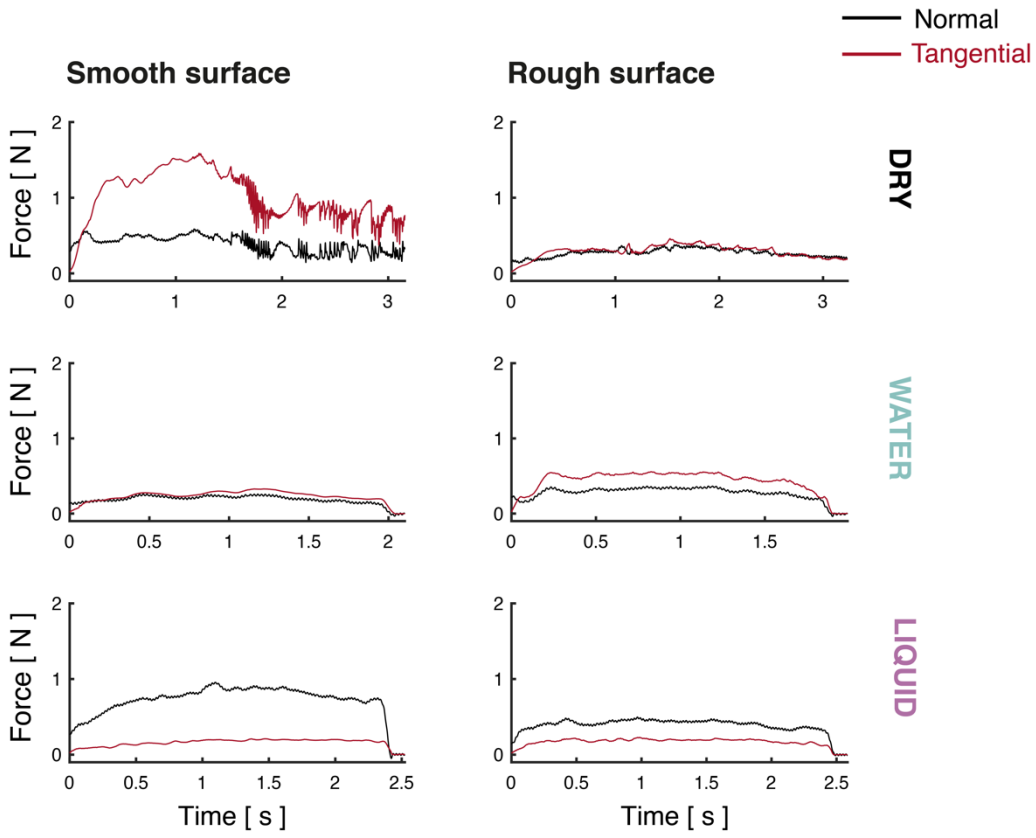

Figure 5.5. Force traces. Example of Normal **(black)** and Tangential **(red)** force traces recorded for participant 2 (trial 22, first interval) for Smooth **(left)** and Rough surfaces **(right).** The traces shown in the figure are trimmed and filtered following the procedure detailed in section 5.3.6 – Analysis of contact forces.

5.4.2.1 Scanning speed

Group average scanning speed is shown in Figure 5.6 for each condition. Scanning speed was computed by dividing the length of the surface (40 mm) by contact duration, assuming that all participants initiated and ended the scanning movement exactly from edge to edge. The mean (SD) speed was 18.45 mm/s (6.39) for Smooth/Dry surfaces, 17.24 mm/s (4.74) for Smooth/Water, and 18.09 mm/s (5.38) for Smooth/Liquid. For Rough/Dry surfaces mean (SD) scanning speed was 15.84 mm/s (4.12), 15.61 mm/s (3.31) for Rough/water, and 15.87 mm/s (3.53) for Rough/Liquid.

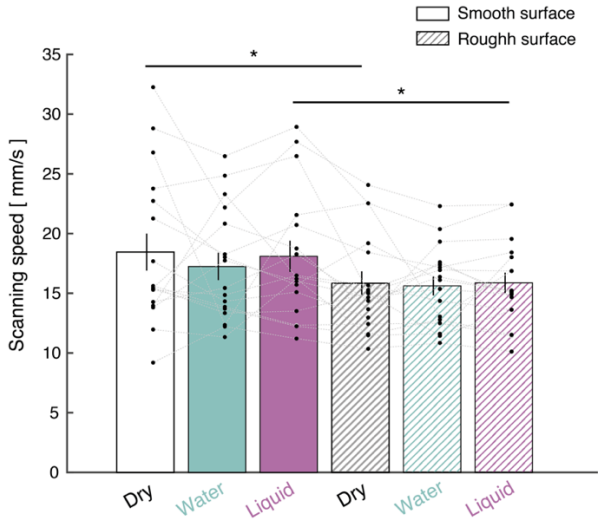

Figure 5.6. Scanning speed. Group average scanning speed for each condition. Uniform bars show data for Smooth surfaces. Striped bars for Rough surfaces. Black dots represent individual data; grey dotted lines connect individual data point between different conditions. Error bars show SEM. * $p < 0.05$, Bonferroni corrected.

Repeated measures ANOVA revealed that there was a significant main effect of Surface geometry ($F(1,16) = 12.836$, $p = 0.002$, $\eta_p^2 = 0.445$), but no main effect of Finger condition ($F(2,32) = 0.434$ $p = 0.651$, $\eta_p^2 = 0.02$), nor significant interaction ($F(2,32) = 0.754$, $p = .479$, $\eta_p^2 = 0.045$). Three two-tailed dependent-sample t-tests were performed to test which pair of Finger condition was significantly different between Smooth and Rough surfaces, p-values were corrected with Bonferroni method. Results showed that scanning speed was significantly higher in the Smooth/Dry when compared to Rough/Dry condition with means difference of 2.61 mm/s ($t(16) = 4.421$, $p_{corrected} = 0.01$, 95% CI [0.99 4.22]). Scanning speed

was also significantly higher in the Smooth/Liquid when compared to Rough/Liquid condition with means difference of 2.22 mm/s (t(16) = 2.817, $p_{corrected}$ = 0.036, 95% CI [0.55 3.89]). No significant difference was found between Smooth/Water and Rough/Water condition (t(16) = 2.216, $p_{corrected}$ = 0.123).

5.4.2.2 Normal forces

Group average normal force and standard deviation for each condition are summarised in Table 5.1 and illustrated more in detail in Figure 5.7a. Mauchly's test of Sphericity (Finger: $\chi^2(2) = 16.609$, p = 0.0002; Surface*Finger: $\chi^2(2) = 6.746$, p = 0.034) revealed that the normal force variances of the differences between each pair of Finger conditions and the interaction term were unequal and degrees of freedom to determine the significance of the F-ratio were adjusted using Greenhouse-Geisser correction.

	Smooth			**Rough**		
	Dry	*Water*	*Liquid*	*Dry*	*Water*	*Liquid*
Normal force (N)	0.36 (0.24)	0.58 (0.39)	1.22 (0.72)	0.75 (0.54)	0.86 (0.52)	1.13 (0.67)
Tangential force (N)	0.57 (0,50)	0.70 (0.35)	0.28 (0.15)	0.64 (0.41)	0.70 (0.44)	0.57 (0.31)
Coeff. Dynamic Friction	1.76 (0.90)	1.28 (0.17)	0.24 (0.04)	0.90 (0.21)	0.88 (0.31)	0.51 (0.06)
RMS of tangential force (N/s)	3.13 (1.58)	0.64 (0.96)	0.21 (0.11)	1.02 (0.57)	0.59 (0.46)	0.40 (0.15)

Table 5.1. Summary table of contact dynamics. Table shows the group average (SD) of normal and tangential force, coefficient of dynamic friction and rms of tangential force (normalised).

Results of a repeated measures ANOVA showed that there was no main effect of Surface geometry on the applied normal force (F(1,16) = 4.063, p = 0.061, η_p^2 = 0.203). Instead, a significant main effect of Finger condition was found (F(1.202, 19.239) = 27.718, p =

0.0000001, η_p^2 = 0.634), and a significant interaction between Surface geometry and Finger Condition (F(1.468, 23.491) = 4.478, p = 0.032, η_p^2 = 0.219). To reveal which pairs of means were statistically different across the levels of Finger condition, six two-tailed dependent-sample t-tests (i.e., three comparisons for each Surface geometry) were performed and the significance values were corrected with Bonferroni method. There was no significant difference between the normal force in the Smooth/Dry and Smooth/Water condition with means difference of -0.22 N (t(16) = -2.830, $p_{corrected}$ = 0.072, 95% CI [-0.38 -0.05]). Instead, a significantly lower normal force was found in the Smooth/Dry when compared to the Smooth/Liquid condition with means difference of -0.86 N (t(16) = -5.343, $p_{corrected}$ = 0.00039, 95% CI [-1.20 -0.52]), and in the Smooth/Water when compared to the Smooth/Liquid condition with means difference of -0.63 N (t(16) = -4.846, $p_{corrected}$ = 0.0011, 95% CI [-0.91 -0-36]). For what concerns the Rough surfaces, no significant difference was found in the applied normal force between any pair of the Finger conditions. The means difference between Rough/Dry and Rough/Water was -0.11 N (t(16) = -1.700, $p_{corrected}$ = 0.65, 95% CI [-0.24 0.03]; Rough/Dry – Rough/Liquid = -0.38 N (t(16) = -2.722, $p_{corrected}$ = 0.09, 95% CI [-0.68 -0.08]; Rough/Water – Rough/Liquid = -0.27 N (t(16) = -2.389, $p_{corrected}$ = 0.18, 95% CI [-0.51 -0.03]).

The overall trend was similar across the Finger Conditions for the two Surface geometries with lower normal forces applied in the Dry condition, slightly higher normal force in the Water condition, and highest normal forces in the Liquid condition.

5.4.2.3 Tangential forces

Group average tangential force and standard deviation for each condition are summarised in Table 5.1 and illustrated more in details in Figure 5.7b. Mauchly's test showed that sphericity assumption was met for the Finger condition factor (Finger: $\chi^2(2) = 2.776$, p = 0.25), but it was not for the interaction term (Surface*Finger: $\chi^2(2) = 6.793$, p = 0.033). Degrees of

freedom to determine the significance of the F-ratio were adjusted using Greenhouse-Geisser correction.

Results showed that there was no statistically significant difference in tangential force between the two Surface geometry conditions ($F(1,16) = 3.508$, $p = 0.079$, $\eta_p^2 = 0.180$), nor significant interaction between Surface geometry and Finger Condition ($F(1.466, 23.457) = 2.839$, $p = 0.092$, $\eta_p^2 = 0.151$). Instead, a significant difference was found for the three Finger conditions ($F(2, 32) = 8.064$, $p = 0.0014$, $\eta_p^2 = 0.335$). To reveal which pairs of means were statistically different across the levels of Finger condition, six two-tailed dependent-sample t-tests (i.e., three comparisons for each Surface geometry) were performed and the significance values were corrected with the Bonferroni method. Post-hoc multiple comparisons analysis showed that the average tangential force was significantly higher in the Smooth/Water when compared to Smooth/Liquid condition with means difference of 0.43 N ($t(16) = 6.463$, $p_{corrected} = 0.000048$, 95% CI [0.29 0.57]), and no significant difference was found in the other t-tests (Smooth/Dry– Smooth/Water = -0.14 N, $t(16) = -1.056$, $p_{uncorrected} = 0.307$, 95% CI [-0.42 0.14]; Smooth/Dry – Smooth/Liquid = 0.29 N, $t(16) = 2.345$, $p_{corrected} = 0.194$, 95% CI [0.02 0.55]; Rough/Dry – Rough/Water = -0.06, $t(16) = -0.713$, $p_{uncorrected} = 0.486$, 95% CI [-0.24 0.12]; Rough/Dry – Rough/Liquid = 0.07 N, $t(16) = 1.0002$, $p_{uncorrected} = 0.332$, 95% CI [-0.08 0.23]; Rough/Water – Rough/Liquid = 0.13 N, $t(16) = 1.894$, $p_{uncorrected} = 0.076$, 95% CI [-0.01 0.28]).

Overall, these results highlight that tangential forces did not vary systematically for the two surface geometries nor between dry and water conditions, while a decrease in tangential force was observed when wetting the finger with a solution of water and surfactant.

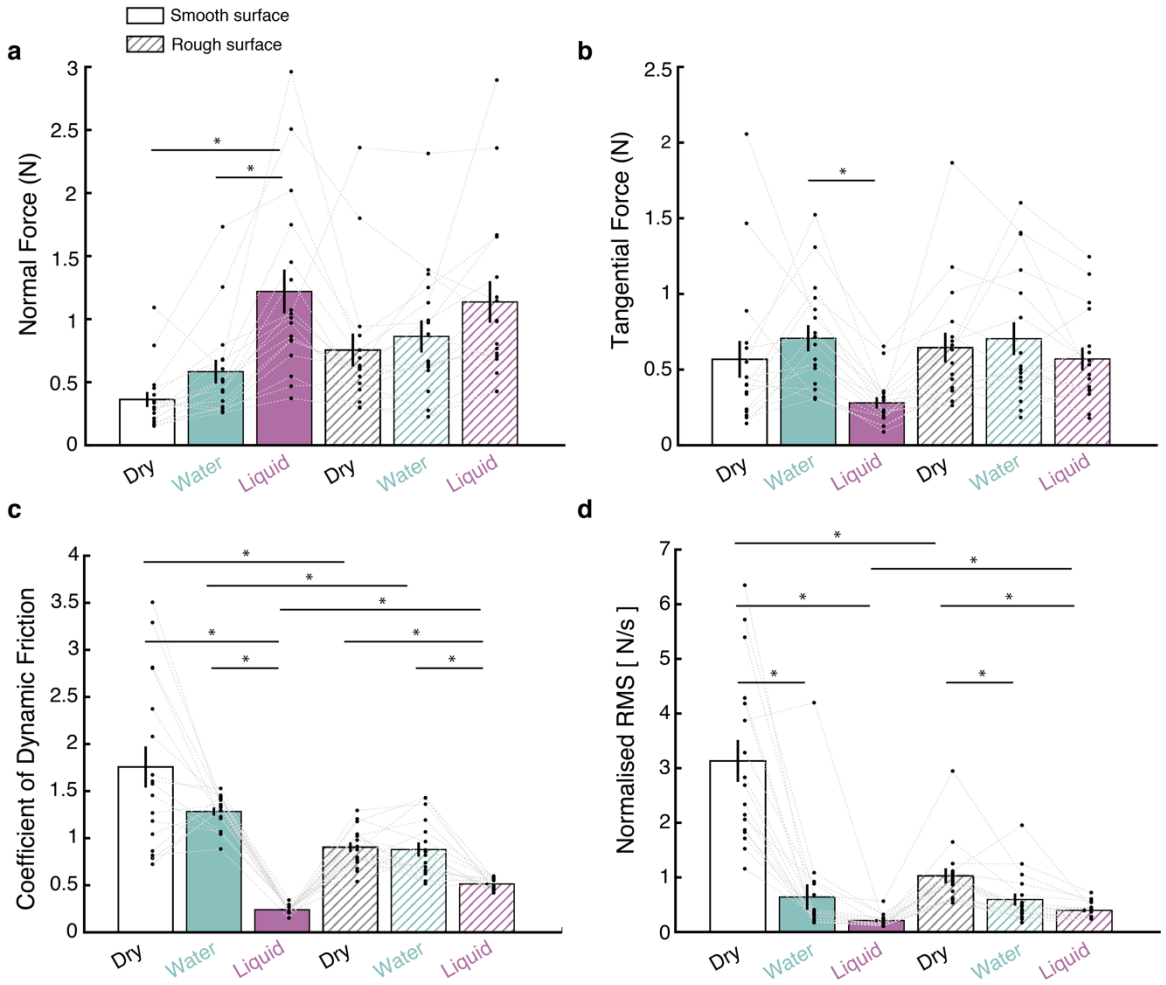

Figure 5.7. Contact dynamics. a) Group average normal forces, **b)** Group average tangential forces, **c)** Group average Coefficient of Dynamic friction (Fx / Fz), **d)** Group average normalised RMS of tangential force variations, plotted for each condition. Uniform bars show data for Smooth surfaces. Striped bars for Rough surfaces. Black dots represent individual data; grey dotted lines connect individual data point between different conditions. Error bars show SEM. * $p < 0.05$, Bonferroni corrected.

5.4.2.4 Coefficient of dynamic friction

Group average coefficient of dynamic friction and standard deviation for each condition are summarised in Table 5.1 and illustrated in more detail in Figure 5.7c. Mauchly's test showed that sphericity assumption was not met for the Finger condition factor (Finger: $\chi^2(2) = 21.978$, $p = 0.000017$), nor for the interaction term (Surface*Finger: $\chi^2(2) = 8.954$, $p = 0.011$). Degrees of freedom to determine the significance of the F-ratio were adjusted using Greenhouse-Geisser correction.

Results showed that there was a main effect of Surface geometry on the resulting coefficient of dynamic friction ($F(1,16) = 21.437$, $p = 0.0003$, $\eta_p^2 = 0.573$), and a significant main effect of Finger condition ($F(1.131, 18.090) = 44.802$, $p = 0.000002$, $\eta_p^2 = 0.737$). A significant interaction between Surface geometry and Finger Condition was found ($F(1.380, 22.077) = 22.088$, $p = 0.00003$, $\eta_p^2 = 0.580$). To reveal which pairs of means were statistically different across the levels of Finger condition, nine two-tailed dependent-sample t-tests (i.e., three comparisons for each Surface geometry, and three comparisons between surface geometry on each Finger condition) were performed and the significance values were corrected with Bonferroni method.

Post-hoc multiple comparisons analysis showed that the average coefficient of dynamic friction was significantly higher in the Smooth/Dry when compared to Smooth/Liquid condition with means difference of 1.51 ($t(16) = 6.864$, $p_{corrected} = 0.00003$, 95% CI [1.04 1.98]). The dynamic coefficient of friction was also significantly higher in the Smooth/Water than in the Smooth/Liquid condition with means difference of 1.04 ($t(16) = 24.570$, $p_{corrected} = 0.00004$, 95% CI [0.95 1.13]), but no significant difference was found between Smooth/Dry and Smooth/Water condition with means difference of 0.47 ($t(16) = 2.235$, $p_{corrected} = 0.36$, 95% CI [0.02 0.92]). For the Rough set, results showed the same pattern as in the Smooth set. There was no difference between Rough/Dry and Rough/Water condition with means difference of 0.025 ($t(16) = 0.347$, $p_{uncorrected} = 0.733$, 95% CI [-0.13 0.17]). The coefficient of dynamic friction was significantly higher for Rough/Dry than Rough/Liquid condition with means difference of 0.39 ($t(16) = 7.789$, $p_{corrected} = 0.000007$, 95% CI [0.28 0.50]), and significantly higher for Rough/Water than Rough/Liquid condition with means difference of 0.36 ($t(16) = 4.671$, $p_{corrected} = 0.0023$, 95% CI [0.20 0.53]). Analysis of the interaction effect showed that the coefficient of dynamic friction was significantly higher in the Smooth/Dry when compared to Rough/Dry condition with means difference of 0.85 ($t(16) = 4.636$, $p_{corrected} = 0.0025$, 95% CI [0.46 1.24]) and significantly higher for Smooth/Water than Rough/Water

condition with means difference of 0.40 (t(16) = 4.021, $p_{corrected}$ = 0.0089, 95% CI [0.13 0.58]). Finally, coefficient of dynamic friction was significantly lower in the Smooth/Liquid than the Rough/Liquid with means difference of -0.27 (t(16) = -18.489, $p_{corrected}$ = 2.8822e-11, 95% CI [-0.30 -0.24]).

5.4.2.5 RMS of tangential force variations

Group average normalised RMS of tangential force variations and standard deviation for each condition are summarised in Table 5.1 and illustrated more in details in Figure 5.7d. Mauchly's test showed again that sphericity assumption was not met for the Finger condition factor (Finger: $\chi^2(2) = 6.597$, p = 0.037), but it was for the interaction term (Surface*Finger: $\chi^2(2) = 4.186$, p = 0.123). Degrees of freedom to determine the significance of the F-ratio were adjusted using Greenhouse-Geisser correction.

A significant main effect of Surface geometry (F(1,16) = 19.759, p = 0.0004, η_p^2 = 0.553), Finger condition (F(1.475, 23.601) = 48.529, p = 3.1887E-8, η_p^2 = 0.752), and interaction term (F(1.608, 25.734) = 26.898, p = 0.000002, η_p^2 = 0.627) were found. Nine two-tailed t-tests were performed to compare each level of Finger Condition within the same and across Surface geometry. The significance level was corrected with Bonferroni method. The normalised rms of tangential force variations was significantly higher in the Smooth/Dry than the Smooth/Water condition with means difference of 2.49 N/s (t(16) = 6.109, $p_{corrected}$ = 0.00013, 95% Ci [1.62 3.35]). Similarly, the RMS in the Smooth/Dry was significantly higher than the Smooth/Liquid condition with means difference of 2.92 N/s (t(16) = 7.811, $p_{corrected}$ = 6.7922e-06, 95% CI [2.13 3.71]). No difference was found between Smooth/Water and Smooth/Liquid condition with means difference of 0.43 N/s (t(16) = 1.862, $p_{corrected}$ = 0.73, 95% CI [-0.06 0.92]). Again, for the Rough set results showed the same pattern as in the Smooth set. The RMS was significantly higher in the Dry condition when compared to the Water condition with means difference of 0.43 N/s (t(16) = 3.376, $p_{corrected}$ = 0.0347, 95% CI [0.16 0.70]). The rms was also significantly higher in the Rough/Dry compared to

Rough/Liquid condition with means difference of 0.63 N/s (t(16) = 5.290, $p_{corrected}$ = 0.00065, 95% CI [0.38 0.88]). No difference was found between Rough/Water and Rough/Liquid condition with means difference of 0.20 N/s (t(16) = 2.088, $p_{corrected}$ = 0.478, 95% CI [-0.003 0.40]). The comparison between Smooth/Dry and Rough/Dry revealed that the RMS was significantly higher for the Smooth surface with means difference of 2.10 N/s (t(16) = 6.020, $p_{corrected}$ = 0.0016, 95% CI [1.36 2.84]). There was no significant difference between the RMS in the Smooth/Water and the Rough/Water condition with means difference of 0.04 N/s (t(16) = 0.189, $p_{uncorrected}$ = 0.852, 95% CI. [-0.47 0.57]). Finally, the RMS in the Smooth/Liquid condition was significantly lower than the RMS in the Rough/Liquid condition with means difference of -0.19 N/s (t(16) = -6.943, $p_{corrected}$ = 0.00002, 95% CI [-0.24 -0.13]).

Again, we observed a similar trend across conditions showing a reduction of tangential force variations following the decrease in friction generated by the addition of water and a solution of water and liquid soap.

5.4.2.6 Skin hydration in the Dry condition

To determine whether the intrinsic skin hydration affected the way participants interacted with the surfaces and its effects on the sensitivity to our set of stimuli in the dry condition, a correlation analysis was performed between hydration and the estimated JNDs, the coefficient of dynamic friction, as well as the RMS of tangential force variations (Figure 5.8).

Results showed that there was a significant positive relationship between hydration and dynamic friction for Smooth surfaces (Pearson's r = 0.612 p = 0.009, 95% CI [0.19 0.84]) as well as for Rough surfaces (Pearson's r = 0.808 p = 0.0001, 95% CI [0.54 0.93]). In contrast, no significant correlation was found between hydration and the normalised rms of tangential force variations for both surface geometries (Smooth: Pearson's r = -0.14 p = 0.59, 95% CI [-0.58 0.36]; Rough: Pearson's r = -0.28 p = 0.27, 95% CI [-0.67 0.22]), nor between hydration

and detection sensitivity (Smooth: Pearson's r = 0.204 p = 0.43, 95% CI [-0.31 0.62]; Rough: Pearson's r = 0.183 p = 0.48, 95% CI [-0.32 0.61]),

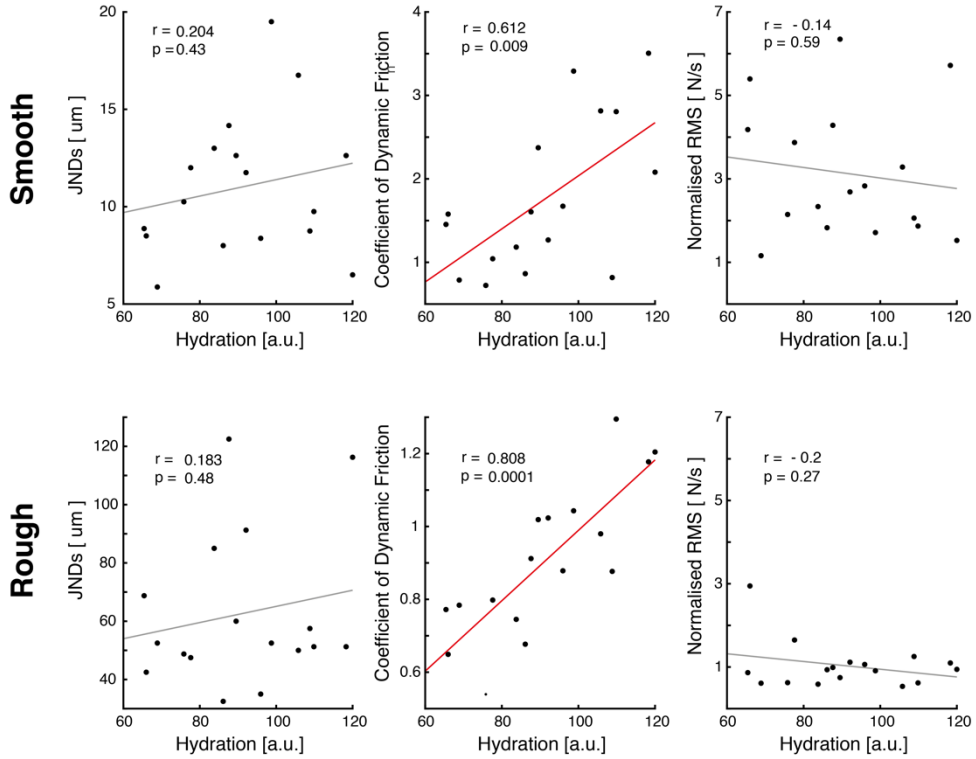

Figure 5.8. Correlation analysis between skin hydration and detection thresholds **(left panels)**, coefficient of dynamic friction **(middle panels)**, and normalised RMS of tangential force variations **(right panels)** for Smooth surfaces **(top row)** and Rough surfaces **(bottom row)**. Black lines show least-squares line for non-significant correlations. Red lines represent significant correlations.

5.5 Discussion

5.5.1 Microdot detection with dry finger

A combination of a psychophysical task with force recordings was employed to explore the effects of surface roughness and fluid environment on the contact dynamics and the detection sensitivity to a single microdot in young participants. To determine the microdot height detected at 75% correct rate, a 2-alternative forced-choice approach was used in which participant were actually asked to discriminate between a 'blank' surface and a target surface featuring a single microdot with different heights. The exploratory movement was

performed freely by the participants with the only constraints being the trial duration and the possibility to slide the finger only once from left to right.

Results showed that people have a very fine sensitivity to features at sub-millimetre scale, similarly to what has been observed previously (e.g., LaMotte and Whitehouse, 1986). In the detection task performed with dry finger, participants were able to detect a square-shape dot placed on a smooth surface with a side length of 300 microns and only 11 microns height. Detection thresholds for a microdot placed on a rough surface were also determined. In this condition, participants were able to detect a single square-shape dot raised about 60 microns above the surrounding dots. The surface roughness caused a 6-fold increase compared to the smooth surfaces. It is suggested that this might be due to skin vibrations generated before, during and after the contact with the single dot, in response to the surrounding rough geometry. These vibrations could have acted as ‘noise’ to the extent to which they activated the rapidly adapting receptors and potentially decreased the signal-to-noise ratio coming from the single dot.

Analysis of force recordings revealed that the coefficient of dynamic friction and the tangential force variations were higher for the smooth surfaces than the rough ones. This is likely due to a combination of the adhesive behaviour and deformation component resulting from the interaction between skin and surface properties. The higher friction and tangential force variations recorded on the smooth surfaces showed that the sliding movement was difficult to perform and characterised by slow and repeated stick-to-slip transitions. This was confirmed by participants who reported that it was difficult to slide on the smooth surface with dry finger and it is reflected in the profile of raw force traces for the Smooth surfaces which shows repeated aperiodic variations for most of the trials (Figure 5.5, top left panel). The presence of multiple stick-slip transitions has been previously reported for smooth polished surfaces (van Kuilenburg et al., 2013) which result in high variability of the friction measurement between and within participants.

Regarding the rough surfaces, the lower friction and tangential force variations compared to the smooth surfaces are likely due to the reduction of the finger real contact area as a result of the interaction between the irregular shape of the finger pad (i.e., fingerprints) and the asperities on the surface top as previously observed (Masen, 2011; Derler and Gerhardt, 2012; Arvidsson et al., 2017).

Interestingly, correlation analysis showed that the dynamic friction was positively related to the skin hydration of participants regardless of surface geometry, as previously shown (Gerhardt et al., 2008). However, no correlation was found between skin hydration and tactile sensitivity, nor between skin hydration and tangential force variations. Although individual variability of skin hydration may generate different frictional forces, this seemed not enough to determine the detection sensitivity to our set of stimuli.

Importantly, friction not only depends on the surface geometry and skin, but also on the material molecular properties which can reduce or increase the adhesion between the finger and the surface top. Thus, it would not be surprising to find different patterns of skin-surface interaction when using another material (e.g., matte/unpolished plexiglass).

5.5.2 Microdot detection with moistened finger

Results showed that moistening the finger with water, or a solution of water and soap, had a similar effect on the contact dynamics for the two surface geometries yet different behavioural outcomes. For the smooth surfaces, higher sensitivity with moistened finger was observed. Participants were able to detect the single dot with height of about 7 microns when task was performed after wetting the finger in water or a solution of water and soap, compared to 11 microns when the task was performed with dry finger. For the rough surfaces, instead, the average detection threshold was lower after wetting the finger.

Detection sensitivity was about 90 microns in the Rough/Water and 77 microns in the Rough/Liquid condition, compared to 60 microns in the Rough/Dry condition.

Coefficient of dynamic friction and tangential force variations were reduced with moistening regardless of surface geometry. It was observed an increase in the applied normal force when the finger was moistened but no major changes in the tangential forces. This pattern of contact dynamics can help explain why moistened finger improved sensitivity for smooth surfaces but worsened it for rough ones.

Sliding the dry finger on the smooth surfaces produced higher variations in tangential forces and frequent stick-slip effects compared to when the task was performed after wetting the finger. This shows that moistening the finger reduced the adhesion between the finger and the object, making the sliding movement easier to perform. This can be beneficial for two related reasons. First, the suppression of the irrelevant skin response caused by stick-slip event could have increased the signal-to-noise ratio for the single dot placed in the centre of the smooth surface. Second, a reduction of adhesion allowed participants to apply higher normal force without increasing the tangential force which could have been beneficial by possibly increasing microdot indentation and enhancing the response of mechanoreceptors when in contact with the microdot. In this context, the signal and noise inputs can be dissociated with positive effects on perception.

In contrast, for the rough surfaces the origin of noise is mostly the rough surface geometry itself rather than the adhesion force alone. As such, the signal coming from the single dot might not be separable from the noise produced by the rough background. The higher normal force observed with moistened finger might have increased the indentation of both the target microdot and the background dots resulting in higher noise and worse performance.

It is worth noting that although tangential force variations were dramatically reduced in the presence of water, there was no difference between the friction with dry finger and moistened finger regardless of surface geometry. This can be explained by two co-existing effects generated by the addition of water. The first is the reduced friction caused by the addition of a great amount of water on the surface top (Andrè et al., 2009), the second is the increased friction following the enlargement of the real contact area due to the softening of the skin with water and the slightly higher normal force applied in the presence of water.

5.6 Conclusion

The findings presented here highlight the complexity of skin-surface interaction and how it affects the way we interact and perceive object properties. The main reason is the nonlinear viscoelastic nature of the finger pad and the multiple factors affecting frictional forces acting during adhesion and sliding. Friction is modulated by the real contact area which in turn is affected by the applied normal force (Spinner et al., 2016), skin properties such as hydration level (Adams et al., 2013), the stiffness of the stratum corneum (Liu et al., 2015), elasticity (Wierteleski and Hayward, 2012), and fingerprint microgeometry (Prevost et al., 2009), as well as by object properties such as surface geometry (van Kuilenburg et al., 2013) and material molecular properties (Gueorgiev et al., 2016), or different fluid environments as shown here. This is further complicated by the high variability of finger properties across individuals which depend on age, sex (Yang et al., 2018), occupation and exposure to environmental factors (Langton et al., 2017), amongst other factors.

The results of this study can be summarised as follows:

1. Surface geometry and fluid environment affected detection sensitivity for a single microdot.

2. Rough surface geometry resulted in a deterioration of detection sensitivity in all fluid environments when compared to the sensitivity for the smooth surfaces.

3. Intrinsic skin hydration was positively related to the resulting friction when the exploration was performed with dry finger, yet it did not affect the variations of tangential force nor detection sensitivity.

4. Scanning speed was higher on the smooth surfaces than on the rough ones.

5. Moistening the finger with water and a solution of water and liquid soap reduced friction and the variations of tangential force regardless of surface geometry but with opposite effects on perception.

6. Microdot detection for smooth surfaces was improved with the addition of water and a solution of water and liquid soap.

7. Microdot detection for rough surfaces was poorer with the addition of water and a solution of water and liquid soap.

Chapter 6

General Discussion, Limitations, and Future Work

6.1 Overview

Psychophysical research on tactile perception has provided extensive evidence regarding human capabilities in detecting and discriminating a wide variety of stimuli. Several studies have investigated the limits of tactile perception suggesting that people are sensitive to features even at a sub-micron scale. Neurophysiology studies have gathered evidence regarding the characteristics of the peripheral neural response involved in the different aspects of touch, including spatial acuity and temporal sensitivity. This line of work also helped to develop computational models to simulate the peripheral neural response and overcome the limitations of microneurography. The investigation of finger tribology has shown the complexity of skin-object interaction and the large number of factors that can affect it, including skin and object properties. However, there are still several open questions regarding the relationship between the properties of the peripheral components of the tactile system and tactile sensitivity. In particular, the research presented in this dissertation is focused on: i) understanding the contribution of skin hydration, elasticity, and afferent density in the deterioration of spatial acuity observed with ageing with static touch (Chapter 4), and ii) providing new insights into how frictional changes generated by different surface geometry and moistening of the finger can influence the sensitivity to detect near-threshold stimuli (Chapter 5). These questions have been addressed by using a combination of simulations of first-order tactile neurons, psychophysics, measurements of finger properties, force recordings, and highly controlled stimuli.

In the following sections, I will summarise the review of simulations models presented in Chapter 3 (section 6.2) as well as the main findings of the empirical chapters (section 6.3 and 6.4) and their significance for tactile perception in relation to existing literature (section

6.5). I will discuss relevant limitations (section 6.6) and introduce future work planned to extend the findings presented here (section 6.7). Finally, I will provide concluding remarks on the relevance of the findings for tactile perception and their translational significance (section 6.8)

6.2 Simulating skin and mechanoreceptor response to tactile stimuli for static touch

In Chapter 3, I reviewed four of the most relevant models to simulate the activity of first-order tactile neurons. This work highlights the importance of having such models to reproduce the known response properties of first-order tactile neurons as well as realistic definition of finger composition and skin biomechanics. Simulation models can help overcoming the limitations embedded in microneurography and answer open questions regarding the function of first-order tactile neurons and the role of skin properties for tactile perception. In particular, simulating skin and mechanoreceptor response allows investigation of population response of afferent units with ease to test potential coding strategies for a wide range of stimuli and to assess how finger properties affect the mechanotransduction process and the informativeness of the neural response. I described four different models which differ in terms of how the skin is modelled, the type and response properties of mechanoafferent units implemented, the stimuli that can be reproduced, and their applications. These models are Gerling et al. (2014), Saal et al. (2017), Ouyang et al. (2020), and Hay and Pruszynski (2020).

The main difference between the models described here is their approach to simulate skin composition and its mechanical properties. Gerling et al. (2014) used finite element modelling to provide a realistic representation of the skin composition including different layers and hard structures (e.g., bone and nail) and its viscoelastic properties. This allows study of the contribution of individual factors (e.g., thickness of stratum corneum) to how the stress caused by mechanical input propagates through the skin and activates mechanoreceptors located at different depths. By contrast, Saal et al., (2017) employed

continuum mechanics to create a simplified definition of the skin while focusing on the modelling of the response properties of the afferent units. Their model treats the skin as flat, homogenous and elastic to facilitate the calculation of the stresses acting on the mechanoreceptors and to allow real-time generation of spike trains with precise spike timing as well as the implementation of most of the known response properties. Another approach is shown by Ouyang et al. (2020) who simplified the definition of the skin further to improve the efficiency of their model. Here, the skin is built as a resistance network consisting of multiple connected node each representing a first-order tactile neuron. Finally, Hay and Pruszynski (2020) did not include any aspect of skin biomechanics. Their virtual skin is modelled as a 12x12 mm grid uniquely designed for the arrangement of a set of virtual RA1 mechanoreceptors. The neural output is determined only by the distance between the stimulus and the receptors. Importantly, they included a model of second-order neurons (i.e., spinal cord and cuneate nucleus) and the integration of the signals coming from first-order neurons.

I highlighted how these models can be used in combination with psychophysics to investigate the nature of the tactile inputs and their relation to individual differences (e.g., skin properties in the ageing population) in order to clarify the peripheral mechanisms underlying tactile perception. I provided several application examples, including an edge orientation task (Delhaye et al., 2019), an experiment involving localising the point at which a hand-held rod is hit (Miller et al., 2018), and the experiment presented in Chapter 4 aimed at determining the contribution of skin elasticity, hydration and afferent density in the deterioration of tactile spatial acuity with ageing.

6.3 Finger properties in the deterioration of spatial acuity with ageing

In the experiment presented in Chapter 4, I investigated the link between finger properties and tactile spatial acuity in young and elderly people to understand which peripheral factors affect the deterioration of sensitivity observed with aging.

Participants were asked to discriminate between a single pin and a pair of adjacent pins at several separation distances (2-point discrimination task). The stimuli were indented orthogonally and statically on to the central portion of the finger pad through a robotic device to accurately control the stimulus parameters (e.g., applied force, speed of indentation, interstimulus interval). Being able to achieve a consistent stimulation across trials and participants allowed isolation of the contribution of individual finger properties to the peripheral neural response and subsequent perceptual judgments.

Skin biological elasticity, hydration and finger size were measured before the psychophysical task. In addition, I used a modelling approach (Saal et al., 2017) to generate the response of first-order tactile neurons to the same stimuli used in the actual experiment for the two age-groups. Simulation for young and elderly group differed in terms of Young's modulus and afferent density. The elderly group was modelled with lower value for Young's modulus (Boyer et al., 2009; Yang et al., 2018) and lower afferent density (Garcia-Piqueras et al., 2019). These parameters relate to biological elasticity and finger size, respectively.

Behavioural results confirmed that the ability to discern the spatial layout of stimuli is poorer in the ageing population compared to their younger counterpart. Analysis of finger measurements and age in relation to discrimination abilities suggested that the difference in spatial acuity between the two groups can be mostly explained by age. The contribution of finger properties was marginal, although commonality analysis revealed that finger size, biological elasticity and hydration were to some extent useful to explain the variance in the measured 2-point JNDs.

The simulation outcomes provided further insights into the relationship between finger properties and spatial acuity. Results showed that lower Young's modulus and loss of SA1 and RA1 afferent units negatively affected the encoding of stimulus information based on spike count, although the effects of Young's modulus was minimal. The simulated neural

activity showed higher variability for the young group than the older counterpart in terms of the neural spatial activation for the different stimuli. This variability was likely exploited by the classifier resulting in lower simulated thresholds for the young group.

The strong contribution of age to tactile sensitivity was expected as ageing involves not only a deterioration of skin properties but also changes that happen at a central level. Simulation results showed that lower afferent density had a great impact on the simulated JNDs which is associated with both ageing and finger size. However, behavioural thresholds were about two times higher than those derived from the simulations. This is not surprising as the simulations did not include higher stages of sensory processing (i.e., cortical somatosensory neurons). For example, cortical somatosensory representations may become less sharp (Kalisch et al., 2009), and older participants might have experienced difficulties in deploying sustained attention or in recalling sensory information after the interstimulus interval. Also, simulations did not include other peripheral changes that might occur with ageing such as altered size, morphology, and depth of mechanoreceptors (Garcia-Piqueras et al., 2019), and slower conduction velocities of peripheral nerve due to demyelination (Peters, 2002).

In regard to skin elasticity and hydration, results suggest that they might only play a marginal role in the deterioration of tactile spatial acuity. Although the elderly group had significantly lower skin elasticity and hydration than young participants, these factors did not show a strong relationship with the behavioural outcome. This was confirmed by simulations results showing only a minimal increase of the virtual thresholds (i.e., 0.09 mm increase) when elasticity was the only manipulation applied to the model.

Interestingly, lower afferent density, and to some extent lower skin elasticity, not only increased the asymptotic level of performance but also affected the temporal dynamics of the neural response. In particular, these manipulations resulted in a slower build-up of stimulus information which in turn may influence the way elderly people interact with objects.

Finally, it is interesting to note that the simulation results showed that different types of afferent unit can have overlapping functions (Chapter 4) as shown by the similar contribution of SA1 and RA1 to convey stimulus information. This is in contrast with the classical segregation model (Johnson et al., 2000; Johnson, 2001) but more and more evidence supports a convergence of functions, discussed by Saal and Bensmaia (2014).

6.4 The effects of finger tribology on detection sensitivity

In the second experimental chapter, I explored the effects of surface geometry and finger moistening on the ability to detect a single microdot. These manipulations were chosen to alter finger tribology in order to gauge the extent to which tactile sensitivity is associated with these changes.

Participants were asked to freely slide their finger once across smooth and rough surfaces featuring a single target dot raised a few microns above the surrounding area. They performed the same task with dry finger, after moistening the finger in water, or in a solution of water and soap. I measured skin hydration prior to the session performed with dry finger as well as the contact forces in all conditions to estimate normal and tangential forces, the coefficient of dynamic friction, and the variations of tangential force.

Results showed that people are very sensitive to tactile features at micron scale as previously shown (e.g., LaMotte and Whitehouse,1986). Participants were able to detect a square-shape microdot with a side length of 300 microns and only 11 microns height when the scanning movement was performed with dry finger on smooth surfaces. In contrast, the average detection threshold was 60 microns for the rough surface, 6-fold higher than for the smooth surface. This might have been caused by the reduction of the signal-to-noise ratio of the target dot due to the skin deformation generated by sliding the finger on the rough texture.

Force recordings showed that the contact with smooth surfaces was characterised by multiple stick-slip events reflecting strong adhesion between the finger and surface and suggestive of difficulty in performing the sliding movement. On the other hand, the contact with rough surfaces was characterised by periodic oscillations which suggest that this pattern was caused by the geometry itself. Correlation analysis for the data obtained when the task was performed with dry finger revealed that the intrinsic hydration of the finger pad was related to the dynamic friction, but no relationship was found with detection sensitivity and tangential force variations.

Interestingly, moistening the finger with water, or a solution of water and soap had similar effects on the contact dynamics yet opposite behavioural results. Detection sensitivity improved for smooth surfaces and decreased for the rough ones. The estimated threshold for the smooth set was about 7 microns when the finger was wet with water, or a solution of water and soap, compared to 11 microns with dry finger. For the rough texture, the threshold was about 90 microns and 77 microns for the task performed with moistened finger with water and with water and soap, respectively, compared to 60 microns with dry finger.
In contrast, the coefficient of dynamic friction and RMS of tangential force variations were reduced regardless of surface geometry. Also, normal force was higher when the task was performed with moistened finger on smooth surfaces, but no significant increase was observed for tangential force across conditions. These changes of contact dynamics can help explain the different behavioural outcome of moistening the finger for the two textures. This is likely due to the different nature of neural noise generated when making contact with smooth or rough surfaces, and the extent to which moistening the finger modulated the forces acting on the skin with consequences for the neural response.

The reduction of tangential force variations and less frequent stick-to-slip transitions for the smooth surfaces with moistened finger suggest that the adhesion between finger and object was lower and the sliding movement was easier to perform compared to when the task was

performed with a dry finger. The absence of irrelevant skin response due to continuous stick-slip events and the possibility to apply higher normal force without affecting friction are likely to have enhanced the neural signal-to-noise ratio for the single dot on the smooth surfaces. In regard to rough surfaces, the origin of noise is mostly the rough surface geometry itself rather than the adhesion force alone. In this case, the signal for the single microdot is yoked to the noise generated by the surrounding rough background. Applying higher normal force with moistened finger compared to dry finger, was detrimental as it increased the indentation of both the target microdot as well as of the surrounding microdots resulting in higher noise and worse performance.

6.5 The role of skin properties and finger tribology on tactile perception

The transformation of external inputs into a meaningful signal for tactile perception is not straightforward. This is due to the complexity of the mechanical response of the skin and the variability of its properties across individuals as well as changes that happens throughout our lifespan because of intrinsic and extrinsic factors. This is further complicated by the uncertainty regarding the function of the four types of first-order tactile neurons (e.g., segregated versus overlapped) and the presence of different potential encoding strategies (e.g., rate code versus temporal code). The research presented in this dissertation was focused on gaining a better understanding of the role of finger properties and tribology on tactile perception by leveraging on a combination of behavioural and modelling approaches. I investigated the contribution of skin elasticity, hydration and afferent density to static touch and spatial acuity as well as the effects of hydration and manipulation of finger tribology on detecting a microfeature with sliding touch.

Results of the two-point discrimination task (Chapter 4) showed that skin elasticity and hydration were not critical to determine the spatial sensitivity in young and elderly participants. Although the two age-groups significantly differed in terms of skin properties, this difference was not strongly related to the observed difference in behavioural

performance. Similarly, intrinsic skin hydration was not related to the sensitivity to detect a single microdot while the external manipulation of hydration and finger friction did affect the behavioural outcome. These findings corroborate previous studies showing that hydration and skin compliance, related to skin elasticity, are not the main determinants of the sensitivity to statically indented stimuli, although their role is more evident for dynamic touch. For example, Woodward (1993) showed that cutaneous compliance is not a significant predictor of the performance in the two-point and gap discrimination tasks assessed on 102 participants ranging from 18 to 84 years of age on the finger pad. Similarly, Vega-Bermudez and Johnson (2004) observed that elderly performance was poorer than the younger counterpart in the grating orientation task although the skin conformance of the two group did not differ substantially. Moreover, Leveque and colleagues (2000) found no correlation between skin hydration of the cheek and changes in sensitivity threshold for the gap-detection task measured before and after the application of a moisturiser on 12 elderly women (69.5 ± 5 years old).

On the other hand, skin hydration and biological elasticity seems to be relevant when sensing the object with active exploration, as shown in Chapter 5 and several previous studies. In particular, the external manipulation of these properties by using water, moisturiser, or solution of water and surfactant, can have consequences on perceptual abilities. Verrillo (1998) showed that moistening the finger with distilled water, or a solution of water and surfactant (sodium dodecyl sulphate) results in a reduction of perceived roughness of sandpaper samples sensed by active movement. Smith et al. (2002) reported similar results. In their experiment, participants provided lower magnitude estimates of roughness for surfaces featuring rectangular arrays of truncated cones coated in lubricant compared to the same dry surfaces. More recently, Skedung et al. (2018) showed that applying a moisturiser containing glycerol increased the hydration and the elasticity of the finger pad skin of elderly women with improvements on their abilities to discriminate between two surfaces with different roughness.

These findings suggest that the role of hydration and elasticity for discriminating or detecting tactile features becomes evident in the presence of tangential displacement acting on the skin and friction. Abrupt changes of hydration due to external manipulations can have both positive or negative effects depending on the task and initial state of the finger (e.g., very dry skin versus hydrated skin). It is worth mentioning that the amount of intrinsic hydration was not predictive of detection sensitivity in our pool of participants while individual differences were correlated to differences in friction generated when sliding the dry finger across the surfaces, regardless of surface geometry (Chapter 5). This might be due to the fact that the tactile system can, to some extent, adapt to the actual skin properties through experience in order to maximise perception.

A methodological consideration that stems from this thesis is the importance of controlling, or at least measuring, stimulus parameters, or in general the contact dynamics when sensing tactile objects. In the experiment presented in Chapter 4, I employed a robotic arm to deliver parameter-controlled stimuli indented orthogonally and statically into the skin. Being able to achieve a consistent pattern of stimulation in terms of indentation force, speed, and interstimulus interval, together with measurements of finger properties, allowed the effects of stimulation protocol and finger properties to be disentangled from the actual tactile sensitivity. On the other hand, the recordings of contact dynamics carried out in the experiment illustrated in Chapter 5 allowed examination of the effects of skin-object interaction on detection sensitivity in the presence of an unconstrained sliding movement to sense the surface. Using unconstrained movements allowed participants to freely choose and adapt their movement to maximise perception and then analyse the forces acting on the skin to gain insights into the role of skin properties (e.g., hydration) and frictional changes.

6.6 Limitations

There are several issues related to the methods used in this thesis. In this section, I will focus on the general limitations of the simulation models to generate the activity of first-order

tactile neurons, the caveats of using the Cutometer to measure skin mechanical properties, and the potential lack of generalisability of the results presented in Chapter 4 and 5 to different stimuli.

Simulation models have gained momentum in recent years as they allow the limitations of microneurography to be overcome. Recording the activity of nerve fibres is invasive, slow and technically difficult to perform, sessions are usually short and stimulation is passive to avoid nerve damage, and it is possible to record only from a single or a few afferent fibres at the time. Modelling the skin response and the subsequent activation of mechanoafferent units offer the possibility to perform virtual experiments and test new hypothesis with ease. The main advantage is to look at the population activity which is critical to understand tactile coding strategies. However, the current state-of-the-art models have two major limitations. First, there is a trade-off between a realistic definition of the finger structure and skin composition and the efficiency of computing the mechanical deformation and the stresses acting on the mechanoreceptors. Finite element modelling allows the creation of the different layers of the skin with their own characteristics (e.g., stiffness, elasticity) and even subject-specific definition of the finger including bones and muscles, yet it requires long computation time to estimate skin deformation and it is not accessible to every researcher. On the other hand, continuum mechanics simplifies the definition of finger composition and skin properties which makes this approach computationally efficient and easy to implement but limited in the extent to which the relationship between skin properties and neural activation can be studied. Second, there is a lack of understanding of the skin biomechanical response and subsequent neural activation under active touch (e.g., sliding). Although finite element modelling is suited to simulate the evolution of skin deformation and the neural response with active exploration, there is limited evidence to validate the models and compare results on this aspect.

Measuring skin mechanical properties is critical to investigate the relationship between tactile inputs and perception. For example, it offers the possibility of ruling out the potential contribution to tactile sensitivity of individual differences in skin properties.

In the experiment presented in Chapter 4, I used the Cutometer to characterise skin biological elasticity in young and elderly in order to assess whether loss of elasticity is predictive of the poorer performance in the elderly group. Although this device is widely used in cosmetics and fundamental research, the lack of a standardised measurement protocol as well as its susceptibility to factors other than the property of interest requires careful consideration when interpreting the results and their generalisability. The measurements are usually carried out by the experimenter holding the probe in their hand and making contact with the area of the skin that they want to study. This approach is susceptible to the details of the interaction between the probe and the skin including the applied load, the exact location of the measurement, and small movements between the experimenter and the participant. Moreover, the absolute parameters of the Cutometer are a function of skin thickness making difficult to compare results between participants or body area, unless skin thickness can be measured, and corrections are made. Finally, measures of elasticity and stiffness are also dependent on the method used to record them (e.g., suction versus indentation) due to the intrinsic properties of the skin which results in contrasting findings, for example, on ageing effects on skin. Taken together, these concerns should be kept in mind when relating previous studies to each other or, in general, when analysing this type of data.

The last concern is related to the stimuli used in the experimental chapters and the generalisability of the results. In Chapter 4, I investigated tactile spatial acuity by employing the 2-point discrimination task. Although this classic paradigm is widely used in clinical settings and research, there are several authors questioning its reliability. The main issues are the low sensitivity to assess sensory deficit or recovery of peripheral components of tactile system in clinical application, the highly variable results across participants reported in perception studies, and sometimes lack of correlation with other measures of spatial acuity

(e.g., grating orientation discrimination). Usually, this test is carried out manually by the experimenter who might not press the two-points simultaneously and so generate a temporal delay that can be used to detect the two-point stimulus. In addition, there is variability in the method used to estimate sensitivity threshold in terms of instructions given to participants (e.g., “respond one-point if unsure”), and the presence of a comparison stimulus (e.g., both single- and two-point presented on each trial versus either one or the other). These factors are likely to contribute to the poor sensitivity and reliability of this paradigm. In the two-point discrimination experiment (Chapter 4), stimuli were highly controlled and indentation parameters consistent across and within participants thanks to the Force Dimension Delta 3 robot. However, it has not been established that the findings generalise to other tasks regarded as more rigorous such as the grating orientation task, and future experiment are needed to corroborate results.

In Chapter 5, I investigated the effects of surface geometry and moistening of the finger on the contact forces and the detection sensitivity for a single microdot in young participants. The stimuli used in this experiment were stainless steel plates which have hydrophilic properties. This means that the water tends to spread across and stick to the surface, maximising contact. Results showed a decrease in friction with the addition of water and behavioural results also showed the influence of surface geometry on detection sensitivity. However, due to the wide variety of materials, surface geometries, and the highly variable properties of the skin between people, there are several questions that were not addressed in this study. How does skin-surface friction change when adding water on hydrophobic materials, and what are the consequences for perception? How does moistening of the finger affect perception in subjects with very dry skin (e.g., elderly)? What is the contribution of, and to what extent does specific surface roughness affect skin-object interaction and perception?

6.7 Future work (planned experiments)

In this section, I will describe the ideas and motivation for two experiments to further study the relationship between finger properties and tactile perception. These include an extension of the microdot results to elderly participants (section 6.6.1) and a vibrotactile frequency discrimination task in young and elderly (section 6.6.2).

6.7.1 The effects of age and restoring hydration on finger tribology and the detection of a single microdot

Finger tribology depends on a variety of factors including skin and object properties. The former includes skin hydration and in general the biomechanical behaviour of the skin which depends on individual difference, exposure to environmental factors, and age. The latter refers to surface geometry, compliance, as well as material molecular properties. All together, these aspects determine the way we interact with objects and, as shown in Chapter 5, they can affect our detection sensitivity when friction is manipulated by surface geometry and moistening of the finger.

In this planned experiment, the goal is to further investigate the relationship between detection abilities and finger tribology in the elderly population. The progressive decrease of hydration and elasticity observed with ageing determine the frictional forces between the finger and the surface as shown by Skedung et al. (2018). They also showed that temporarily restoring hydration and elasticity with the application of a moisturiser increase the ability to discriminate between different surface roughness. The research question of this experiment is whether detection sensitivity to a single microdot is affected by age and the loss of hydration and elasticity, and to determine whether increasing hydration of the skin can improve performance.

The experiment is designed in the same way as the one presented in Chapter 5 so that results can be compared between age-groups. The method of constant stimuli with two-

alternative forced-choice and force recordings will be used to estimate friction and other contact dynamics of interest. Elderly participants will perform the task with dry finger, moistened finger in water and a solution of water and soap on both smooth and rough surfaces.

6.7.2 The role of skin and mechanoreceptors properties on frequency discrimination in young and elderly

Vibrotaction, or vibrotactile (temporal) sensitivity is involved with the ability to detect and discriminate stimuli that generate an oscillatory response in the skin. Vibrational inputs generated by active movement allow perception of different textures and materials that would be otherwise impossible with static contact such as surface roughness in the submicron scale (LaMotte and Srinivisan, 1991). Vibrotaction is also important in tool use where vibrations propagating across the tool are the only source of information. For example, Klatzky and Lederman (1999) showed that roughness discrimination can be achieved through a rigid link with similar sensitivity to bare finger.

Measurements of vibration perception threshold (VPT) has been widely used to investigate the detection sensitivity to vibrations delivered across a variety of frequency in both young and elderly. VPT is traditionally used in neurological assessment to evaluate the state of the tactile peripheral sensory components such as potential peripheral neuropathy following medical treatment (e.g., chemotherapy), or a medical condition (e.g., diabetes). Several studies have reported a worsening of VPT with healthy ageing (Verrillo, 1980) in both low and high frequency range. Vibrotaction detection thresholds have been investiaged across a range of frequenices. However, vibrotactle frequency discrimination itself has received little attention and its progression throughout the lifespan is unknown.

The aim of this experiment is to investigate the relationship between finger properties and frequency discrimination abilities in young and elderly, with a focus on afferent density and

simulations of first-order tactile neurons response, skin biological elasticity and hydration. To do so, this study will employ psychophysics, simulation of tactile neurons' activity and measurements of finger properties. The goal is also to evaluate frequency discrimination as an additional measure (in addition to VPT) to assess vibrotaction in people who suffer, or may suffer, from peripheral neuropathy (diabetic, chemotherapy patients, elderly). The advantage of having two measures could be important for a thorough evaluation so to provide a more accurate picture of the current state of the peripheral components of touch with only a minimal increase of testing time. In addition, knowing the relationship between skin properties and frequency discrimination can also help to rule out other factors when assessing the state of the peripheral neurons.

The experiment will individually address the discrimination ability at low frequencies, which mainly activate Merkel's and Meissner's cells, and at high frequencies, which mainly activates Pacinian corpuscles. To target specific sensory channels, two frequencies will be used as the comparison stimuli. 30 Hz was selected to target RA1 units (Meissner's cell) with likely some response from SA1 units (Merkel's cell), while 300 Hz to target RA2 units (Pacinian Corpuscles). RA1 units respond to frequencies in the range 1 to 300 Hz and are most sensitive between 5 and 50 Hz. RA2 units have a broader sensitivity from 5 to 1000 Hz and are most sensitive between 5 and 300 Hz (Bolanowski et al., 1988). As aging is accompanied by a major loss of Merkel's and Meissner's cell, ageing effects are expected to have a bigger impact on the lower frequency range.

To corroborate behavioural findings, simulations of the experiment will be performed with the model of Saal et al. (2017). The virtual experiment will accurately reproduce the stimulus parameters (e.g., contact area, vibration frequency, etc) and test whether introducing the manipulations that characterise the elderly group (e.g., lower afferent density, lower elasticity) affect the informativeness of the neural response.

6.8 Concluding remarks

The work described in this thesis has spanned the use of computational modelling informing robust psychophysical methods for determining detection and discrimination thresholds under conditions with contact forces accurately controlled or measured for high resolution tactile stimuli.

The results have provided a clearer understanding of the peripheral factors involved in tactile processing with important implications for fundamental research. It has been shown that the progressive loss of mechanoafferent units plays a crucial role in the deterioration of spatial acuity observed with ageing and static touch. This was the case when only the firing rate of the simulated neurons was taken into account to determine the informativeness of the neural response. These findings represent a starting point to evaluate different coding strategies in relation to afferent density and tactile perception with both static and sliding touch.

Skin biomechanics was found to be relevant in the context of sliding touch when manipulations of friction were introduced to affect the interaction between the skin and the object. The complex relationship between skin properties and surface geometry provided interesting results that needs to be extended to different materials, geometries, age-groups, and other factors (e.g., wearing gloves) to better understand how they affect tactile sensitivity.

Finally it is worth noting the collaborative nature of this project, jointly funded by University of Birmingham and Procter & Gamble, which suggests the translational potential of the work. The experiments summarised in the thesis describe important factors affecting touch that may have a bearing on the ability to detect food deposits when washing dishes by hand. The methods used may be expected to help understand the impact of changing the formulation of dishwashing products to benefit the experience of customers. For example, the findings of the microdot detection experiment suggest that subjective experience of cleanliness might

depend on the material and roughness of the object we are assessing when washing up. Thus, a food deposit is likely to be easier to detect on a smooth metal spoon rather than on a rough cast iron pan, and this will also be dependent on whether the user is exploring the surface under water or with dry hands. The methods developed in this thesis will allow practical issues such as these to be taken forward.

References

Abraira, V. E., & Ginty, D. D. (2013). The sensory neurons of touch. *Neuron*, *79*(4), 618-639.

Adams, M. J., Johnson, S. A., Lefèvre, P., Lévesque, V., Hayward, V., André, T., & Thonnard, J. L. (2013). Finger pad friction and its role in grip and touch. *Journal of the Royal Society Interface*, *10*(80).

Agache, P. (Ed.). (2000). *Physiologie de la peau et explorations fonctionnelles cutanées*. Edition Medicale International.

Aktar, T., Chen, J., Ettelaie, R., Holmes, M., & Henson, B. (2017). Human roughness perception and possible factors effecting roughness sensation. *Journal of Texture Studies*, *48*(3), 181-192.

Alloway KD, Burton H (1991) Differential effects of GABA and bicuculline on rapidly- and slowly-adapting neurons in primary somatosensory cortex of primates. Exp Brain Res 85:598–610.

Amaied, E., Vargiolu, R., Bergheau, J. M., & Zahouani, H. (2015). Aging effect on tactile perception: Experimental and modelling studies. *Wear*, *332*, 715-724.

Andersen P, Eccles JC, Sears TA (1964b) The ventrobasal complex of the thalamus: types of cells, their responses and their functional organization. J Physiol (Lond) 174:370–399.

André, T., Lefèvre, P., & Thonnard, J. L. (2009). A continuous measure of fingertip friction during precision grip. *Journal of neuroscience methods*, *179*(2), 224-229

André, T., Lévesque, V., Hayward, V., Lefevre, P., & Thonnard, J. L. (2011). Effect of skin hydration on the dynamics of fingertip gripping contact. *Journal of The Royal Society Interface*, *8*(64), 1574-1583.

Andrews, J. W., Adams, M. J., & Montenegro-Johnson, T. D. (2020). A universal scaling law of mammalian touch. *Science advances*, *6*(41), eabb6912.

Arvidsson, M., Ringstad, L., Skedung, L., Duvefelt, K., & Rutland, M. W. (2017). Feeling fine - the effect of topography and friction on perceived roughness and slipperiness. *Biotribology*, *11*(October 2016), 92–101.

Ayer, M., Brunk, H.D., Ewing, G.M., Reid, W.T., & Silverman, E. (1955). An empirical distribution function for sampling with incomplete information. Annals of Mathematical Statistics, 26, 641-647.

Bäuerle D. Ultrashort pulse laser ablation. In: Laser Processing and Chemistry, New York: Springer, 2000, pp.259-281.

Bensmaia, S. J., & Hollins, M. (2003). The vibrations of texture. *Somatosensory & motor research*, *20*(1), 33-43.

Bensmaia, S. J., Denchev, P. V., Dammann, J. F., Craig, J. C., & Hsiao, S. S. (2008b). The representation of stimulus orientation in the early stages of somatosensory processing. *Journal of Neuroscience*, *28*(3), 776-786.

Bensmaia, S. J., Hsiao, S. S., Denchev, P. V., Killebrew, J. H., & Craig, J. C. (2008). The tactile perception of stimulus orientation. *Somatosensory & motor research*, *25*(1), 49-59.

Birznieks, I., Jenmalm, P., Goodwin, A. W., & Johansson, R. S. (2001). Encoding of direction of fingertip forces by human tactile afferents. *Journal of Neuroscience*, *21*(20), 8222–8237.

Blake, D. T., Hsiao, S. S., & Johnson, K. O. (1997). Neural coding mechanisms in tactile pattern recognition: the relative contributions of slowly and rapidly adapting mechanoreceptors to perceived roughness. *Journal of Neuroscience*, *17*(19), 7480-7489.

Bolanowski Jr, S. J., Gescheider, G. A., Verrillo, R. T., & Checkosky, C. M. (1988). Four channels mediate the mechanical aspects of touch. *The Journal of the Acoustical society of America*, *84*(5), 1680-1694.

Bowden, J. L., & McNulty, P. A. (2013). Age-related changes in cutaneous sensation in the healthy human hand. *Age*, *35*(4), 1077-1089.

Boyer, G., Laquièze, L., Le Bot, A., Laquièze, S., & Zahouani, H. (2009). Dynamic indentation on human skin in vivo: ageing effects. *Skin Research and Technology*, *15*(1), 55-67.

Bradley, R. M., & Mistretta, C. M. (1975). Fetal sensory receptors. *Physiological reviews*, *55*(3), 352-382.

Brothers, T., & Hollins, M. (2014). Two sensory channels mediate perception of fingertip force. *Perception*, *43*(10), 1071-1082.

Chichkov BN, Momma C, Nolte S, von Alvensleben, F and Tunnermann A. Femtosecond, picosecond and nanosecond laser ablation of solids. Applied Physics A 1996; 63(2): 109–115.

Cole, J. (2016). *Losing touch: a man without his body*. Oxford University Press.

Connor, C. E., & Johnson, K. O. (1992). Neural coding of tactile texture: comparison of spatial and temporal mechanisms for roughness perception. *Journal of Neuroscience*, *12*(9), 3414-3426.

Corniani, G., & Saal, H. P. (2020). Tactile innervation densities across the whole body. *Journal of Neurophysiology*, *124*(4), 1229-1240.

Craig, J. C. (1999). Grating orientation as a measure of tactile spatial acuity. *Somatosensory & motor research*, *16*(3), 197-206.

Crosby, P. M., & Lee Dellon, A. (1989). Comparison of two-point discrimination testing devices. *Microsurgery*, *10*(2), 134-137.

Daly, C. H. (1982). Biomechanical properties of dermis. *Journal of Investigative Dermatology*, *79*(Suppl. 1), 17–20.

Dandekar K, Raju BI, Srinivasan MA. 3-D finite-element models of human and monkey fingertips to investigate the mechanics of tactile sense. J. Biomech. Eng.-Trans. ASME. Oct; 2003 125(5): 682–691.

de Haan, E. H., & Dijkerman, H. C. (2020). Somatosensation in the brain: A theoretical re-evaluation and a new model. *Trends in Cognitive Sciences*.

Delhaye, B. P., Xia, X., & Bensmaia, S. J. (2019). Rapid geometric feature signaling in the simulated spiking activity of a complete population of tactile nerve fibers. *Journal of neurophysiology*, *121*(6), 2071-2082.

Dellon, A. L., Mackinnon, S. E., & Crosby, P. M. (1987). Reliability of two-point discrimination measurements. *The Journal of hand surgery*, *12*(5), 693-696.

Dequeker, J., & Vadakethala, P. (1979). Soft-tissue measurements at the index finger: age and sex characteristics. *Clinical Radiology*, *30*(5), 513-515.

Derler, S., & Gerhardt, L. C. (2012). Tribology of skin: review and analysis of experimental results for the friction coefficient of human skin. *Tribology Letters*, *45*(1), 1-27.

Detorakis, G. I., & Rougier, N. P. (2012). A neural field model of the somatosensory cortex: formation, maintenance and reorganization of ordered topographic maps. *PloS one*, *7*(7), e40257.

DiCarlo, J. J., Johnson, K. O., & Hsiao, S. S. (1998). Structure of receptive fields in area 3b of primary somatosensory cortex in the alert monkey. *Journal of neuroscience*, *18*(7), 2626-2645.

Dillon, Y. K., Haynes, J., & Henneberg, M. (2001). The relationship of the number of Meissner's corpuscles to dermatoglyphic characters and finger size. *The Journal of Anatomy*, *199*(5), 577-584.

Diridollou, S., Vabre, V., Berson, M., Vaillant, L., Black, D., Lagarde, J. M., Grégoire, J. M., Gall, Y., & Patat, F. (2001). Skin ageing: Changes of physical properties of human skin in vivo. *International Journal of Cosmetic Science*, *23*(6), 353–362.

Dodson MJ, Goodwin AW, Browning AS, Gehring HM. 1998. Peripheral neural mechanisms determining the orientation of cylinders grasped by the digits. The Journal of Neuroscience 18:521–530.

Duvefelt, K., Olofsson, U., Johannesson, C. M., & Skedung, L. (2016). Model for contact between finger and sinusoidal plane to evaluate adhesion and deformation component of friction. *Tribology International*, *96*, 389–394.

Fallon, J. B., & Macefield, V. G. (2007). Vibration sensitivity of human muscle spindles and Golgi tendon organs. *Muscle & Nerve: Official Journal of the American Association of Electrodiagnostic Medicine*, *36*(1), 21-29.

Friedman RM, Khalsa PS, Greenquist KW, LaMotte RH. 2002. Neural coding of the location and direction of a moving object by a spatially distributed population of mechanoreceptors. The Journal of Neuroscience 22: 9556–9566.

Fruhstorfer, H., Abel, U., Garthe, C. D., & Knüttel, A. (2000). Thickness of the stratum corneum of the volar fingertips. *Clinical Anatomy: The Official Journal of the American Association of Clinical Anatomists and the British Association of Clinical Anatomists*, *13*(6), 429-433.

García-Piqueras, J., García-Mesa, Y., Cárcaba, L., Feito, J., Torres-Parejo, I., Martín-Biedma, B., ... & Vega, J. A. (2019). Ageing of the somatosensory system at the periphery: age-related changes in cutaneous mechanoreceptors. *Journal of anatomy*.

Gardner, E. P. (1988). Somatosensory cortical mechanisms of feature detection in tactile and kinesthetic discrimination. *Canadian journal of physiology and pharmacology*, *66*(4), 439-454.

George, J. A., Kluger, D. T., Davis, T. S., Wendelken, S. M., Okorokova, E. V., He, Q., ... & Marasco, P. D. (2019). Biomimetic sensory feedback through peripheral nerve stimulation improves dexterous use of a bionic hand. *Science Robotics*, *4*(32), eaax2352.

Gerhardt, L. C., Strässle, V., Lenz, A., Spencer, N. D., & Derler, S. (2008). Influence of epidermal hydration on the friction of human skin against textiles. *Journal of the Royal Society Interface*, *5*(28), 1317-1328.

Gerling, G. J., & Thomas, G. W. (2005). The effect of fingertip microstructures on tactile edge perception. *Proceedings - 1st Joint Eurohaptics Conference and Symposium on Haptic Interfaces for Virtual Environment and Teleoperator Systems; World Haptics Conference, WHC 2005*, *January*, 63–72.

Gerling, G. J., Rivest, I. I., Lesniak, D. R., Scanlon, J. R., & Wan, L. (2013). Validating a population model of tactile mechanotransduction of slowly adapting type I afferents at

levels of skin mechanics, single-unit response and psychophysics. *IEEE transactions on haptics*, *7*(2), 216-228.

Gescheider, G. A. (2013). *Psychophysics: the fundamentals*. Psychology Press.

Gescheider, G. A., Beiles, E. J., Checkosky, C. M., Bolanowski, S. J., & Verrillo, R. T. (1994). The effects of aging on information-processing channels in the sense of touch: II. Temporal summation in the P channel. *Somatosensory & motor research*, *11*(4), 359-365.

Gibson, T., Stark, H., & Evans, J. H. (1969). Directional variation in extensibility of human skin in vivo. *Journal of Biomechanics*, *2*(2).

Gniadecka, M., & Quistorff, B. (1996). Assessment of dermal water by high-frequency ultrasound: comparative studies with nuclear magnetic resonance. *British Journal of Dermatology*, *135*(2), 218-224.

Goldreich, D., & Kanics, I. M. (2003). Tactile acuity is enhanced in blindness. *Journal of Neuroscience*, *23*(8), 3439-3445.

Goodwin, A. W., John, K. T., & Marceglia, A. H. (1991). Tactile discrimination of curvature by humans using only cutaneous information from the fingerpads. *Experimental brain research*, *86*(3), 663-672.

Greenspon, C. M., McLellan, K. R., Lieber, J. D., & Bensmaia, S. J. (2020). Effect of scanning speed on texture-elicited vibrations. *Journal of the Royal Society, Interface*, *17*(167), 20190892.

Gueorguiev, D., Bochereau, S., Mouraux, A., Hayward, V., & Thonnard, J. L. (2016). Touch uses frictional cues to discriminate flat materials. *Scientific reports*, *6*(1), 1-7.

Harrington, G. S., & Downs III, J. H. (2001). FMRI mapping of the somatosensory cortex with vibratory stimuli: Is there a dependency on stimulus frequency?. *Brain research*, *897*(1-2), 188-192.

Hay, E., & Pruszynski, J. A. (2020). Orientation processing by synaptic integration across first-order tactile neurons. *PLoS computational biology*, *16*(12), e1008303.

Heller, M A (1989). Texture perception in sighted and blind observers. *Perception & Psychophysics* 45: 49-54.

Hihara S, Taoka M, Tanaka M, Iriki A (2015) Visual responsiveness of neurons in the secondary somatosensory area and its surrounding parietal operculum regions in awake macaque monkeys. Cereb Cortex 25(11):4535-4550. https://doi.org/10.1093/cercor/bhv095

Hollins M, Bensmaïa SJ, Washburn S. Vibrotactile adaptation impairs discrimination of fine, but not coarse, textures. Somatosens Mot Res. 2001;18(4):253-62. doi: 10.1080/01421590120089640. PMID: 11794728.

Hollins, M., & Risner, S. R. (2000). Evidence for the duplex theory of tactile texture perception. *Perception & psychophysics*, *62*(4), 695-705.

Hollins, Sliman J. Bensmaïa, Sean Washburn, M. (2001). Vibrotactile adaptation impairs discrimination of fine, but not coarse, textures. *Somatosensory & motor research*, *18*(4), 253-262.

Hsiao SS, O'Shaunessy DM, Johnson KO. 1993. Effects of selective attention on spatial form processing in monkey primary and secondary somatosensory cortex. J Neurophysiol 70:444–447.

Jarocka, E., Pruszynski, J. A., & Johansson, R. S. (2021). Human touch receptors are sensitive to spatial details on the scale of single fingerprint ridges. *Journal of Neuroscience*, *41*(16), 3622-3634.

Jenmalm, P., Birznieks, I., Goodwin, A. W., & Johansson, R. S. (2003). Influence of object shape on responses of human tactile afferents under conditions characteristic of manipulation. *European Journal of Neuroscience*, *18*(1), 164–176.

Johansson, R. S. (1978). Tactile sensibility in the human hand: receptive field characteristics of mechanoreceptive units in the glabrous skin area. *The Journal of physiology*, *281*(1), 101-125.

Johansson, R. S., & Birznieks, I. (2004). First spikes in ensembles of human tactile afferents code complex spatial fingertip events. *Nature neuroscience*, *7*(2), 170-177.

Johansson, R. S., & LaMotte, R. H. (1983). Tactile detection thresholds for a single asperity on an otherwise smooth surface. *Somatosensory research*, *1*(1), 21-31.

Johansson, R. S., & Vallbo, A. B. (1979). Tactile sensibility in the human hand: relative and absolute densities of four types of mechanoreceptive units in glabrous skin. *The Journal of physiology*, *286*(1), 283-300.

Johansson, R. S., & Vallbo, Å. B. (1980). Spatial properties of the population of mechanoreceptive units in the glabrous skin of the human hand. *Brain research*, *184*(2), 353-366.

Johnson, K. O. (2001). The roles and functions of cutaneous mechanoreceptors. *Current opinion in neurobiology*, *11*(4), 455-461.

Johnson, K. O., & Phillips, J. R. (1981). Tactile spatial resolution. I. Two-point discrimination, gap detection, grating resolution, and letter recognition. *Journal of neurophysiology*, *46*(6), 1177-1192.

Johnson, K. O., Yoshioka, T., & Vega–Bermudez, F. (2000). Tactile functions of mechanoreceptive afferents innervating the hand. *Journal of Clinical Neurophysiology*, *17*(6), 539-558.

Kaas JH. 2008. The somatosensory thalamus and associated pathways. In: JH Kaas, EP Gardner (eds). The Senses: A Comprehensive Reference, Vol. 6 Somatosensation, pp. 117–141. Oxford: Elsevier.

Kaim, L., & Drewing, K. (2011). Exploratory strategies in haptic softness discrimination are tuned to achieve high levels of task performance. *IEEE Transactions on Haptics*, *4*(4), 242-252.

Kalichman, L., Malkin, I., Seibel, M. J., Kobyliansky, E., & Livshits, G. (2008). Epiphyseal expansion in hand bones: association with age, sex, and hand osteoarthritis. *Osteoarthritis and cartilage*, *16*(5), 560-565.

Kalisch, T., Ragert, P., Schwenkreis, P., Dinse, H. R., & Tegenthoff, M. (2009). Impaired tactile acuity in old age is accompanied by enlarged hand representations in somatosensory cortex. *Cerebral Cortex*, *19*(7), 1530-1538.

Kalra, A., Lowe, A., & Jumaily, A. A. (2016). An overview of factors affecting the skins Youngs modulus. *J. Aging Sci*, *4*(2), 1000156.

Kandel, E. R., Schwartz, J. H., Jessell, T. M., Siegelbaum, S. A., & Hudspeth, A. J. Hg.(2013/2021). Principles of Neural Science.

Katz, D. (1925). Der Aufbau der Tastwelt. Zeitschrift für Psychologie, Ergänzungsband 11.

Kauffman, T., Théoret, H., & Pascual-Leone, A. (2002). Braille character discrimination in blindfolded human subjects. *Neuroreport*, *13*(5), 571-574.

Klatzky, R. L., & Lederman, S. J. (1999). Tactile roughness perception with a rigid link interposed between skin and surface. *Perception & psychophysics*, *61*(4), 591-607.

Knüttel, A.; Boehlau-Godau, M. Spatially confined and temporally resolved refractive index and scattering evaluation in human skin performed with optical coherence tomography. J. Biomed. Opt. 2000, 5, 83–93.

LaMotte, R. H., & Srinivasan, M. A. (1991). Surface microgeometry: Tactile perception and neural encoding. In *Information processing in the somatosensory system* (pp. 49-58). Palgrave, London.

LaMotte, R. H., & Srinivasan, M. A. (1996). Neural encoding of shape: responses of cutaneous mechanoreceptors to a wavy surface stroked across the monkey fingerpad. *Journal of neurophysiology*, *76*(6), 3787-3797.

LaMotte, R. H., & Whitehouse, J. (1986). Tactile detection of a dot on a smooth surface: peripheral neural events. *Journal of neurophysiology*, *56*(4), 1109-1128.

Langer, K. (1861). Zur Anatomie und Physilogie der Haut. *Sitzungsbericht Der Mathematisch-Naturwissenschaftlichen Classe Der Kaiserlichen Academie Der Wissenschaften*, *44*, 19-48

Langton, A. K., Graham, H. K., McConnell, J. C., Sherratt, M. J., Griffiths, C. E. M., & Watson, R. E. B. (2017). Organization of the dermal matrix impacts the biomechanical properties of skin. *British Journal of Dermatology*, *177*(3), 818-827.

Lederman, S J (1979). Auditory texture perception. *Perception* 8: 93-103.

Lederman, S. J., & Klatzky, R. L. (1987). Hand movements: A window into haptic object recognition. *Cognitive psychology*, *19*(3), 342-368

Lederman, S. J., Loomis, J. M., & Williams, D. A. (1982). The role of vibration in the tactual perception of roughness. *Perception & Psychophysics*, *32*(2), 109-116.

Lenz, M., Tegenthoff, M., Kohlhaas, K., Stude, P., Höffken, O., Tossi, M. A. G., ... & Dinse, H. R. (2012). Increased excitability of somatosensory cortex in aged humans is associated with impaired tactile acuity. *Journal of Neuroscience*, *32*(5), 1811-1816.

Libouton, X., Barbier, O., Berger, Y., Plaghki, L., & Thonnard, J. L. (2012). Tactile roughness discrimination of the finger pad relies primarily on vibration sensitive afferents not necessarily located in the hand. *Behavioural brain research*, *229*(1), 273-279.

Lieber, J. D., & Bensmaia, S. J. (2020). Emergence of an invariant representation of texture in primate somatosensory cortex. *Cerebral Co*

Liu, X., Gad, D., Lu, Z., Lewis, R., Carré, M. J., & Matcher, S. J. (2015). The contributions of skin structural properties to the friction of human finger-pads. *Proceedings of the Institution of Mechanical Engineers, Part J: Journal of Engineering Tribology*, *229*(3), 294-311.

Mackevicius, E. L., Best, M. D., Saal, H. P., & Bensmaia, S. J. (2012). Millisecond precision spike timing shapes tactile perception. *Journal of Neuroscience*, *32*(44), 15309-15317.

Macmillan, N. A., & Creelman, C. D. (2004). *Detection theory: A user's guide*. Psychology press.

Manfredi, L. R., Saal, H. P., Brown, K. J., Zielinski, M. C., Dammann III, J. F., Polashock, V. S., & Bensmaia, S. J. (2014). Natural scenes in tactile texture. *Journal of neurophysiology*, *111*(9), 1792-1802.

Manschot, J. F. M. (1985). *The mechanical properties of human skin in vivo* (Doctoral dissertation, Radboud University, Nijmegen).

Martin, K. Direct measurement of moisture in skin by NIR spectroscopy. J. Soc. Cosmet. Chem. 1993, 44, 249–261.

Masen, M. A. (2011). A systems based experimental approach to tactile friction. *Journal of the mechanical behavior of biomedical materials*, *4*(8), 1620-1626.

Maurel, W., Thalmann, D., Wu, Y., & Thalmann, N. M. (1998). *Biomechanical models for soft tissue simulation* (Vol. 48). Berlin: Springer.

McGlone, F., Vallbo, A. B., Olausson, H., Loken, L., & Wessberg, J. (2007). Discriminative touch and emotional touch. *Canadian Journal of Experimental Psychology/Revue canadienne de psychologie expérimentale*, *61*(3), 173.

Metzger, A., & Drewing, K. (2021). A Kalman filter model for predicting discrimination performance in free and restricted haptic explorations. In *2021 IEEE World Haptics Conference (WHC)* (pp. 439-444). IEEE.

Miller, J., & Ulrich, R. (2001). On the analysis of psychometric functions: The Spearman-Kärber method. *Perception & Psychophysics*, *63*(8), 1399-1420.

Miller, L. E., Fabio, C., Ravenda, V., Bahmad, S., Koun, E., Salemme, R., ... & Farne, A. (2019). Somatosensory cortex efficiently processes touch located beyond the body. *Current Biology*, *29*(24), 4276-4283.

Morley, J. W., & Goodwin, A. W. (1987). Sinusoidal movement of a grating across the monkey's fingerpad: temporal patterns of afferent fiber responses. *Journal of Neuroscience*, *7*(7), 2181-2191.

Mountcastle, V. B. (2005). *The sensory hand: neural mechanisms of somatic sensation*. Harvard University Press.

Muniak, M. A., Ray, S., Hsiao, S. S., Dammann, J. F., & Bensmaia, S. J. (2007). The neural coding of stimulus intensity: linking the population response of mechanoreceptive

afferents with psychophysical behavior. *Journal of Neuroscience*, *27*(43), 11687-11699.

Nakazawa, N., Ikeura, R., & Inooka, H. (2000). Characteristics of human fingertips in the shearing direction. *Biological Cybernetics*, *82*(3), 207–214.

Nolano M, Provitera V, Crisci C, Stancanelli A, Wendelschafer-Crabb G, Kennedy WR, et al. (2003). Quantification of myelinated endings and mechanoreceptors in human digital skin. Ann Neurol. 54: 197–205.

Nolano M, Provitera V, Crisci C, Stancanelli A, Wendelschafer-Crabb G, Kennedy WR, et al. (2003). Quantification of myelinated endings and mechanoreceptors in human digital skin. Ann Neurol. 54: 197–205.

Ouyang, Q., Wu, J., Shao, Z., Chen, D., & Bisley, J. (2020). A Simplified Model for Simulating Population Responses of Tactile Afferents and Receptors in the Skin. *IEEE Transactions on Biomedical Engineering*.

Ouyang, Q., Wu, J., Shao, Z., Wu, M., & Cao, Z. (2019). A Python Code for Simulating Single Tactile Receptors and the Spiking Responses of Their Afferents. *Frontiers in neuroinformatics*, *13*, 27.

Pan, L., Zan, L., & Foster, F. S. (1997). In vivo high frequency ultrasound assessment of skin elasticity. *Proceedings of the IEEE Ultrasonics Symposium*, *2*, 1087–1091.

Parandoush P, Hossain A. A review of modeling and simulation of laser beam machining. International Journal of Machine Tools and Manufacture 2014; 85: 135-145.

Pare, M., Behets, C., & Cornu, O. (2003). Paucity of presumptive ruffini corpuscles in the index finger pad of humans. *Journal of Comparative Neurology*, *456*(3), 260-266.

Paré, M., Smith, A. M., & Rice, F. L. (2002). Distribution and terminal arborizations of cutaneous mechanoreceptors in the glabrous finger pads of the monkey. *Journal of Comparative Neurology*, *445*(4), 347-359

Pawluk, D. T., & Howe, R. D. (1999). Dynamic contact of the human fingerpad against a flat surface.

Peelle, J. (2020). E. Age-Related Sensory Deficits and Their Consequences. In A.K. Thomas & A. Gutchess (Eds.). The Cambridge Handbook of Cognitive Ageing: A Like Course Perspective, Cambridge Handbooks in Psychology (pp. 179.199).

Penchev, Pavel Nedyalkov. Reconfigurable laser micro-processing systems: development of generic system-level tools for implementing modular laser micro-manufacturing platforms. PhD Thesis, University of Birmingham, UK, 2016.

Persson, J., & Nyberg, L. (2006). Altered brain activity in healthy seniors: what does it mean?. *Progress in brain research*, *157*, 45-385.

Peters, A. (2002). The effects of normal aging on myelin and nerve fibers: a review. *Journal of neurocytology*, *31*(8-9), 581-593.

Petkov P. Laser milling: Surface Integrity, Removal strategies and Process accuracy. PhD Thesis, Cardiff University, UK, 2011.

Phillips, J. R., & Johnson, K. O. (1981a). Tactile spatial resolution. II. Neural representation of bars, edges, and gratings in monkey primary afferents. *Journal of Neurophysiology*, *46*(6), 1192–1203.

Phillips, J. R., & Johnson, K. O. (1981b). Tactile spatial resolution. III. A continuum mechanics model of skin predicting mechanoreceptor responses to bars, edges, and gratings. *Journal of neurophysiology*, *46*(6), 1204-1225.

Phillips, J. R., Johnson, K. O., & Hsiao, S. S. (1988). Spatial pattern representation and transformation in monkey somatosensory cortex. *Proceedings of the National Academy of Sciences*, *85*(4), 1317-1321.

Prevost A, Scheibert J, Debrégeas G. 2009 Effect of fingerprints orientation on skin vibrations during tactile exploration of textured surfaces. Commun. Integr. Biol. 2, 422–424. (doi:10.4161/cib.2.5.9052)

Pruszynski, J. A., & Johansson, R. S. (2014). Edge-orientation processing in first-order tactile neurons. *Nature neuroscience*, *17*(10), 1404-1409.

Pruszynski, J. A., Flanagan, J. R., & Johansson, R. S. (2018). Fast and accurate edge orientation processing during object manipulation. *ELife*, *7*, 1–22.

Qassem, M., & Kyriacou, P. (2019). Review of modern techniques for the assessment of skin hydration. *Cosmetics*, *6*(1), 19.

Roberts, R. D., Loomes, A. R., Allen, H. A., Di Luca, M., & Wing, A. M. (2020). Contact forces in roughness discrimination. *Scientific reports*, *10*(1), 1-9.

Robinson CJ, Burton H. Organization of somatosensory receptive fields in cortical areas 7b, retroinsula, postauditory and granular insula of M. fascicularis. J Comp Neurol. 1980 Jul 1;192(1):69-92. doi: 10.1002/cne.901920105. PMID: 7410614.

Romo R, Hernandez A, Zainos A, Lemus L, Brody CD. 2002. Neuronal correlates of decision-making in secondary somatosensory cortex. Nat Neurosci 5:1217–1235.

Ruben, J., Schwiemann, J., Deuchert, M., Meyer, R., Krause, T., Curio, G., ... & Villringer, A. (2001). Somatotopic organization of human secondary somatosensory cortex. *Cerebral cortex*, *11*(5), 463-473.

Ryun, S., Kim, J. S., Lee, H., & Chung, C. K. (2017). Tactile Frequency-Specific High-Gamma Activities in Human Primary and Secondary Somatosensory Cortices. *Scientific reports*, *7*(1), 15442. https://doi.org/10.1038/s41598-017-15767-x

Saal HP, Suresh AK, Solorzano LE, Weber AI, Bensmaia SJ. 2018 The effect of contact force on the responses of tactile nerve fibers to scanned textures. Neuroscience 389, 99–103. (doi:10.1016/j. neuroscience.2017.08.024)

Saal, H. P., & Bensmaia, S. J. (2014). Touch is a team effort: interplay of submodalities in cutaneous sensibility. *Trends in neurosciences*, *37*(12), 689-697.

Saal, H. P., Delhaye, B. P., Rayhaun, B. C., & Bensmaia, S. J. (2017). Simulating tactile signals from the whole hand with millisecond precision. *Proceedings of the National Academy of Sciences*, *114*(28), E5693-E5702.

Sandford, E., Chen, Y., Hunter, I., Hillebrand, G., & Jones, L. (2013). Capturing skin properties from dynamic mechanical analyses. *Skin Research and Technology*, *19*(1), e339-e348.

Shao, Y., Hayward, V., & Visell, Y. (2020). Compression of dynamic tactile information in the human hand. *Science Advances*, *6*(16).

Shoham D, Grinvald A. 2001. The cortical representation of the hand in macaque and human area S-I: high resolution optical imaging. J Neurosci 21:6820–6835.

Skedung L, El Rawadi C, Arvidsson M, Farcet C, Luengo GS, Breton L, Rutland MW. Mechanisms of tactile sensory deterioration amongst the elderly. Scientific reports. 2018 Apr 19;8(1):1-0.

Slatineanu L, Coteata M, Besliu I and Dodun O. Thermal Phenomena at the laser beam machining. Int J Mater Form 2010; 3:1103 1106.

Smith, A. M., Chapman, C. E., Deslandes, M., Langlais, J. S., & Thibodeau, M. P. (2002). Role of friction and tangential force variation in the subjective scaling of tactile roughness. *Experimental brain research*, *144*(2), 211-223.

Spinner, M., Wiechert, A. B., & Gorb, S. N. (2016). Sticky fingers: Adhesive properties of human fingertips. *Journal of Biomechanics*, *49*(4), 606-610.

Srinivasan MA. (1989). Surface deflection of primate fingertip under line load. *Journal of Biomechanics*, 22(4):343–9.

Srinivasan, M. A., & LaMotte, R. H. (1987). Tactile discrimination of shape: responses of slowly and rapidly adapting mechanoreceptive afferents to a step indented into the monkey fingerpad. *Journal of Neuroscience*, *7*(6), 1682-1697.

Sripati AP, Yoshioka T, Denchev P, Hsiao SS, Johnson KO. (2006a). Spatiotemporal receptive fields of peripheral afferents and cortical area 3b and 1 neurons in the primate somatosensory system. J Neurosci 26:2101–2114.

Sripati, A. P., Bensmaia, S. J., & Johnson, K. O. (2006b). A continuum mechanical model of mechanoreceptive afferent responses to indented spatial patterns. *Journal of neurophysiology*, *95*(6), 3852-3864.

Stevens, J. C. (1992). Aging and spatial acuity of touch. *Journal of gerontology*, *47*(1), P35-P40.

Stevens, J. C., & Choo, K. K. (1996). Spatial acuity of the body surface over the life span. *Somatosensory & motor research*, *13*(2), 153-166.

Stevens, J. C., & Cruz, L. A. (1996). Spatial acuity of touch: ubiquitous decline with aging revealed by repeated threshold testing. *Somatosensory & motor research*, *13*(1), 1-10.

Suresh, A. K., Saal, H. P., & Bensmaia, S. J. (2016). Edge orientation signals in tactile afferents of macaques. *Journal of Neurophysiology*, *116*(6), 2647-2655.

Tong, J., Mao, O., & Goldreich, D. (2013). Two-point orientation discrimination versus the traditional two-point test for tactile spatial acuity assessment. *Frontiers in human neuroscience*, *7*, 579. https://doi.org/10.3389/fnhum.2013.00579

Tymms, C., Gardner, E. P., & Zorin, D. (2018). A quantitative perceptual model for tactile roughness. *ACM Transactions on Graphics (TOG)*, *37*(5), 1-14.

Ulrich, R., & Miller, J. (2004). Threshold estimation in two-alternative forced-choice (2AFC) tasks: The Spearman-Kärber method. *Perception & Psychophysics*, *66*(3), 517-533.

Van Kuilenburg, J., Masen, M. A., & Van Der Heide, E. (2013). Contact modelling of human skin: What value to use for the modulus of elasticity? *Proceedings of the institution of mechanical engineers, Part J: Journal of Engineering Tribology*, *227*(4), 349-361.

van Kuilenburg, J., Masen, M. A., & van der Heide, E. (2013). The role of the skin microrelief in the contact behaviour of human skin: Contact between the human finger and regular surface textures. *Tribology International*, *65*, 81-90.

Vega-Bermudez, F., & Johnson, K. O. (1999). SA1 and RA receptive fields, response variability, and population responses mapped with a probe array. *Journal of neurophysiology*, *81*(6), 2701-2710.

Verrillo, R. T. (1980). Age related changes in the sensitivity to vibration. *Journal of gerontology*, *35*(2), 185-193.

Wang, Q., & Hayward, V. (2007). In vivo biomechanics of the fingerpad skin under local tangential traction. *Journal of Biomechanics*, *40*(4), 851–860.

Warren S, Hamalainen HA, Gardner EP. Objective classification of motion- and direction-sensitive neurons in primary somatosensory cortex of awake monkeys. J Neurophysiol. 1986 Sep;56(3):598-622. doi: 10.1152/jn.1986.56.3.598. PMID: 3783213.

Weber, A. I., Saal, H. P., Lieber, J. D., Cheng, J. W., Manfredi, L. R., Dammann, J. F., & Bensmaia, S. J. (2013). Spatial and temporal codes mediate the tactile perception of natural textures. *Proceedings of the National Academy of Sciences of the United States of America*, *110*(42), 17107–17112.

Weber, E. (1835). Uber den tastsinn. *Arch Anat Physiol, Wissen Med (Muller's Archives)*, *1*, 152-159.

Weinstein, S. (1968). Intensive and extensive aspects of tactile sensitivity as a function of body part, sex and laterality. *The skin senses*.

Westheimer, G. (1975). Visual acuity and hyperacuity. *Investigative Ophthalmology & Visual Science*, *14*(8), 570-572.

Westling, G., & Johansson, R. S. (1987). Responses in glabrous skin mechanoreceptors during precision grip in humans. *Experimental brain research*, *66*(1), 128-140

Wiertlewski, M., & Hayward, V. (2012). Mechanical behavior of the fingertip in the range of frequencies and displacements relevant to touch. *Journal of biomechanics*, *45*(11), 1869-1874.

Wilhelm, K.P., Cua, A.B., Maibach, H.I. (1993). In Vivo Study on Age-Related Elastic Properties of Human Skin. In: Frosch, P.J., Kligman, A.M. (eds) Noninvasive Methods for the Quantification of Skin Functions. Springer, Berlin, Heidelberg. https://doi.org/10.1007/978-3-642-78157-5_12

Wilhelmi, B. J., Blackwell, S. J., Mancoll, J. S., & Phillips, L. G. (1998). Creep vs. stretch: a review of the viscoelastic properties of skin. *Annals of plastic surgery*, *41*(2), 215-219.

Won, S. Y., Kim, H. K., Kim, M. E., & Kim, K. S. (2017). Two-point discrimination values vary depending on test site, sex and test modality in the orofacial region: a preliminary study. *Journal of applied oral science : revista FOB*, *25*(4), 427–435. https://doi.org/10.1590/1678-7757-2016-0462

Woodward, K. L. (1993). The relationship between skin compliance, age, gender, and tactile discriminative thresholds in humans. *Somatosensory & motor research*, *10*(1), 63-67.

Yang, Y., Wang, L., Yan, F., Xiang, X., Tang, Y., Zhang, L., ... & Qiu, L. (2018). Determination of normal skin elasticity by using real-time shear wave elastography. *Journal of Ultrasound in Medicine*, *37*(11), 2507-2516.

Yao YL, Chen H and Zhang W. Time scale effects in laser material removal: a review. International Journal of Advanced Manufacturing

Yokota, H., Otsuru, N., Kikuchi, R., Suzuki, R., Kojima, S., Saito, K., ... & Onishi, H. (2020). Establishment of optimal two-point discrimination test method and consideration of reproducibility. *Neuroscience letters*, *714*, 134525.

Zhou, X., Masen, M. A., Li, Y. Y., Yap, K. K., Murali, M., & Jin, Z. M. (2022). Influence of different fluid environments on tactile perception and finger friction. *Journal of the Royal Society Interface*, *19*(188), 20210783.